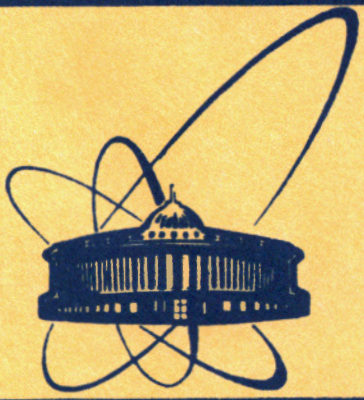

сообщения
объединенного
института
ядерных
исследований
дубна

E4-84-446

D.N.Poenaru,[1] M.Ivaşcu,[1] A.Săndulescu, W.Greiner[2]

NUCLEAR DECAY BY EMISSION OF CHARGED PARTICLE – SUPERASYMMETRIC FISSION PROCESS

[1] Central Institute of Physics, 76900-Bucharest, Romania
[2] Johann-Wolfgang-Goethe Universität, D-6000 Frankfurt am Main, BRD

1984

1. INTRODUCTION

The induced fission (Hahn and Strassmann 1939, Meitner and Frisch 1939) and the spontaneous fission (Petrjak and Flerov 1940) have been discovered long time after the alpha decay (Becquerel 1896, Rutherford and Geiger 1908). One of the first successes of the quantum mechanics was the explanation of the alpha tunnelling through the Coulomb barrier (Gamow 1928, Condon and Gurney 1929).

The similarity between fission and alpha decay was recognized in the early stages of the fission theory (Bohr and Wheeler 1939, Frenkel 1946). Nevertheless, the theories of these phenomena were developed on essentially different grounds. Nuclear reaction microscopic methods have been used in alpha decay, but for many years the phenomenological liquid-drop model (LDM) dominated the fission.

The asymmetrical distribution of the fragment masses from the spontaneous or low excitation energy induced fission was a longstanding puzzle of the theory.

The first attempt to consider both the collective nature of the nucleonic motion and the single particle effects by adding the shell corrections to the LDM energy (Myers and Swiatecki 1966) offered a good estimation of nuclear ground state (gs) deformations. The next important step, producing a renewed interest for the development of the fission theory was the idea of deformed nuclear shells and the microscopic shell correction method (Strutinsky 1967) strongly stimulated by the experimental discovery (Polikanov et al.1962) of fission isomers (Poenaru 1977, Metag et al. 1980, Bjørnholm and Lynn 1980).

In this way it was possible to explain qualitatively the fission asymmetry (Möller and Nilsson 1970, Pashkevich 1971, Adeev et al. 1970, Brack et al. 1972, Möller 1972, Mustafa et al. 1972) as it is essentially due to shell effects. The fragmentation theory (Fink et al. 1974) was also successful in both regions of low and high mass asymmetry (Maruhn 1976, Săndulescu et al. 1980).

Alternatively, the phenomenological shell corrections were extended (Schultheis et al. 1970) to the high deformations encountered in a fission process. New variants of the LDM: the finite range of nuclear forces model (FRNFM) (Krappe and Nix 1974) and the Yukawa-plus-exponential folding model (Y+EM) (Krappe et al. 1979) were especially developed to describe both the fission and fusion processes taking place in the heavy ion

reactions. The extension of these models to the systems with different charge densities (Poenaru et al. 1979d, 1980a, 1980c) offered a good basis for the fission theory of the alpha decay (Poenaru et al. 1979a, 1979b, 1979c, Poenaru and Ivaşcu 1980, 1982) - an attempt toward a unified treatment of these only apparently distinct processes.

Another model describing in a continuous way the transition from light particle emission to fission in the decay of the compound nucleus at higher excitation energies above the barrier was developed by Moretto (1975) and by Swiatecki (quoted by Sobotka et al.1983); it was recently tested (Sobotka et al. 1983) by studying the production of ^{4}He, Li, $^{7,9}Be$, B, C, N, O, and F in the reaction 90 MeV ^{3}He - ^{nat}Ag. It is based on the statistical transition state formalism and allows to compute the angular and energy distributions. Unlike this model dealing with excited states above the barrier, we are concerned with ground states or lower excited states, below the barrier where quantum-mechanical tunnelling and shell effects are extremely important.

The purpose of this paper is to present the formalism used in our model, the results obtained and its extensions allowing to predict other decaying modes intermediate between alpha decay and fission (Sandulescu et al.1980a,Poenaru and Ivascu 1980, poenaru et al. 1983a, 1984). The first evidence for such a mode was reported recently by Rose and Jones (1984); they discovered the spontaneous emission of ^{14}C from ^{223}Ra. The results were confirmed by Dr.Ogloblin from Kurchatov Institute in Moscow *.

2. NUCLEAR STABILITY

2.1. Metastability

In order to see whether a nucleus ^{A}Z is stable or not with respect to the split in two nuclei $^{A_1}Z_1$ and $^{A_2}Z_2$, one can use (Blatt and Weisskopf 1956) the deformation energy curve of the system vs. separation distance between fragments (fig.1). If the energy of the two nuclei at infinite separation is taken as the origin of the potential, the initial energy

$$E(R)|_{R=0} = Q(A_2, Z_2) = M(A, Z) - [M(A_1, Z_1) + M(A_2, Z_2)] \qquad (2.1)$$

is the Q-value (the energy release), which can be easily computed from the well-known experimental masses (Wapstra and Bos 1977). The fission barrier height is the difference

$$E_b = E_{sp} - Q. \qquad (2.2)$$

*Talk presented at the 34th conference on nuclear spectroscopy and structure of atomic nucleus (Alma-Ata, 1984).

Fig.1. Stability (1), metastability (2), and instability (3) of the nuclear systems with respect to the fission process.

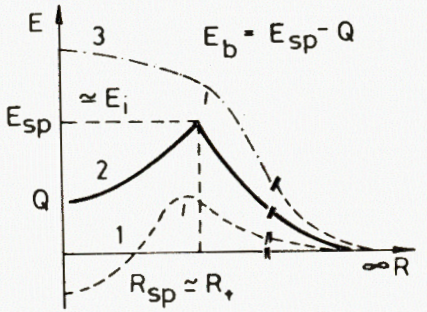

Three distinct cases are shown in figure 1:

1) STABILITY: $Q < 0$, $E_b > 0$. The nucleus ^{A}Z is in the position of minimum potential energy; its split is prevented by an infinitely thick barrier.

2) METASTABILITY: $Q > 0$, $E_b > 0$. The fragments are held together temporarily by a potential barrier. Because of the quantum-mechanical tunnelling effect, there is a finite probability P per unit time for the penetration through this barrier which decreases with an increase in E_b and in the reduced mass $\mu = (A_1A_2/A)m$, where m is the nucleon mass. The radioactive nuclei are metastable.

3) INSTABILITY: $Q > 0$, $E_b < 0$. The compound nucleus is unstable mainly due to the spontaneous fission.

One has to consider also the beta instability, which is beyond the scope of this work.

2.2. The Lifetime

Like in fission (Brack et al. 1972) the half-life T of the metastable system is given by

$$T = \hbar \ln 2/\Gamma = \ln 2/\nu P, \qquad (2.3)$$

where Γ is the partial width and $\nu = \omega/2\pi = 2E_{vib}/h$ represents the number of assaults on the barrier per second (the characteristic frequency of the collective mode). If the time T for a particular split is very long in comparison with the half-life of the other one, this emission cannot be experimentally observed. In spite of the metastability with respect to many disintegration modes, only the faster processes are observed.

According to the WKB theory the probability per unit time of penetration through the barrier is expressed as

$$P = \exp(-K); K = \frac{2}{\hbar}\int_{R_a}^{R_b} \{2\mu[E(R) - Q']\}^{1/2}\, dr, \qquad (2.4)$$

where K is the action integral, $Q' = Q + E_{vib}$ is the initial excitation energy, $E_{vib} = \hbar\omega/2$ is the zero point vibration energy and μ is the mass parameter approximated by the reduced mass, R_a and R_b are the entrance and exit points $E(R_a) = E(R_b) = Q'$. This approximation is valid for a barrier height high enough; otherwise

$$P = [1 + \exp(-K)]^{-1} . \qquad (2.5)$$

In the framework of the R-matrix theory of alpha decay, the disintegration constant $\lambda = \ln 2/T$, is given by

$$\lambda = \delta^2 P/\hbar , \qquad (2.6)$$

where δ^2 is the reduced width, which is proportional to the alpha preformation probability. In fission theory, the role of δ^2 is played by the zero point vibration energy E_{vib}, but this quantity is present also in P, as it is shown by eq.(2.4). Consequently, E_{vib} has smaller variations than δ^2 with Z and N, even in the neighbourhood of magic numbers.

3. DEFORMATION ENERGIES FOR BINARY SYSTEMS WITH CHARGE ASYMMETRY DIFFERENT FROM THE MASS ASYMMETRY

The LDM of Myers and Swiatecki (1966, 1967) and its generalisation replacing the surface energy by double folded Y+EM over a sharp surface density distribution (Krappe et al.1979) are used in fission theory and heavy-ion physics. The Y+EM parameters have been determined by fitting nuclear ground state masses, fission barriers, heavy ion elastic scattering and elastic electron scattering data. New physical effects have been introduced (Möller and Nix 1981) in the mass formulae: a proton form factor, an exact diffuseness correction, a charge asymmetry term,and microscopic zero point energies.

In order to reduce the number of independent parameters, some authors (Krappe 1976, Möller and Nix 1977) have assumed the same charge-to-mass ratio (Z/A) by choosing one of the reaction partners to be off the line of beta stability. On the other hand, Zohni and Blann (1978) considered the realistic combinations but ignored the different charge-to-mass ratio. The difference between the mass-, η_A, and charge-, η_Z, asymmetry parameters has been considered by only some authors (Gupta et al. 1975, Adeev et al. 1976, Gupta 1977) when potential energy surfaces (PES) have been calculated, though the asymmetric mass and charge fragmentation (Fink et al. 1974) in a case frequently met in heavy-ion collisions, due to the fact that for the light beta-stable nuclei $Z_2 = N_2$, but for the heavy ones $N_1 > Z_1$.

We have shown (Ivaşcu and Poenaru 1978, Poenaru and Ivaşcu 1979, Poenaru et al. 1979d) both for LDM and FRNFM that the deformation energy could be underestimated if this difference is ignored. An extension for systems with charge asymmetry different from the mass asymmetry of these two models (Poenaru et al. 1979d) and of Y+EM (Poenaru et al.1980a, 1980c) has been developed.

It is obvious that the condition

$$\eta_A \equiv (A_1 - A_2)/A \neq \eta_z \equiv (Z_1 - Z_2)/Z \qquad (3.1)$$

for mass- and charge-asymmetry parameters, where $A = A_1 + A_2$ and $Z = Z_1 + Z_2$, is equivalent to

$$I \equiv (N - Z)/A \neq I_i \equiv (N_i - Z_i)/A_i \quad (i = 1,2) \qquad (3.2)$$

for the nuclear composition, where $N = A - Z$ and with

$$\rho_{1e} \neq \rho_{2e} \neq \rho_{0e} \equiv eZ/(\tfrac{4}{3}\pi r_0^3 A) \qquad (3.3)$$

for the charge densities, where e is the electron charge and r_0 the radius constant.

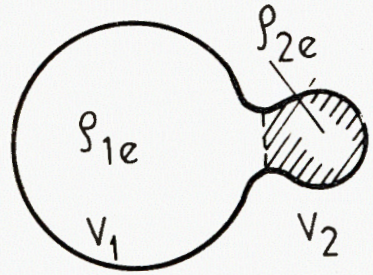

Fig.2. Binary system with different charge densities.

If we ignore the difference $\eta_Z - \eta_A$, we have actually the pair of nuclei $^{A_1}Z_a$, $^{A_2}Z_b$, instead of $^{A_1}Z_1$, $^{A_2}Z_2$, where

$$Z_b = Z/(1 + q) \quad Z_b = Z - Z_a . \qquad (3.4)$$

We take into consideration the difference in charge densities for fusion or binary fragmentation assuming uniformity in each of the two fragments. In an intermediate stage of a fusion (or fission) reaction, when the two fragments are closed together, like in figure 2, we assume that the nuclear volume V is divided in two parts V_1 and V_2 and that each fragment is homogeneously charged with a density

$$\rho_e(\vec{r}) = \begin{cases} \rho_{1e} & \vec{r} \in V_1 \\ \rho_{2e} & \vec{r} \in V_2 \end{cases} . \qquad (3.5)$$

The deformation dependent terms of the potential energy, E_d,

$$E_d = E_s + E_c + E_v \qquad (3.6)$$

are the surface energy, E_s, the Coulomb energy, E_c, and the volume energy E_v.

3.1. LDM Surface Energy

Due to the proportionality between the surface energy E_s and the surface area, one has

$$E_s = c_{s1} A^{2/3} B_{s1} + c_{s2} A^{2/3} B_{s2}\ ,\ B_s \equiv E_s/E_s^\circ = (c_{s1}/c_s) B_{s1} + (c_{s2}/c_s) B_{s2}, \tag{3.7}$$

where

$$B_{si} = S_i/S^\circ\ ,\quad c_{si} = a_s(1 - \kappa I_i^2)\quad (i = 1,2)\ ,\ a_s = 17.9439\ \text{MeV},\ \kappa = 1.7826 \tag{3.8}$$

S_i is the surface area of the fragment i (without the separation area between V_1 and V_2) and S° is the surface area of the spherical fused nucleus $^A Z$, for which

$$E_s^\circ = c_s A^{2/3} \tag{3.9}$$

with c_s calculated as in equation (3.8) but with I_i substituted by I.

3.2. Coulomb Energy for Various Macroscopic Models

The general expression of the Coulomb energy can be split into three parts: by taking into account the two integration domains

$$E_c = \frac{1}{2}\rho_{1e}^2 \int_{V_1} d^3r_1 \int_{V_1} r_{12}^{-1} d^3r_2 + \frac{1}{2}\rho_{2e}^2 \int_{V_2} d^3r_1 \int_{V_2} r_{12}^{-1} d^3r_2 + \tag{3.10}$$

$$+ \rho_{1e}\rho_{2e} \int_{V_1} d^3r_1 \int_{V_2} r_{12}^{-1} d^3r_2\ ;\ r_{12} = |\vec{r}_1 - \vec{r}_2|\ ,$$

$$B_c = (\rho_{1e}/\rho_{0e})^2 B_{c1} + (\rho_{2e}/\rho_{0e})^2 B_{c2} + (\rho_{1e}\rho_{2e}/\rho_{0e}^2) B_{c12},$$

where the first two terms represent the self-energies of the two fragments; and the last one, their interaction energy. For a spherical homogeneously charged nucleus

$$E_c^\circ = 3e^2Z^2/5r_0A^{1/3} \tag{3.11}$$

with $r_0 = 1.2249$ fm for LDM, $r_0 = 1.16$ fm for FRNFM and $r_0 = 1.18$ fm for Y+EM. A more recent value (Möller and Nix 1981) is $r_0 = 1.16$ fm for Y+EM.

3.3. FRNFM Surface Energy

In the FRNFM (Krappe and Nix 1974), the surface energy is replaced by the folded Yukawa potential energy* E_n, from which the spurious contribution to the volume energy, E_{nV}, has to be subtracted out. If the nuclear matter is homogeneously distributed in the two fragments ($\rho_1 = \rho_2 = \rho_0$) one has similarly

$$E_n = -\frac{1}{4\pi a^3}(V_{01} \int_{V_1} d^3r_1 \int_{V_1} d^3r_2\, g(x) + 2(V_{01}V_{02})^{1/2} \int_{V_1} d^3r_1 \int_{V_2} d^3r_2 g(x) + \tag{3.12}$$

$$+ V_{02} \int_{V_2} d^3r_1 \int_{V_2} d^3r_2\, g(x))\ ,$$

$$g(x) = \exp(-x)/x;\ x = r_{12}/a\ ,$$

$$B_n \equiv (E_n - E_{nV})/(E_n^\circ - E_{nV}^\circ) = (c_{s1}/c_s) B_{n1} + (c_{s2}/c_s) B_{n2} + \frac{(c_{s1}c_{s2})^{1/2}}{c_s} B_{n12},$$

where we have assumed

$$V_0 = [V_0(r_1) V_0(r_2)]^{1/2},\ V_0(r) = V_{0i} = c_{si}/2\pi a r_0^2,\ r \in V_i\ \ (i = 1,2) \tag{3.13}$$

and $a = 1.4$ fm, $a_s = 24.7$ MeV, $\kappa = 4$ as usual.

For separated nuclei

$$E_{nV} = E_{nV_1} + E_{nV_2} = (2r_0/3a)(c_{s1}A_1 + c_{s2}A_2) \tag{3.14}$$

and for a spherical fused nucleus

$$E_n^\circ - E_{nV}^\circ = c_s[A^{2/3} - (a/r_0)^2 + (A^{1/3} + a/r_0)^2 \exp(-2R_0/a)\ ,\ R_0 = r_0A^{1/3}. \tag{3.15}$$

3.4. Y+EM Surface Energy

The double folded Yukawa-plus-exponential potential energy is also splitted into three parts

$$E_Y = -\frac{1}{8\pi^2 r_0^2 a^4}[c_{s1} \int_{V_1} d^3r_1 \int_{V_1} f(x)\, d^3r_2 + c_{s2} \int_{V_2} d^3r_1 \int_{V_2} f(x)\, d^3r_2 +$$

$$+ 2(c_{s1}c_{s2})^{1/2} \int_{V_1} d^3r_1 \int_{V_2} f(x)\, d^3r_2],\quad f(x) = (x-2)\, g(x)\ ;\ x = r_{12}/a,$$

*This type of potential energy was used by Greiner and coworkers: see, for example, Holm and Greiner (1970).

$$B_Y \equiv E_Y/E_Y^\circ = (c_{s1}/c_s)B_{Y1} + (c_{s2}/c_s)B_{Y2} + [(c_{s1}c_{s2})^{1/2}/c_s]B_{Y12},$$

$$E_Y^\circ = c_s A^{2/3}\{1 - 3(a/R_0)^2 + (1 + R_0/a)[2 + 3a/R_0 + 3(a/R_0)^2]e^{-2R_0/a}\}. \quad (3.16)$$

In spite of the same notations, for Y+EM we have c_s = 21.7 MeV, κ = 3 and a = 0.65 fm or the new values, allowing one to obtain smaller RMS errors for the ground state masses without microscopic zero point corrections (Möler and Nix 1981): a_s = 21.14 M κ = 2.4 and a = 0.68 fm.

3.5. Volume Energy

Because in the LDM the symmetry energy is included in the volume energy E_V, for $\eta_Z \neq \eta_A$ one also has to add the volume contribution to the deformation energy (though the volume conservation is assumed):

$$E_{V_1} + E_{V_2} - E_V^\circ \neq 0; \quad E_{V_1} = -c_{V_i}A_i; \quad c_{V_i} = a_V(1 - \kappa_V I_i^2), \quad (3.17)$$

where a_V = 15.4941 MeV, $\kappa_V = \kappa$ for LDM and a_V = 16.4696, κ_V = = 2.31015 for FRNFM (Möller and Nix 1976). These values are only slightly different from those adopted by Möller et al. (1974) For Y+EM, the corresponding quantities are: a_V = 16.012 MeV, κ_V = 2.64 and the new ones a_V = 16.0053 MeV, κ_V = 1.959.

The equations (3.7), (3.10), (3.12), and (3.16) are generally valid for binary fragmentation even in the absence of axial symmetry. They can be easily generalized for ternary or quaternary fragmentation.

4. COMPUTATION OF THE DEFORMATION DEPENDENT TERMS OF THE POTENTIAL ENERGY

4.1. Reducing the Order of Integration for General Shapes

Only for very simple nuclear surface shapes (see section 4.5) the eqs. (3.8), (3.10), (3.12), and (3.16) could be integrated in order to obtain an analytical result. Usually for a given parametrization $\rho = \rho(z, \phi)$ of the nuclear shape, this is not possible; one has to apply appropriate method of numerical quadrature. Unfortunately, in order to achieve the required accuracy (more than 5 significant digits) in case of six fold integrals like those from eqs.(3.10), (3.12), and (3.16), one has to spend a long time even with a fast computer. Consequently, it is very important to try to reduce the problem complexity.

If (ρ, ϕ, z) are the cylindrical coordinates of a point on the nuclear surface, the surface area (Junker 1974) is given by

$$S = \int_{z_1}^{z_2} dz \int_0^{2\pi} d\phi \{\rho^2(z, \phi)[1 + (\frac{\partial\rho}{\partial z})^2] + (\frac{\partial\rho}{\partial\phi})^2\}^{1/2}; \quad (4.1)$$

where z_1, z_2 are the intersection points of the z-axis with the nuclear surface. This double integral needs negligible short computer time in comparison with all other. Of course, the calculation of the volume energy with eq.(3.17) is even faster, once the quantities A_i and I_i are determined for a given deformation.

The double-volume integral expressing the Coulomb energy of a uniform charge distribution, or the gravitational potential energy of a uniform mass distribution, can be converted (Davies and Sierk 1975) in various ways into a double-surface integral by using Gauss divergence theorem twice. In this way one has

$$E_c = -\frac{1}{12} \oint\oint \rho_e^2 \frac{(d\vec{S}_1\vec{r}_{12})(d\vec{S}_2\vec{r}_{12})}{r_{12}}, \quad (4.2)$$

or

$$E_c = \frac{1}{10} \oint\oint \rho_e^2 \frac{(d\vec{S}_1\vec{r}_1)(d\vec{S}_2\vec{r}_{12})}{r_{12}}, \quad (4.3)$$

or

$$E_c = \frac{1}{2} \oint\oint \rho_e^2 \frac{(d\vec{S}_1\vec{r}_2)(d\vec{S}_2\vec{r}_{12})}{r_{12}}. \quad (4.4)$$

The computer time can be reduced by exploiting the symmetry of the eq. (4.2) under the interchange of $\vec{r}_1$ and $\vec{r}_2$. In cylindrical coordinates, the eq. (4.3) is written as

$$E_c = \frac{1}{20} \int_{z_1}^{z_2} dz \int_{z_1}^{z_2} dz' \int_0^{2\pi} d\phi \int_0^{2\pi} d\phi' \rho_e^2 \{(\rho'^2 - \frac{z'}{2}\frac{\partial\rho'^2}{\partial z'})[2\rho^2 - 2\rho'\rho\cos(\phi' - \phi) - (z - z')\frac{\partial\rho^2}{\partial z} - 2\rho'\frac{\partial\rho}{\partial\phi}\sin(\phi - \phi')\}/[(z - z')^2 + \rho^2 + \rho'^2 - 2\rho\rho'\cos(\phi - \phi')]^{1/2}, \quad (4.5)$$

where $\rho' = \rho'(z', \phi')$ and $\rho = \rho(z, \phi)$ is the nuclear surface equation. Similarly, one gets for E_n and E_y the double-surface integrals:

$$E_n = \frac{1}{8\pi^2 r_0^2 a^4} \oint\oint c_s(d\vec{S}_1\vec{r}_{12})(d\vec{S}_2\vec{r}_{12})(\frac{a}{r_{12}})^4[\frac{r_{12}}{a} - 2 + (\frac{r_{12}}{a} + 2)e^{-r_{12}/a}] \quad (4.6)$$

and

$$E_y = \frac{1}{8\pi^2 r_0^2 a^4} \oint \oint c_s (d\vec{S}_1 \vec{r}_{12})(d\vec{S}_2 \vec{r}_{12}) \left(\frac{a}{r_{12}}\right)^4 \{[\frac{r_{12}}{a}(\frac{r_{12}}{a} + 2) + 2] e^{-r_{12}/a} - 2\}. \quad (4.7)$$

To pass from Cartesian coordinates (x, y, z) to cylindrical ones (ρ, ϕ, z) (like from eq.(4.3) to eq.(4.5)) one uses the following expressions

$$\vec{r} = x\vec{i} + y\vec{j} + z\vec{k}; \quad x = \rho \cos\phi; \quad y = \rho \sin\phi, \quad d\vec{S} = (\frac{\partial \vec{r}}{\partial \phi}) \times (\frac{\partial \vec{r}}{\partial z}) dz\, d\phi, \quad (4.8)$$

where $\vec{i}$, $\vec{j}$, $\vec{k}$ are the unit vectors of the Cartesian system of coordinates.

The general relationships given in this section are not particularized for binary systems with different charge densities. In order to obtain such expressions one has to apply the method used in the precedent section.

If the nuclear shape has a symmetry with respect to z-axis, the order of integration in the eqs.(4.1)-(4.7) could be reduced further by one unit.

4.2. Various Methods for the Computation of the Coulomb Energy of an Axially Symmetric Nucleus

Three methods were frequently used in the past to compute the electrostatic energy E_c of an axially symmetric nucleus: Lawrence (1965) method in which E_c is expressed as a three fold integral; Hill and Wheeler (1953) method derived from the eq.(4.5), in which E_c is a two fold integral, and Beringer (1963) method containing only a sum of terms. A comparison of these methods was made by Poenaru and Galeriu (1975).

4.2.1. Beringer method

In the Beringer method, the nucleus is divided into N slices of the same thickness Δ, and each slice is replaced by one cylinder with the height Δ and the radius R_{ci}, $(i = 1,2,...,N)$ derived from the condition that the two equivalent bodies have the same volume. The Coulomb energy is composed from the self-energy of cylinders, E_i and the interaction energy E_{ij} between them:

$$E_c = \sum_{i=1}^{N} E_i + \sum_{i>j}^{N} E_{ij}, \quad (4.9)$$

where E_i is approximated by a semiempirical relatioship:

$$E_i = \frac{8\pi}{3}\rho_e^2 \Delta^2 R_{ci}^3 \{1 - \frac{\pi}{8}(\frac{\Delta}{R_{ci}}) + \frac{\pi}{8}(\frac{\Delta}{R_{ci}})^2 [B + \frac{7D}{12} - D \ln(\frac{\Delta}{R_{ci}})]\} \quad (4.10)$$

and

$$E_{ij} = 4\pi^2 \rho_e^2 \Delta^2 R_{ci}^3 \{-\frac{1}{2} k_{ij} g_{ij}^2 + \frac{1}{2}(1 + k_{ij}^2)^{1/2} g_{ij}^2 + \quad (4.11)$$

$$+ \sum_{n=1}^{\infty} C_{2n} P_{2n}(0) [\frac{g_{ij}^{2n+2}}{2n+2} - \frac{n g_{ij}^2}{6}(\frac{\Delta}{R_{ci}})^2](1 + k_{ij}^2)^{-2n+1/2} F(-n, -n+1, \frac{1}{2}; -k_{ij}^2)\}$$

in which $D = 0.155241$; $B = 0.257729$; $g_{ij} = R_{cj}/R_{ci} < 1$; $k_{ij} = (j-1)\Delta/R_{ci}$; $C_{2n} = \frac{(3/2 + n)}{n} C_{2(n-1)}$ the coefficient of the x^{2n} term in the binomial expansion of $(1 + x^2)^{1/2}$; $P_{2n}(0) = \frac{1-2n}{2n} P_{2(n-1)}(0)$ is the Legendre polynomial $(C_0 = P_0(0) = 1)$ and F is the hypergeometric function (Abramowitz and Stegun 1964) which is calculated by using the relationships:

$$F = 1 + \sum_{\ell=1}^{n-1} T_\ell; \quad T_\ell = k_{ij}^2 \frac{(n - \ell + 1)(\ell - n)}{(\ell - 0.5)\ell} T_{\ell-1}; \quad T_0 = 1. \quad (4.12)$$

For reflexion symmetric body, the amount of numerical computations can be significantly reduced (Galeriu and Poenaru 1976) because $R_{ci} = R_{cN+1-i}$; $i \in (1, m)$; $m = (N-1)/2$; N - odd positive integer

$$E_c = 2 \sum_{i=1}^{m} E_i + E_{m+1} + \sum_{i=1}^{m} (2 \sum_{j=i+1}^{m+1} E_{ij} + \sum_{j=m+2}^{N} E_{ij}). \quad (4.13)$$

One obtains an error smaller than 5.10^{-5} if $0 \leq \Delta/R_{ci} \leq 0.5$.

4.2.2. Lawrence method

Usually the integrals in the above formula are computed by using Gauss-Legendre numerical quadrature. It is convenient (Poenaru and Ivaşcu 1979) to express the equation of the nuclear surface in cylindrical coordinates $y = y(x)$ with a properly selected scale factor $[y = \rho/(z_2 - z_1); x = z/(z_2 - z_1)]$ leading to $(-1, +1)$ instead of (z_1, z_2) intercepts of the surface with the symmetry axis.

This interval is reduced to $(0,1)$ in case of the Lawrence method for which the nuclear surface eq. is $v_1 = v_1(u)$. For a uniformly charged body, Lawrence (1965) slices the volume

into infinitesimal disks. He obtains an exact equation for the electrostatic energy expressed as a three-dimensional integral with a relatively simple integrand

$$B_c = 120d^5 \int_0^1 v_1^2 u\,du \int_0^1 v_2^2 dy \int_0^1 \frac{\sin^2(\pi w)\,dw}{u(1-y)+[u^2(1-y)^2+v_1^2+v_2^2-2v_1v_2\cos(\pi w)]^{1/2}}, \quad (4.14)$$

where $2d = (z_2 - z_1)/R_0$ is the nuclear length along the symmetry axis, in units of R_0 and $v_2 = v_1(uy)$.

4.2.3. Davies-Sierk method

For axially symmetric shapes one can reduce further the order of integration in the eq.(4.5). The integration over one of the angles ϕ gives a factor of 2π and from the remaining angular integration one gets an integrand containing complete elliptic integrals (Hill and Wheeler 1953). With a reliable method for evaluating the elliptic integrals (Cody 1965), Hill-Wheeler integral should be faster to compute than eq.(4.14) involving an extra numerical integration. All three methods based on eqs. (4.2)-(4.4) are much more accurate in a given time than the methods of Beringer or Lawrence. The symmetry of eq.(4.2) for interchange of $\vec{r}_1$ to $\vec{r}_2$ makes this Davies-Sierk formula faster than eqs. (4.3) or (4.4).

This formula adapted to our case of a binary system with charge asymmetry different from the mass asymmetry (Poenaru et al. 1980a) leads to the following relationships for the quantities from eq.(3.10)

$$B_{c1} = b_c \int_{-1}^{x_3} dx \int_{-1}^{x_3} dx' F(x,x'); \; B_{c2} = b_c \int_{x_3}^{1} dx \int_{x_3}^{1} dx' F(x,x'); \; B_{c12} = b_c \int_{-1}^{x_3} dx \int_{x_3}^{1} dx' F(x,x'), \quad (4.15)$$

where $b_c = 5d^5/8\pi$, x_3 is the position of separation planes between fragments and

$$F(x,x') = \{yy_1[(K-2D)/3][2(y^2+y_1^2) - (x-x')^2 + 1.5(x-x')(\frac{dy_1^2}{dx'} - \frac{dy^2}{dx})] + \quad (4.16)$$

$$+ K\{y^2y_1^2/3 + [y^2 - 0.5(x-x')\frac{dy^2}{dx}][y_1^2 + 0.5(x-x')\frac{dy_1^2}{dx'}]\}\}/a_\rho ,$$

in which $y_1 = y(x')$ is the nuclear surface eq. with -1,+1 intercepts on the symmetry axis and

$$a_\rho^2 = (y+y_1)^2 + (x-x')^2; \; D = (K-K')/k^2; \; k^2 = 4yy_1/a_\rho^2, \quad (4.17)$$

where K and K′ are complete elliptic integrals of the first and second kind, respectively with argument k, ,

$$K(k) = \int_0^{\pi/2} (1 - k^2\sin^2 t)^{-1/2}\,dt; \quad K'(k) = \int_0^{\pi/2} (1 - k^2\sin^2 t)^{1/2}\,dt.$$

These elliptic integrals are computed by using Chebyshev polynomial approximation.

By removing the indetermination arising for $x = x'$, the function to be integrated takes the value $F(x,x) = 4y^3/3$.

4.3. Surface Energies

The expressions of B′s from the eqs.(3.7), (3.12), and (3.16) will be explicitly written in this section.

4.3.1. LDM

The quantities B_{s1} and B_{s2} from eq.(7) are given by

$$B_{s1} = 0.5d^2 \int_{-1}^{x_3} dx\,[y^2 + 0.25(\frac{dy^2}{dx})^2]^{1/2}, \; B_{s2} = 0.5d^2 \int_{x_3}^{1} dx\,[y^2 + 0.25(\frac{dy^2}{dx})^2]^{1/2} \quad (4.18)$$

for the axially symmetric nuclei. We use the same notations as in the preceding section.

4.3.2. FRNFM

One has, similarly, for B_{n1}, B_{n2} and B_{n12} from eq.(3.12)

$$B_{n1} = b_n(-0.5d^3 \int_{-1}^{x_3} dx \int_{-1}^{x_3} dx' \int_0^1 dw\,F_1F_2Q + 2A_1/3A),$$

$$B_{n2} = b_n(-0.5d^3 \int_{x_3}^{1} dx \int_{x_3}^{1} dx' \int_0^1 dw\,F_1F_2Q + 2A_2/3A), \quad (4.19)$$

$$B_{n12} = -0.5b_n d^3 \int_{-1}^{x_3} dx \int_{x_3}^{1} dx' \int_0^1 dw\,F_1F_2Q,$$

where

$$F_1 = y^2 - yy_1\cos\phi - 0.5(x-x')\frac{dy^2}{dx}; \; F_2 = y_1^2 - y_1y\cos\phi + 0.5(x-x')\frac{dy_1^2}{dx'}, \quad (4.20)$$

$$b_n = c_s A_{r_o}/[a(E_n^\circ - E_{nV}^\circ)], \quad (4.21)$$

$$Q = [P^{1/2} - 2a/R_0 d + (P^{1/2} + 2a/R_0 d)\exp(-R_0 d P^{1/2}/a)]/P^2, \quad (4.22)$$

$$P = y^2 + y_1^2 - 2yy_1\cos\phi + (x - x')^2; \quad \phi = 2\pi w. \quad (4.23)$$

When $x = x'$, we have $y = y_1$ and the integrand becomes

$$(F_1 F_2 Q)_{ii} = 0.5\{y\sin(\phi/2) - a/R_0\ell + [y\sin(\phi/2) + a/R_0 d] \times \times \exp[-(2R_0 d/a)\, y\sin(\phi/2)]\}. \quad (4.24)$$

Unlike B_{ci}, which depends only on the nuclear shapes and allows fast computation for many nuclei simultaneously, B_{ni} depends also on the nuclear mass. Hence the computation for this model has to be done for each nucleus separately. The same is true for B_y's in the Y+EM.

4.3.3. Y+EM

B_{Y1}, B_{Y2} and B_{Y12} from eq.(3.16) are expressed by:

$$B_{Y1} = b_Y \int_{-1}^{x_3} dx \int_{-1}^{x_3} dx' \int_0^1 dw F_1 F_2 Q_Y, \quad B_{Y2} = b_Y \int_{x_3}^{1} dx \int_{x_3}^{1} dx' \int_0^1 dw F_1 F_2 Q_Y,$$

$$B_{Y12} = b_Y \int_{-1}^{x_3} dx \int_{x_3}^{1} dx' \int_0^1 dw F_1 F_2 Q_Y, \quad (4.25)$$

where

$$b_Y = -d^4 (r_0/2a^2)\, c_s R_0 A/E_Y^\circ, \quad (4.26)$$

$$Q_Y = \{[P^{1/2}(P^{1/2} + 2a/R_0 d) + 2a^2/(R_0 d)^2]\exp(-R_0 d P^{1/2}/a) - 2a^2/(R_0 d)^2\}/P^2$$

and F_1, F_2 and P remain unchanged.

4.4. Numerical Integration

4.4.1. Reflection asymmetric nuclei

The integral

$$J_1 = \int_{-1}^{1} dx F(x) \quad (4.27)$$

like that of eq.(4.18), can be computed numerically with a Gauss-Legendre quadrature of order N (Davis and Rabinowitz 1975), using the relationship:

$$J_1 = \sum_{i=1}^{N} w_i F(x_i), \quad (4.28)$$

where x_i are the abscissas and w_i the weights, tabulated (Abramowitz and Stegun 1964) for some values of N. A FORTRAN program allowing to compute $\{x_i, w_i\}$ for any value of N is presented by Davis and Rabinowitz (1975).

In order to obtain a nuclear shape with neck, the nuclear parametrization is usually given (Nix 1972) by three different geometric bodies (for example two ellipsoids and a hyperboloid in the neck region) smoothly joined. In spite of the maching condition for the function $y(x)$ and its first derivative $dy(x)/dx$, there still remain the discontinuities of the higher order derivatives at the two junction planes. In this case the accuracy and speed of numerical quadrature are improved by dividing the integration interval $-1,+1$ along $0x$ in four subintervals with the following boundary values: the intercepts on $0x$ axis $z_1 = -1$ and $z_5 = +1$; the positions of two junction planes z_2 and z_4 and the position of extremum of $\rho(z)$ in the neck region z_3. In our case, z_3 gives the position of separation plane between fragments as it was mentioned above. If the shape has no discontinuity, z_2 and z_4 are arbitrarily chosen.

The transformation from abscissas t_i and weights v_i for the interval $(-1,+1)$ to abscissas x_j and weights w_j, for the four subintervals is made easily by using the following relationships:

$$x_j = a_p t_i + b_p; \quad w_j = a_p v_i; \quad (p = 1, 2, 3, 4), \quad (4.29)$$

where

$$a_p = (z_{p+1} - z_p)/2; \quad b_p = (z_{p+1} + z_p)/2; \quad (i = 1,2,\ldots,M); \quad (j = 1,2,\ldots,N = 4M). \quad (4.30)$$

The integral implied in the computation of B_c, of the following type

$$J_2 = \int_{-1}^{1} dx \int_{-1}^{1} dy G(x, y) \quad (4.31)$$

is computed with double Gauss-Legendre numerical quadrature

$$J_2 = \sum_{i=1}^{4M}\sum_{j=1}^{4M} w_i w_j G(x_i, x_j) = \sum_{i=1}^{4M} w_i [w_i G(x_i, x_i) + 2\sum_{j=i+1}^{4M} w_j G(x_i, x_j)], \quad (4.32)$$

where we have used the symmetry of the function to be integrated

$$G(x_i, x_j) = G(x_j, x_i). \quad (4.33)$$

In the same way, for the computation of B_n and B_Y one needs

$$J_3 = \int_{-1}^{1} dx \int_{-1}^{1} dy \int_{0}^{1} dz\, H(x,y,z)\,, \tag{4.34}$$

$$J_3 \simeq \sum_{i=1}^{4M} \sum_{j=1}^{4M} \sum_{k=1}^{L} w_i w_j u_k H(x_i, x_j, s_k) =$$

$$= \sum_{i=1}^{4M} w_i \left[w_i \sum_{k=1}^{L} u_k H(x_i, x_i, s_k) + 2 \sum_{j=i+1}^{4M} \sum_{k=1}^{L} w_j u_k H(x_i, x_j, s_k) \right], \tag{4.35}$$

where s_k and u_k are the abscissas and weights for L-order Gauss Legendre quadrature on the interval (0,1). The abscissas for angular quadrature in B_n and B_Y appears as $\sin(\phi/2)$ and $\cos\phi$; hence the functions $\sin(\pi s_i)$, $\cos(2\pi s_i)$ $(i = 1,2,\ldots,L)$ are computed only once for given L, and are transmitted through a COMMON statement to the subroutine for computation of B_s, B_c, B_n, or B_Y by (Poenaru and Ivaşcu 1978, Poenaru et al. 1980a).

The integrals (4.15), (4.19) and (4.25) are computed by Gauss-Legendre numerical quadrature with 4m.4m and 4m.4m.n mesh points, respectively. The variation of IBM 370/135 running time, T, with the time of mesh points n and m is presented in fig.3 (solid lines). On the same figure one can see that the CDC-6500 computer (dotted lines) is approximately two times faster. For most purposes n = m = 12 allow to obtain satisfactory small errors even for large deformations.

The three fold integrals in the eqs. for B_{n1}, B_{n2}, B_{n12} and B_{Y1}, B_{Y2}, B_{Y12} are computed by using the eq.(4.35) where the summation is performed over the following indices: ($i = 1,2,\ldots,K$; $j = 1,2,\ldots,K$; $k = 1,2,\ldots,L$) ($i = K+1,\ldots,4M$; $j = K+1,\ldots,4M$; $k = 1,2,\ldots,L$) and ($i = 1,2,\ldots,K$; $j = K+1,\ldots,4M$; $k = 1,2,\ldots,L$), respectively.

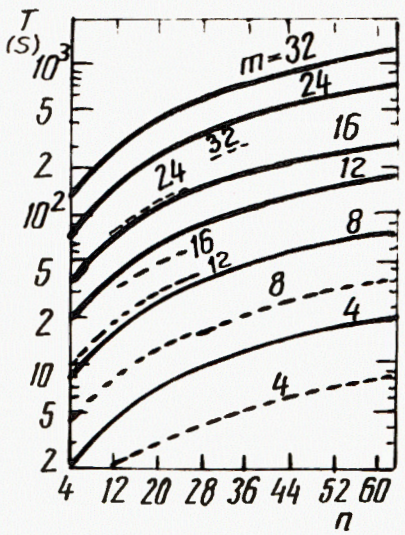

Fig.3. Variation of running time for one deformation set with the number of integration mesh point on IBM 370/135 (solid line) and CDC-6500 (dotted line) computers.

4.4.2. Reflection symmetric nuclei

If the nuclear shape has reflection symmetry, one can write:

$$x_{2M+i} = -x_{2M+1-i}\,; \quad w_{2M+i} = w_{2M+1-i} \qquad (i = 1,2,\ldots,2M) \tag{4.36}$$

and, consequently, the number of summation terms in eqs.(4.28) and (4.32) can be reduced. In fact, eqs.(4.28) and (4.32) become in this case:

$$J_1 \simeq 2 \sum_{i=1}^{2M} w_i F(x_i)\,, \tag{4.37}$$

$$J_2 \simeq 2 \sum_{i=1}^{2M} w_i \left(w_i G_{ii} + 2 \sum_{j=i+1}^{2M} w_j G_{ij} + \sum_{j=2M+1}^{4M} w_i G_{ij} \right), \tag{4.38}$$

where $G_{ij} \equiv G(x_i, x_j)$.

By using eq.(4.38) in place of eq.(4.32), the computation time for a given nuclear shape is reduced from 13.2 s to 9.5 s for M = 16; from 7.1 s to 5.3 s for M = 12; from 3.2 s to 2.5 s for M = 8 and from 0.88 s to 0.65 s for M = 4 (Poenaru and Ivaşcu 1979). The effective increase in computation speed is important because usually for potential energy surface (PES) one needs to consider many deformations.

4.5. Analytical Relationships

For spherical shapes we have already shown that simple analytical relationships are available, allowing to calculate in a short time the selfenergies in the framework of all models. In the following we would like to present briefly some other cases for which closed formulae are known to exist.

4.5.1. Self energy of a spheroid and ellipsoid

There are analytical relationships (Beringer and Knox 1961) for the LDM self-energy of a spheriodal nucleus with the semi-axes ratio $\eta = c/a$ (c is the semi-axis along the symmetry axis) and an excentricity $\epsilon = |1 - \eta^{-2}|^{1/2}$:

$$B_s = 0.5\,\eta^{-2/3} \left[1 + \begin{cases} \arcsin\epsilon/(1-\epsilon)]; & \eta > 1 \quad \text{(prolate)} \\ \ln(\epsilon + \eta^{-1})/(\epsilon\,\eta^{-1})]; & \eta < 1 \quad \text{(oblate)}\,, \end{cases} \right. \tag{4.39}$$

$$B_c = (0.5\,\eta^{-2/3}/\epsilon) \cdot \begin{cases} \ln(1+\epsilon)/(1-\epsilon); & \eta > 1 \\ 2\,\mathrm{arctg}\,\epsilon; & \eta < 1\,. \end{cases} \tag{4.40}$$

For an ellipsoid with semiaxes $c > b > a$ expressed in units of R_0, due to the volume conservation condition

$$abc = 1 \qquad (4.41)$$

there are only two independent deformation parameters; one choice can be $s \equiv c/a$, $r \equiv b/a$. In this case Carlson (1961) has found that

$$B_s = 0.5\{a^2 + \frac{b}{(c^2-a^2)^{1/2}}[(c^2-a^2)E(\phi,k_s) + a^2F(\phi,k_s)]\}, \qquad (4.42)$$

$$B_c = \frac{1}{(c^2-a^2)^{1/2}}F(\phi,k_c), \qquad (4.43)$$

where F and E are the generalized elliptic integrals of the first and second kind, respectively

$$F = \int_0^{\phi}(1-k^2\sin^2 t)^{-1/2}\,dt; \quad E = \int_0^{\phi}(1-k^2\sin^2 t)^{1/2}\,dt \qquad (4.44)$$

and

$$tg\phi = \sqrt{s^2-1}; \quad k_s^2 = \frac{1-r^{-2}}{1-s^{-2}}; \quad k_c^2 = \frac{s^2-r^2}{s^2-1} \qquad (4.45)$$

are the arguments of F and E.

4.5.2. Coulomb interaction energy of a spheroid with a sphere

After Cohen and Swiatecki (1962), the Coulomb interaction energy of a spheroid having the semiaxis (c, a) with a sphere of radius R_2 at a separation distance R between centers is given by:

$$E_c = Z_1Z_2e^2s(x)/R; \quad x^2 = |c^2-a^2|/R^2; \quad R \geq R_t \equiv c + R, \qquad (4.46)$$

where $e^2 = 1.4399764$ MeV.fm, and

$$s(x) = \begin{cases} 1; & c = a \\ 0.75\{(x-1/x)\ln[(1+x)/(1-x)] + 2\}/x^2; & c > a \\ 1.5[(x+1/x)\,\mathrm{arctg}(x) - 1]/x^2; & c < a \ \text{(oblate)} \end{cases} \qquad (4.47)$$

For $c = a$ one obtains the Coulomb interaction energy of the two spheres which is expressed as in case of two point charges separated by the distance R. In the overlapping region ($R < R_t$) the deformation dependent terms of the potential energy are calculated by using numerical methods.

4.5.3. Interaction energies between two spheres in FRNFM and Y+EM

At small distances $R - R_t \gtrsim 0$, in case of FRNFM and Y+EM, besides the electrostatic energy, there is also a nuclear interaction term due to finite range of nuclear forces. For separated spherical shapes, in the framework of FRNFM one has

$$E_d(R) = \frac{Z_1Z_2e^2}{R} - 4(\frac{a}{r_0})^2(c_{s1}c_{s2})^{1/2}\,g_1g_2\,\frac{\exp(-R/a)}{R/a}, \qquad (4.48)$$

where

$$g_k = (\frac{R_k}{a})\,ch(\frac{R_k}{a}) - sh(\frac{R_k}{a}) \qquad (k = 1,2). \qquad (4.49)$$

Similarly, in the Y+EM

$$E_d(R) = \frac{Z_1Z_2e^2}{R} - 4(\frac{a}{r_0})^2(c_{s1}c_{s2})^{1/2}[g_1g_2(4+\frac{R}{a}) - g_2f_1 - g_1f_2]\,\frac{\exp(-R/a)}{R/a}, \qquad (4.50)$$

where

$$f_k = (\frac{R_k}{a})^2\,sh(\frac{R_k}{a}). \qquad (4.51)$$

In order to find the separation distance R_M at which the interaction energy has its maximum, one has to find numerically the root of a nonlinear equation $dE_d/dR|_{R=R_M} = 0$, which can be put in the form

$$\begin{aligned} &e^x + p(x+1) = 0 \quad \text{for FRNFM} \\ &e^x + p_1 + x(p_1 + xp) = 0 \quad \text{for Y+EM}; \quad x = R/a, \end{aligned} \qquad (4.52)$$

where $p = -4\frac{a^3}{r_0^2}(c_{s1}c_{s2})^{1/2}\,\frac{g_1g_2}{e^2Z_1Z_2}$; $p_1 = p(4 - f_1/g_1 - f_2/g_2)$.

The first eq.(4.52) is solved by Newton iteration method refining the initial guess $x_0 = 1.5R_0/a$. Mueller iteration scheme of successive bisection and inverse parabolic interpolation in

the range of x from $x_t = R_t/t$ to $x_t + 5$, is used to find the solution of the second eq.(4.52).

4.6. Interaction Barriers. Q -Values and Fission Barriers

One can obtain some information concerning the fission and fusion phenomena, by studying the potential energy of a system of two spherical nuclei (Z_1, A_1), (Z_2, A_2) at the touching point $R_t = R_1 + R_2$ and infinite separation $R = \infty$, relative to the energy E° of a spherical compound nucleus (Z, A) (see fig.4).

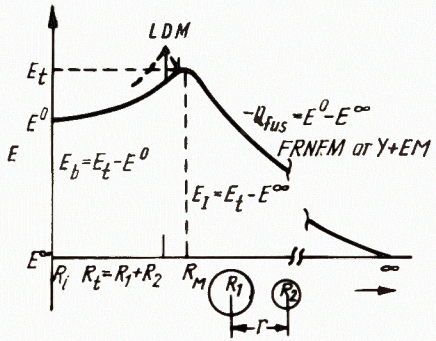

Fig.5. Charge asymmetry parameter η_Z and difference $\Delta\eta = \eta_A - \eta_Z$ between mass and charge asymmetry for nuclear combinations along the Green approximation for the line of beta stability.

Fig.4. Variation of potential energy of a system of two spherical nuclei with the separation distance between centers.

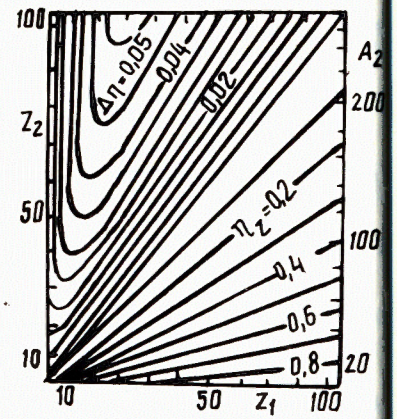

The interaction barrier, E_I, of two heavy ions is usually calculated in a very simple one dimensional parametrisation as the maximum of the interaction potential energy. For two spherical nuclei this maximum occurs at the touching point (LDM) or not far from it (FRNFM or Y+EM), as it is shown schematically in figure 4. In this parametrization E_b is a rough approximation of the fission barrier. In the LDM, E_I is simply the Coulomb interaction at the touching point, but in FRNFM or Y+EM, the interaction due to nuclear forces must be also taken into account.

The general trends in the variation of interaction barriers, fusion Q values and fission barriers for various projectile (Z_1) target (Z_2) combinations along the Green approximation for the line of beta stability can be found by computing the energies

E°, E_t, and E^∞ for the fused system, touching-point configuration and separated fragments.

Values for η_Z and $\Delta\eta = \eta_A - \eta_Z$ for these pairs of nuclei are plotted in figure 5. Due to the interchangeability of Z_1 and Z_2 we have used only half of the figure, from $Z_2 = 0$ to $Z_1 = Z_2$, for η_z and the other one, from $Z_1 = 0$ to $Z_1 = Z_2$, for $\Delta\eta$. One can see that for each target nucleus there is one projectile which gives the maximum of $\Delta\eta$. A similar trend can be expected for the influence of charge density differences on $E_I = E_t - E^\infty$ (figure 6(a),(a'),(a'')), $Q = E^\infty - E^\circ$ (figure 6(b),(b'),(b'')) and $E_b = E_t - E^\circ$ (figure 6(c),(c'),(c'')) for LDM, FRNFM and Y+EM.

At given pair (A_1, A_2) the interaction barrier in the case $\eta_Z \neq \eta_A$ is lower than for $\eta_Z = \eta_A$. For $\Delta\eta$ of the order of 0.05 $\Delta E_I = E_I(\eta_Z = \eta_A) - E_I$ is as high as - 30 MeV. This difference is due mainly to different values of Coulomb energies at the touching point.

A first approximation for a fusion reaction Q value (figure 6(b), (b'),(b'')) is obtained as a difference of deformation-dependent terms of potential energy. In order to get accurate values of Q, one has also to consider the other terms of a mass formula (surface diffuseness and exchange corrections, pairing and shell corrections, Wigner term, etc.). Nevertheless the approximation reproduces the general trend as one can see from figure 6(b),(b'),(b''). For light systems one has positive values of Q (energy release). The transition from positive to negative values of Q occurs at smaller Z in the FRNFM or Y+EM than in LDM. Due to partial compensation of the Coulomb energy by the volume (symmetry) energy at $R = R_i$, $|\Delta Q|$ is lower than $|\Delta E_I|$: 18 MeV for LDM, 10 MeV for FRNFM and 14 MeV for Y+EM compared with 30 MeV. Here $\Delta Q = Q(\eta_Z = \eta_A) - Q$.

E_b overestimates the fission barrier not only because the saddle-point shape is different from two spheres at the touching point, but also because the shell and pairing corrections were not taken into account. As one can see from figure 6(c), (c'),(c'') the region of nuclei stable against fission ($E_b > 0$) is larger than that predicted by more realistic calculations. In spite of these considerations, $\Delta E_b = E_b(\eta_Z = \eta_A) - E_b$ gives the order of magnitude of the difference in energy between the saddle-point energies of systems $(^{A_1}Z_a, {}^{A_2}Z_b)$ and $(^{A_1}Z_1, {}^{A_2}Z_2)$ respectively. For $\Delta\eta \simeq 0.05$, the FRNFM and Y+EM are more sensitive than LDM in this respect: - 20 MeV and -16 MeV compared with -12 MeV. The sign of E_b shows that except for shell effects there is no driving force towards different N/Z ratios in the two fission fragments, at least in case of neutron-deficient systems formed in heavy-ion reactions. In fission, PES for $\eta_Z \neq \eta_A$, are useful for the computation of charge distributions.

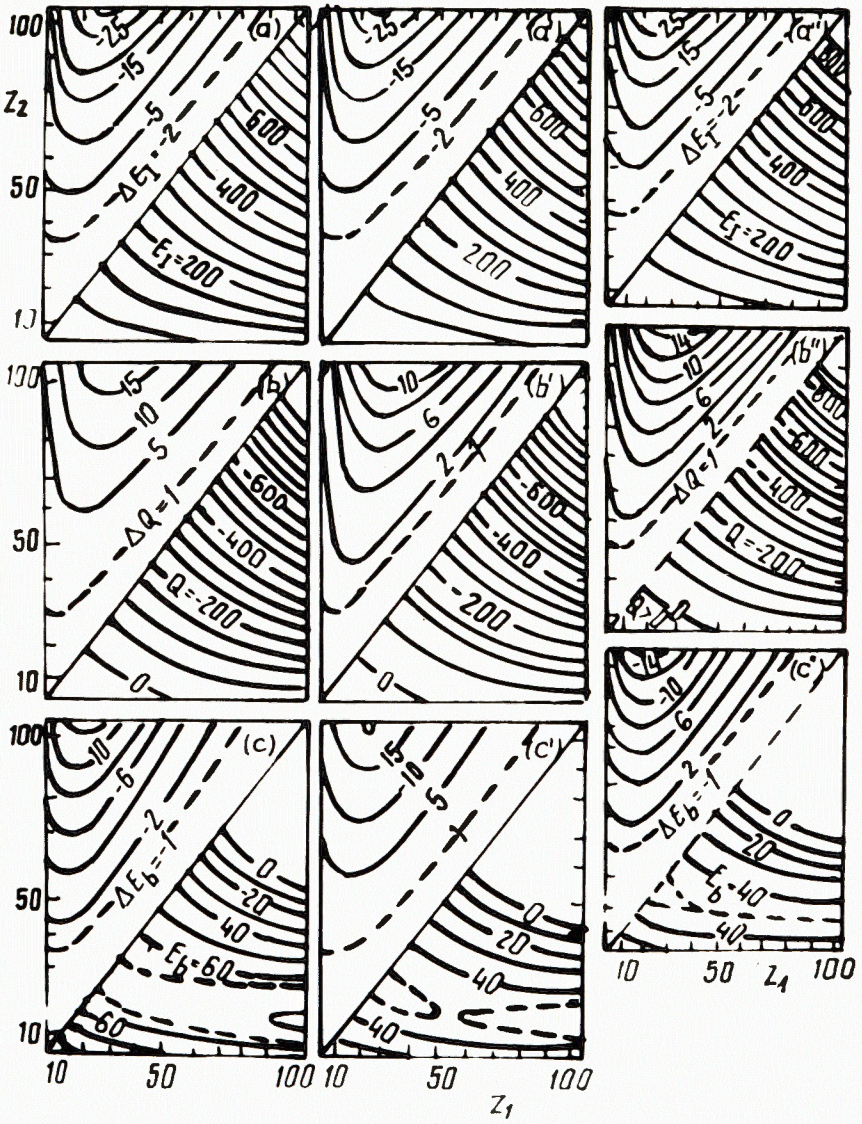

Fig.6. LDM, FRNFM and Y+EM interaction barriers ((a), (a'), (a'')), fusion reaction Q-values ((b), (b'), (b'')) and fusion barriers ((c), (c'), (c'')). The corresponding errors are obtained if the charge density difference is ignored. All energies are expressed in MeV.

Due to the fact that the charge equilibration process is very fast with respect to the fission time, it is important to take

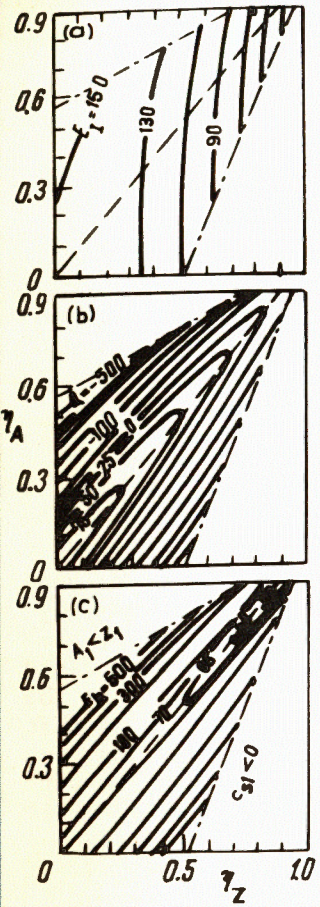

Fig.7. LDM interaction barriers (a), fusion Q-values (b) and fission barriers (c): trend of variation with mass and charge asymmetry for the ^{149}Tb composite system.

into account the charge density asymmetry particularly in the initial stages of fusion reactions. This is also interesting for the calculation of the charge distribution in fission (Gupta et al. 1975, Gupta 1977).

The influence of charge and mass asymmetries on the above-mentioned LDM quantities in the case of the ^{149}Tb composite system is shown in figure 7. Only a relatively narrow surface of the plane $\eta_A - \eta_Z$ has physical meaning. The frontiers of this surface (chain lines) could be set by the requirement $A_1 \geq Z_1$ (the upper limit) and $c_{s1} \geq 0$ (the lower limit). If $\eta_Z = \eta_A$ one follows the dotted lines: the interaction energy (figure 7(a)), fission Q-value $Q_{fis} = -Q_{fus}$ (figure 7(b)) and fission barrier (figure 7(c)) become smaller if the asymmetry is increased. The interaction energy is very sensitive to the charge asymmetry: for a given η, it increases when η_Z is decreased from $\eta_Z = \eta_A$ and decrease when

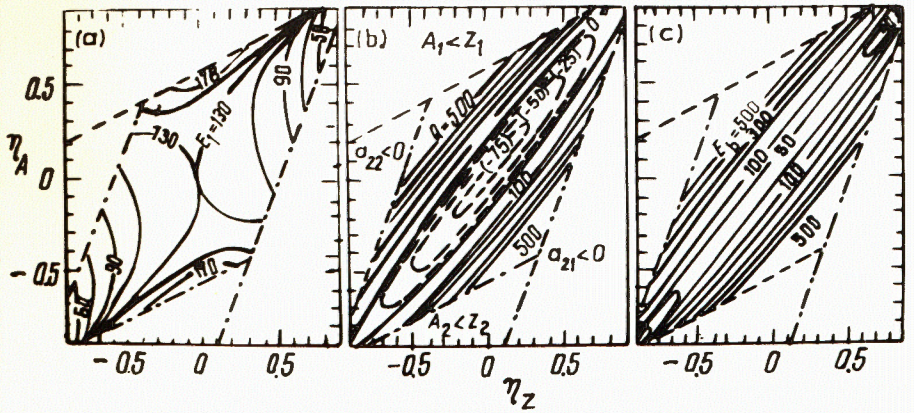

Fig.8. The same quantities as in fig.7, computed in the framework of Y+EM.

η_Z is increased. The fusion Q value and fission barrier are almost symmetric with respect to the line $\eta_Z = \eta_A$: both increase for $\Delta\eta > 0$ and $\Delta\eta < 0$. A similar trend shows the figure 8, displaying the results computed in the framework of Y+EM.

5. ALPHA DECAY AS A FISSION-LIKE PROCESS. NUMERICAL RESULTS

5.1. Nuclear Shape Parametrization

If a simple parametrization of the nuclear shape is used, one needs the numerical time consuming procedure only in the overlapping region of the two fragments; for the touching point configuration and the separated objects, one can get simple analytical relationships.

5.1.1. Spherical nuclei

The ground state shapes of the parent, daughter nuclei and of the alpha particle are approximated by spheres of radii R_0, R_1, and R_2, respectively. In an intermediate stage during the deformation process (see figure 9), the distance between centres is R. It increases from $R_i = R_0 - R_2$ to $R_t = R_{1f} + R_2$ at the touching point in such a way that R_2 is kept constant and the volume $V_1 + V_2$ is conserved. The surface equation $y(x)$, in cylindrical coordinates, with -1, +1 intercepts on the symmetry axis is

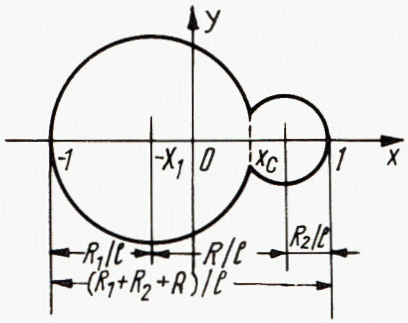

Fig.9. Spherical two centers parametrization of the nuclear surface.

$$y^2 = \begin{cases} R_1^2/\ell^2 - (x + x_1)^2, & x \le x_c \\ R_2^2/\ell^2 - (x + x_1 - R/\ell)^2, & x > x_c, \end{cases} \tag{5.1}$$

where $2\ell = R + R_1 + R_2$; $x_1 = (\ell - R_1)/\ell$, $x_c = z_c/\ell - x_1$. For a given deformation parameter, R, the position of the separation plane between fragments relative to the heavy fragment center, z_c, and the radius of the large fragment, R_1, are determined by solving iteratively the nonlinear system of eqs. expressing the matching and volume conservation conditions:

$$\begin{aligned} &R_1^2 - 2Rz_c + R^2 - R_2^2 = 0, \\ &2R_1^3 + 3R_1^2 z_c - 3R^2 z_c + 3(R^2 - R_2^2)z_c + R_2^2(2R_2 + 3R) - R^3 - 4 = 0, \end{aligned} \tag{5.2}$$

with a first guess $R_{10} = 1$; $z_{c0} = 0.5[(1 - R_2^2)/R + R]$. In this section all the lengths R, R_1, R_2 and z_c are expressed in units of R_0. We presume a proportionality between the fragment mass numbers A_1 and A_2 and their volumes V_1 and V_2. At the touching point $A_{1f} = A_1(R_t) = A - A_2 = A - 4$ and $A_{2f} = A_2(R_2) = 4$.

5.1.2. Deformed parent and daughter

For deformed nuclei, the ground state shapes of the parent and daughter nuclei are approximated by two spheroids of semiaxis a_0, c_0 and a_1, c_1, respectively (see fig.10) the ratio of which can be determined from tables of nuclear deformations (Seeger and Howard 1975)

$$\beta_0 \equiv c_0/a_0 = (1 + \alpha_{20} + \alpha_{40})/(1 - 0.5\alpha_{20} + 0.375\alpha_{40}). \tag{5.3}$$

One assumes a spherical shape with constant radius $R_2 = r_0 A_{2f}^{1/3}$ for the emitted particle. During the deformation process, the distance between centres, R, is increased from $R_i = c_0 - R_2$ to $R_t = c_1 + R_2$ at the touching point, then to ∞ in such a way that the volume is conserved and the ratio of semiaxis of the large fragment $\beta \equiv c/a$ is a linear extrapolation between the parent β_0 and daughter β_1 ratio:

$$\beta = \beta_0 - (\beta_0 - \beta_1)(R - R_i)/(R_t - R_i); \quad R_i \le R \le R_t. \tag{5.4}$$

In cylindrical coordinates (ρ, z) the surface equation is given by

$$\rho^2 = \begin{cases} a^2(1 - z^2/c^2), & z \le z_c \\ R_2^2 - (z - R)^2, & z > z_c. \end{cases} \tag{5.5}$$

Fig.10. Spheroid intersected with a sphere. (a) initial configuration; (b) intermediate position; (c) touching point.

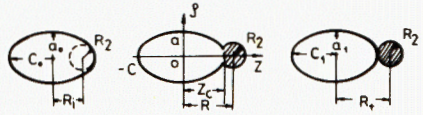

The volume conservation condition can be written as

$$4\pi R_0^3/3 = 4\pi a_0^2 c_0/3 = 4\pi(a_1^2 c_1 + R_2^3)/3 = V_1 + V_2, \tag{5.6}$$

where $R_0 = r_0 A^{1/3}$ and

$$3V_1/\pi = c^2[2c + z_c(3 - z_c^2/c^2)]/\beta^2 \ ,$$
$$3V_2/\pi = z_c^2 - 3Rz_c^2 + 3(R^2 - R_2^2)z_c + R_2^2(2R_2 + 3R) - R^3 \ . \qquad (5.7)$$

We presume a proportionality between the fragment mass numbers A_1 and A_2 (at the touching point A_{1f} and A_{2f}) and their volumes V_1 and V_2. From the matching condition at the separation plane $z = z_c$, we get:

$$c^2 - z_c^2 = \beta^2[R_2^2 - (z_c - R)^2] \ . \qquad (5.8)$$

In this way, for a given value of one independent deformation parameter R, the geometry of the systems is perfectly determined. The two unknown quantities $x \equiv c$ and $y \equiv z_c$ are the simultaneous solutions of the following nonlinear system of eqs.:

$$x^2 + (\beta^2 - 1)y^2 - 2R\beta^2 y + \beta^2(R^2 - R_2^2) = 0 \ ,$$
$$2x^3 + 3x^2y + (\beta^2 - 1)y^3 - 3R\beta^2y^2 + 3(R^2 - R_2^2)\beta^2 y + \beta^2[R_2^2(2R + 3R) - R^3 - 4R_0^3] = 0 \ . \qquad (5.9)$$

This can be solved by refining an initial guess

$$y_0 = c_1 \ ; \ x_0 = \{y_0^2 + \beta^2[R_2^2 - (y_0 - R)^2]\}^{1/2} \qquad (5.10)$$

with the Newton iteration numerical method.

5.2. Variation of the Charge Density

From heavy ion collision studies it is known that the charge density equilibration process is very fast. Hence, the charge densities of the two fragments are considered to be the same until $R = R_7 = R_i + 0.7(R_t - R_i)$; then the charge number Z_2 of the small fragment increases linearly with R up to $Z_{2f} = 2$.

$$Z_2 = Z_{27} + (Z_{2f} - Z_{27})(R - R_7)7/[3(R_7 - R_i)], \quad R \geq R_7 \ . \qquad (5.11)$$

As we mentioned above only deformation dependent terms are taken into account when the macroscopic potential energy is calculated. In the LDM, FRNFM and Y+EM, one has:

$$E_d(R) = E_{LD}(R) - E_{LD}(\infty); \ E_d(R) = E_{FR}(R) - E_{FR}(\infty), \ E_d(R) = E_{Y+E}(R) - E_{Y+E}(\infty), \qquad (5.12)$$

where the potential $E(\infty) = E_1 + E_2$ of the two fragments at infinite separation distance $(R \to \infty)$ is the origin of the energy.

5.3. Fission Q-Values

For $R = R_1$ one obtains the macroscopic model deformation dependent part Q-value of the fission reaction

$$E_d(R)|_{R=R_i} = Q_d \ . \qquad (5.13)$$

This quantity is different from experimental value Q_{exp} because the ground state deformations of the parent and daughter nuclei could not be reproduced by the chosen parametrization, other terms of a macroscopic model mass formula were ignored and the shell correction energy δE was not yet introduced.

For each of the three models mentioned above, one has

$$Q_{exp} = Q = M - (M_1 + M_2) = Q_M + \delta Q; \ \delta Q = \delta E - (\delta E_1 + \delta E_2) \ , \qquad (5.14)$$

where Q_M is the contribution of the macroscopic model terms of the mass formula and δQ is the shell correction part.

If $Q_{exp} < 0$ for a particular nucleus, it is stable with respect to the spontaneous emission of an alpha particle. This is the case of the light - and most of the neutron excess nuclei far off the line of beta stability. The Q-values contour lines for even-even nuclei with Z and N protons and neutrons are given in figure 11. The dashed area corresponds to nuclei with experimentally measured masses tabulated by Wapstra and Bos (1977). Calculated values using the code kindly supplied by Dr.Jänecke (1980), the results of various authors (Maripuu 1976) and the Myers-Swiatecki (1967) mass formula for spherical shapes are used beyond this area.

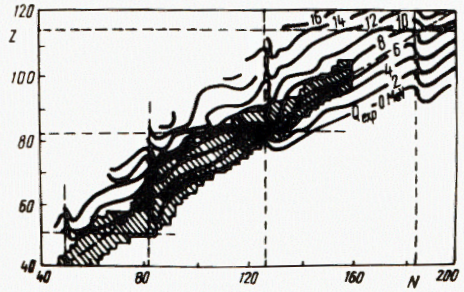

Fig.11. Contour maps of the alpha decay Q_{exp} -value for even-even nuclei with Z protons and N neutrons.

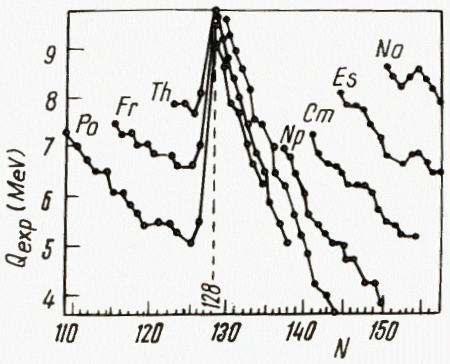

Fig.12. Q_{exp}-value systematics of some alpha emitters.

The point-dotted curve is the Green approximation of the line of beta stability. From this figure one can see the general trend of increased alpha instability toward neutron deficient and heavy nuclei, well explained by the macroscopic part of the mass formula and the important variation from magic parent to magic daughter nuclei, due to the strong increase of the shell effects δQ.

The pronounced instability corresponding to the daughter nuclei with magic neutron number ($N - 2 = 126$) is more transparent from the figure 12.

For a given nucleus (let's say ^{248}Cm) it is interesting to see other possible very asymmetric spontaneous fission activities in competition with alpha decay. As is shown in figure 13 the neighbouring nuclei are not emitted spontaneously because the corresponding processes have negative Q-values, but for emission of many other nuclei with $N_2 Z_2 \geq 4$, ^{248}Cm has $Q > 0$.

The shell effects, δQ favouring the alpha decay of this nucleus with respect to that of its neighbours are presented in figure 14. These were computed with the Myers-Swiatecki (1966) formula, for spherical nuclei, eq.(5.15)). At each of the double shell closure ($N_2 = Z_2 = 2, 8$ and 14 on figure 14), δQ has a maxumum value (3,7 and 12 MeV, respectively). In spite of the increased Q for ^{16}O and ^{28}Si in comparison with ^{4}He, the emission of these clusters (Sandulescu et al.1980) is strongly hindered with respect to the alpha decay. One has to consider also the macroscopic model contribution to the fission barrier, the vibration frequency and the inertial mass parameters, playing an important part in this competition. The delta-function-like mass and charge distributions in this region of asymmetry are due to the fact that the asymmetric fission leading to a light fragment different from ^{4}He is not possible ($Q < 0$) or has a very low probability (10^{-9} for ^{14}C than α).

The barrier shapes for this very asymmetric fission will be plotted in figure 19. The barrier height E_b is given by $E_b = E_d(R_m) - Q = E_I - Q$. For the same nuclei as in figure 12, we have plotted in figure 15a the LDM touching point interaction energy $E_i = E_d(R_t)$, in figure 15b the shell effects δQ, and in figure 15c the barrier heights $E_b = E_i - Q_{exp}$. The figure 15c is almost the figure 12 with the upside down, because E_i is a smoothly varying quantity. The pronounced reduction of the barrier height for the magic neutron number due to the steep variation of δQ (figure 15b) is very clear in figure 15c.

5.4. Shell Corrections

Usually the macroscopic-microscopic method (Brack et al. 1972) is applied to heavy nuclei. For instance the mass table of Seeger and Howard (1975) refers to $Z, N \geq 22$ and that of

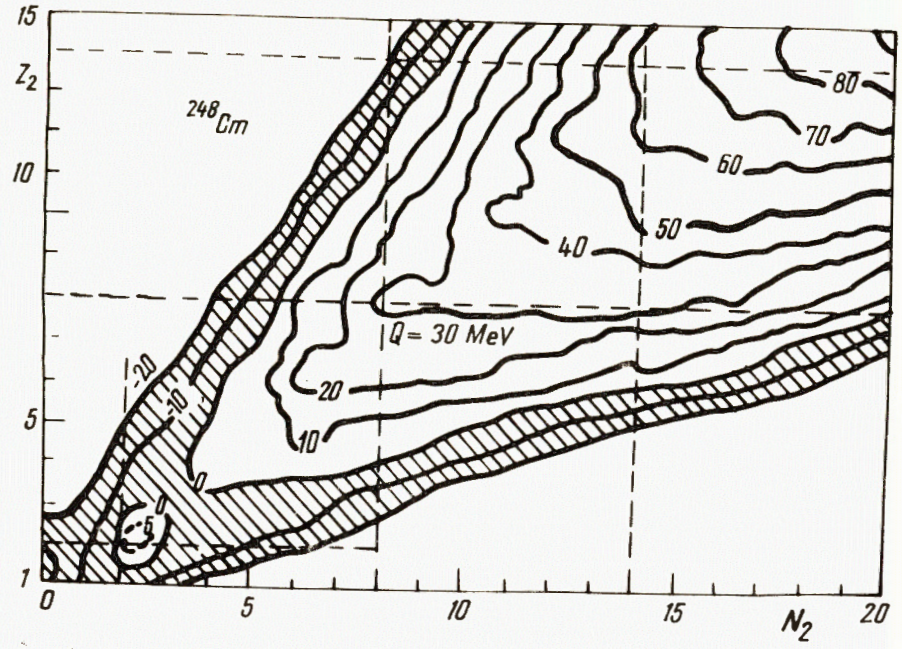

Fig.13. Contour maps of the Q-values for various asymmetric splitting of the ^{248}Cm nucleus.

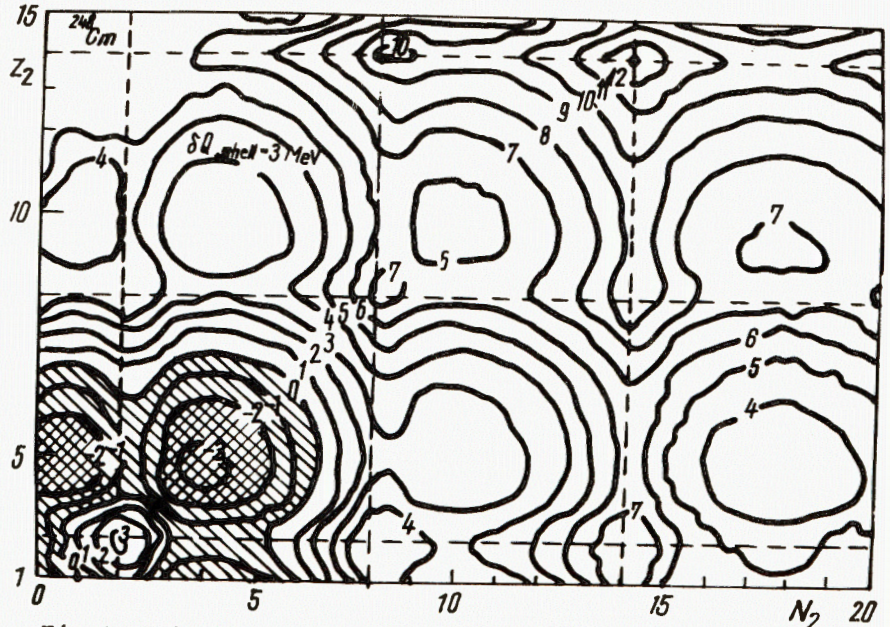

Fig.14. Shell effect contribution δQ to the Q-values for the same processes as in fig.13.

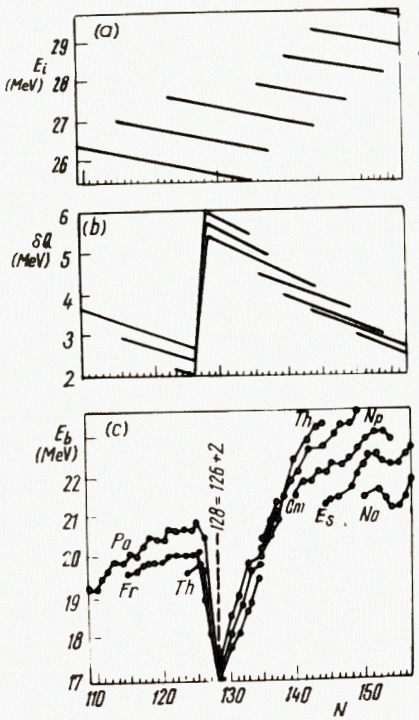

Fig.15. Interaction barriers (a), shell effects (b) and fission barriers (c) for alpha decay of the same nuclei as in figure 12.

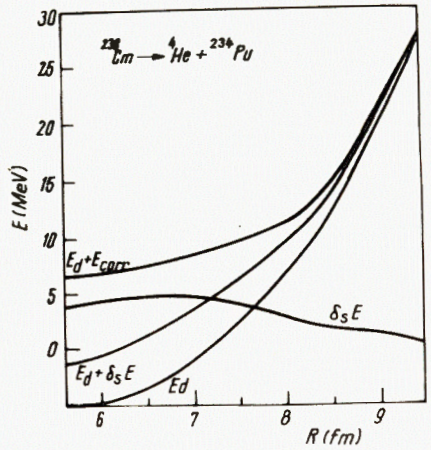

Fig.16. The rising part of the LDM, Schultheis's shell corrections and total fission barrier for the alpha decay of ^{238}Cm.

Möller and Nix (1981) to Z,N $\geq$ 8. The Strutinsky prescription for light nuclei or for very large mass-asymmetry was not yet developed. Nevertheless, one can use a phenomenological shell correction method sometimes called cluster prescription, extending for large deformations the Myers-Swiatecki (1977) formula for the g.s. of spherical nuclei:

$$S(N,Z) = C\{[F(N) + F(Z)]/(0.6A)^{2/3} - cA^{1/3}\},$$
$$F(m) = 0.6[(N_i^{5/3} - N_{i-1}^{5/3})(m - N_{i-1})/(N_i - N_{i-1}) - m^{5/3} + N_{i-1}^{5/3}], \qquad (5.15)$$

where $m \in (N_{i-1}, N_i)$; N_i are the spherical magic numbers N,Z = 2,8, 14, 28, 50, 82; N = 126, 184; Z = 114, and the parameters C = 5.8 MeV; c = 0.325. This eq. was used to calculate δE, δE_1, δE_2 and δQ plotted in figure 14 and fig.15b. According to Schultheis and Schultheis (1973), the damping terms of the Myers-Swiatecki shell correction formula for deformed nuclei, were replaced by a curvature-dependent integration usually performed numerically:

$$\delta S = \frac{C}{4\pi r_0^2 A^{4/3}} \int k\{[F(N/k^3) + F(Z/k^3)]2^{2/3} k^3 - cA\}d\sigma, \qquad (5.16)$$

where

$$k = 2R_0\left(\frac{1-a}{\mathcal{R}_1+\mathcal{R}_2} + \frac{a}{|S|}\int\frac{d\sigma}{\mathcal{R}_1+\mathcal{R}_2}\right);\ a = 0.7\ , \qquad (5.17)$$

$\mathcal{R}_1$, $\mathcal{R}_2$ are the curvature radii and $|S|$ is the surface area. For two intersected spheres (Schultheis et al. 1970) one has a simple formula:

$$\delta S(R) = S(N_1,Z_1)\frac{2\pi R_1(R_1+z_c)}{4\pi R_1^2} + S(N_2,Z_2)\frac{2\pi R_2(R-z_c+R_2)}{4\pi R_2^2}\ . \qquad (5.18)$$

During the deformation, the variation of R induces the variation of z_c, R_1, V_1, V_2, A_1, A_2 and consequently of Z_1, N_1, Z_2 and N_2. Each time when one of the nucleon numbers reaches a magic number, the correction energy has a minimum (negative value) and it has a maximum at mid-shell number.

For alpha decay, the variation of the fission fragment nucleon numbers during the deformation from $R = R_i$ to $R = R_t$ is as low as 2 units at all. Hence the shell correction energy is a smooth function of R (see figure 16).

By assuming that the top of the barrier is not affected by the shell correction, which agree with experimental data on fusion interaction barriers (Poenaru et al. 1979d) the shell correction

$$\delta_s E(R) = \delta S(R) - \delta S(R_t)\ , \qquad (5.19)$$

when added to the deformation energy E_d of the LDM, rises the theoretical Q_d-values of the heavy nuclei with 3-6 MeV. In spite of this improvement, there still remains a smoothly varying shift mentioned above. In order to reproduce the experimental Q-value exactly, we have introduced a phenomenological correction energy $E_{corr}(R)$, containing both the shell correction and the smooth shift:

$$E(R) = E_d(R) + E_{corr}(R);\ E_{corr}(R) = Q_{corr}[1 - V_2(R)/V_{2f}];\ Q_{corr} = Q_{exp} - Q_d. \qquad (5.20)$$

where $V_{2f} = V_2(R_t)$ is the alpha particle volume. It seems reasonable to scale the shell correction with $V_2(R)/V_{2f}$, by relating its variation to the bulk properties of the nascent alpha fragment. Another choice could be the ratio $S_2(R)/S_{2f}$ of the surface area of the small fragment to $S_{2f} = S_2(R_t)$, or the ratio $(R - R_i)/(R_t - R_i)$ as shown in figure 17 for the example of ^{222}Ra. A best choice for the scaling parameters S_2 and R (Poenaru et al. 1979b) have yield a negligible difference of $\log T(S_2)$ and $\log T(R)$ with respect to $\log T(V_2)$, so we decided to use the eq.(5.20).

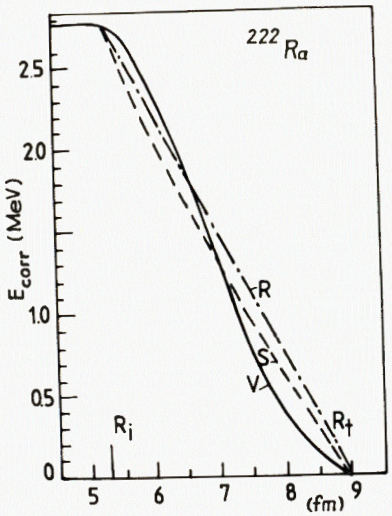

Fig.17. Variation of the ^{222}Ra correction energy for volume (V), surface (S) and separation distance (R) scaling parameters in case of Y+EM.

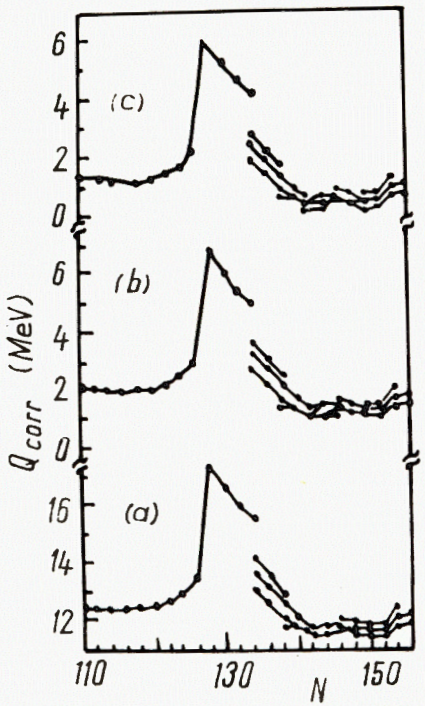

Fig.18. Correction energies vs neutron number N of parent nucleus for various alpha emitters (Po, Ra, Th, U, Pu, Cm, Cf, Fm and No); a - LDM, b - FRNFM; c - Y+EM.

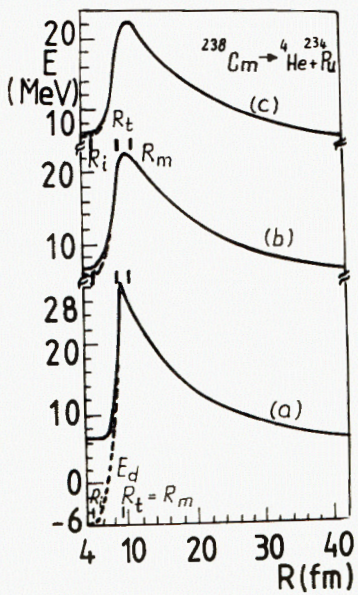

Fig.19. Barrier shapes for the alpha decay of ^{238}Cm, without (broken curve) and with (full curve) shell correction. a - LDM; b - FRNFM; c - Y+EM.

The experimental corrections Q_{corr} defined by eq. (5.20) are plotted in figure 18a for the LDM, in figure 18b for the FRNFM and in figure 18c for the Y+EM. As was expected, the very strong shell effects at the magic neutron number in the daughter nucleus are the same, but the deformation dependent part Q_d of the Y+EM and FRNFM give a good approximation of the alpha Q-values. On the other hand LDM, giving a large error for the alpha particle mass leads to large discrepancies (even negative Q_d-values).

5.5. Barrier Shape

The corrections of the barrier for the alpha decay of non-magic nuclei are very small in the framework of FRNFM and Y+EM. As an example in figure 19 the barrier shapes for the alpha decay of ^{238}Cm are shown. The LDM (a), FRNFM (b) and Y+EM (c) potential energies without (broken lines) and with (full line) corrections are plotted. As we have mentioned in the preceeding section, one can see that in the last two models $R_m > R_t$. In the LDM, $R_m = R_t$; the top of the barrier is very sharp and higher in energy. Due to the different values of the radius constant r_0 the initial separation distance R_i (in fm) is also different from model to model.

5.6. Alpha Decay Lifetime of Heavy and Superheavy Nuclei

After replacement of numerical values of the parameters, from eqs.(2.3) and (2.4), one obtains:

$$T = \frac{1.4333 \times 10^{-21}}{E_{vib}} \exp\left(0.4239 \int_{R_a}^{R_b} \{\mu_A(R)[E(R) - Q']\}^{\frac{1}{2}} dR\right), \qquad (5.21)$$

where T is expressed in s; R, R_a and R_b in fm; E_{vib}, E and Q' in MeV. The penetrability integral is computed by Gauss-Legendre numerical quadrature, dividing the whole range (R_a, R_b) in two subintervals (R_a, R_m) and (R_m, R_b). For $R \in (R_i, R_t)$ the potential energy E(R) is calculated numerically, hence the lower limit of the integral, R_a, the solution of the eq. $E(R_a) = Q'$ in this interval, is found by a searching computer code. The upper limit, R_b, is given by the Coulomb interaction energy: $R_b = Z_1 Z_2 e^2/Q$, because the nuclear interaction term is vanishingly small at large distances.

For the mass parameter $\mu_A(R) \equiv \mu(R)/m$, where m is the nucleon mass, we have tried three kinds of variations: 1) the instantaneous reduced mass

$$\mu_i(R) = A_1(R) A_2(R)/A, \qquad (5.22)$$

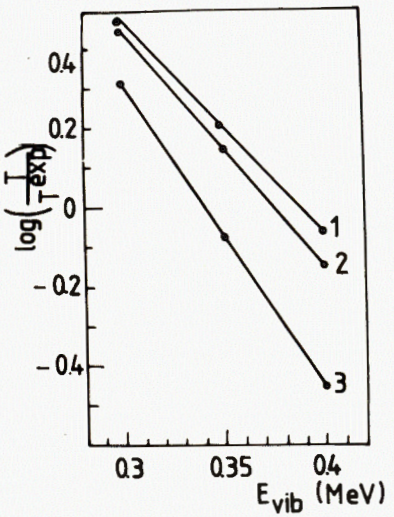

Fig.20. Half-life sensitivity to the variation of zero point vibration energy. 1 - ^{230}Th; 2 - ^{248}Cf; 3 - ^{252}No.

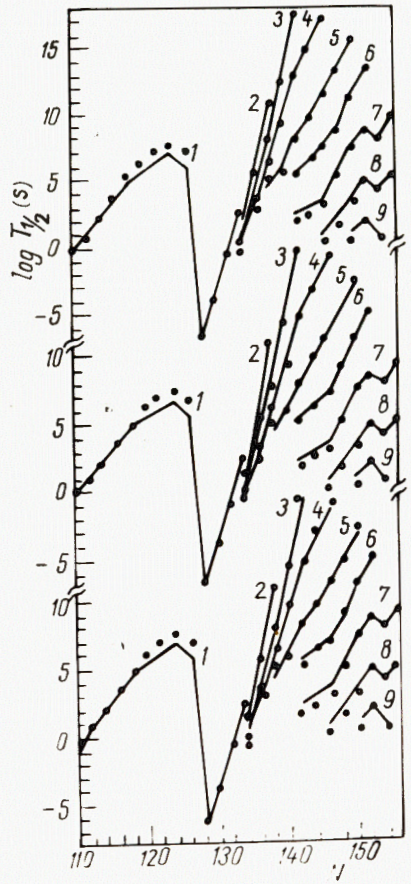

Fig.21. Experimental (points) and theoretical (lines) alpha decay half-lives for the same even-even nuclei as in figure 18. a - LDM; b - FRNFM; c - Y+EM. 1 - Po; 2 - Ra; 3 - Th; 4 - U ; 5 - Pu; 6 - Cm; 7 - Cf; 8 - Fm; 9 - No.

which is an increasing function of R; 2) the final reduced mass

$$\mu_f(R) = A_{1f} A_{2f}/A = 4(A-4)/A = \text{const}. \qquad (5.23)$$

and 3) the semiempirical relationship suggested by Randrup et al. (1973) for the almost symmetrical fission

$$\mu_s(R) = \mu_f[1 + 7.37 \exp(-2.452\frac{R-R_i}{R_t-R_i})] . \qquad (5.24)$$

The zero point vibration energy E_{vib} was adjusted for each time: 0.37 MeV for μ_i; 0.4 MeV for μ_f and 0.63 MeV for μ_s in the LDM. The difference between the maximum and minimum value of $\log(T/T_{exp})$ for the seven isotopes of U is a good measure

of the deviation of theoretical values from the experimental ones. This is practically the same (1.4 and 1.5) for μ_i and μ_f but much higher (2.2) for μ_s. Hence we decided to use for the moment the simple law of μ_f.

As one can see from figure 20, on the example of ^{230}Th (1), ^{248}Cf (2) and ^{252}No (3), the half-life is very sensitive to the variation of E_{vib}. In order to obtain a good overall fit with experimental data, following values of E_{vib} = 0.37; 0.37 and 0.30 MeV were chosen for LDM, FRNFM and Y+EM respectively, with μ_i.

5.6.1. Heavy nuclei

Experimental half-lives (heavy points) after Rytz (1979) and Nuclear Data Sheets (vol.5, no.3 and 6; vol.6, no.4; vol.7, no.2 and vol.8, no.2) are used in figure 21. By comparing this, with figure 15c, one can see an almost identical trend, revealing the importance of the barrier height in this process. The good agreement with experimental data of the theoretical lifetimes irrespective of the model used for the macroscopic energy E_d, in the range of T of 24 orders of magnitude, suggests that the alpha decay process could be interpreted as a fission phenomenon. This conclusion is also supported by the fact that a new semiempirical relationship (Poenaru et al.1980b, 1982, Poenaru and Ivaşcu 1983 a) for $T_{½}(Q)$, derived on the basis of fission theory of alpha decay, gives the best agreement with experimental data. In the following we will use the LDM, by exploiting the advantage of its simplicity.

When compared with other theories of alpha decay, these computations are faster and more accurate. To calculate the lifetime for one nucleus, the IBM 370/135 computer running time is of the order of 45 s for LDM and 2m 20 s for FRNFM or Y+EM.

5.6.2. Superheavy nuclei

On the basis of our method one can predict reliable values of the alpha decay lifetimes in the new region of nuclei including the superheavies. Alpha disintegration of these nuclei is particularly important because in many cases it puts a limit of the survival.

As an example we have studied (Poenaru et al.1981) the even-even isotopes of the elements with Z = 106-120 and N = 172-190, where there are no experimental data. In order to have a complete systematic trend of variation with N between 110 and 190 (see fig.22) the isotopes of the element 104 with N = 154-190 have been also considered. The Q-values for correction energy

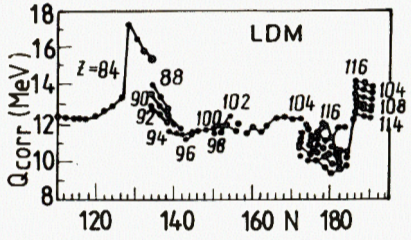

Fig.22. Correction energies vs neutron number of parent nucleus for alpha emitters including superheavies.

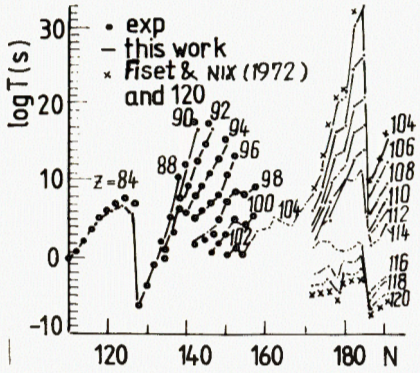

Fig.23. Alpha decay half-lives of some heavy and superheavy even-even nuclei.

were taken from Fiset and Nix (1972). As it is seen on the fig.22, the shell effects of the daughter nuclei with magic number of neutrons, for which N = 128 and 186, induces a steep increase of the Q_{corr}. The same thing happens at the magic proton number 114 (Z = 116).

A corresponding increase of the decay probability is shown in fig.23. One can see that nuclei with Z > 114 decay particularly faster. For some isotopes of the elements 104, 106 and 108 we predict lower half-lives than Fiset and Nix (1972), but in general the present results are more optimistic: about an order of magnitude larger. When other competing modes of decay (fission and beta decay) are also taken into account, the nucleus $^{294}110$ has the longest calculated total half-life. Of course the centrifugal barrier (Möller and Aberg 1980) can change drastically the situation.

5.7. Transitions between Deformed Ground States and Fission Isomers Alpha Decay

5.7.1. Transitions between ground states

In section 5.6. the g.s. nuclear deformations of the parent and daughter nuclei (Seeger and Howard 1975) was not taken into consideration explicitly; it was introduced only through the experimental Q-value in the correction energy. The parametrization of a spheroid intersected with a sphere, presented in section 5.1.2. (Poenaru and Ivascu 1981b) is able to consider the deformations and at the same time preserves the ad-

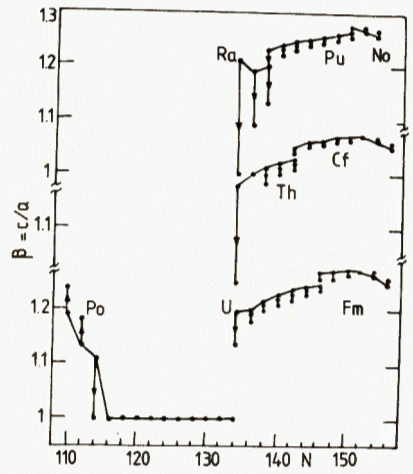

Fig.24. Nuclear deformations of some parent and daughter even-even nuclei.

Fig.25. Nuclear deformation contribution to the alpha decay Q-values.

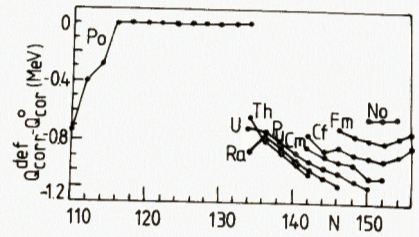

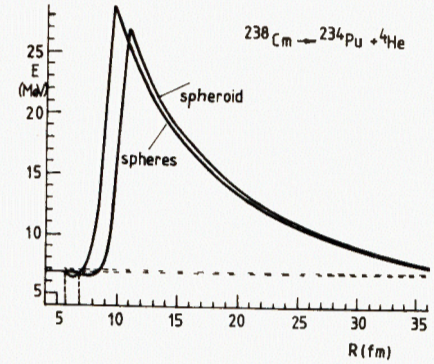

Fig.26. Influence of the deformation on LDM barrier shape for the alpha decay of ^{238}Cm.

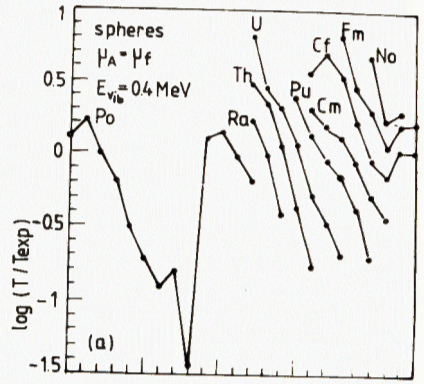

Fig.27. Residual discrepancies between the theoretical and experimental life-times without deformation (a) and with deformation (b) taken into account.

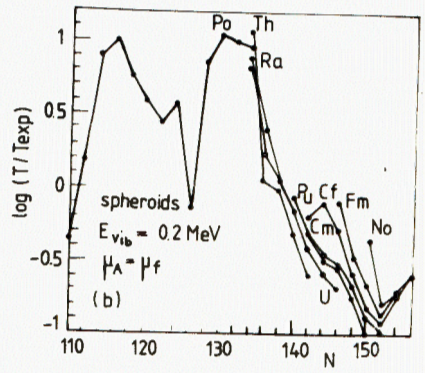

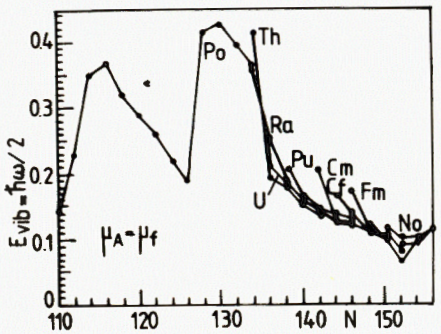

Fig.28. Zero point vibration energy of some spherical and deformed nuclei.

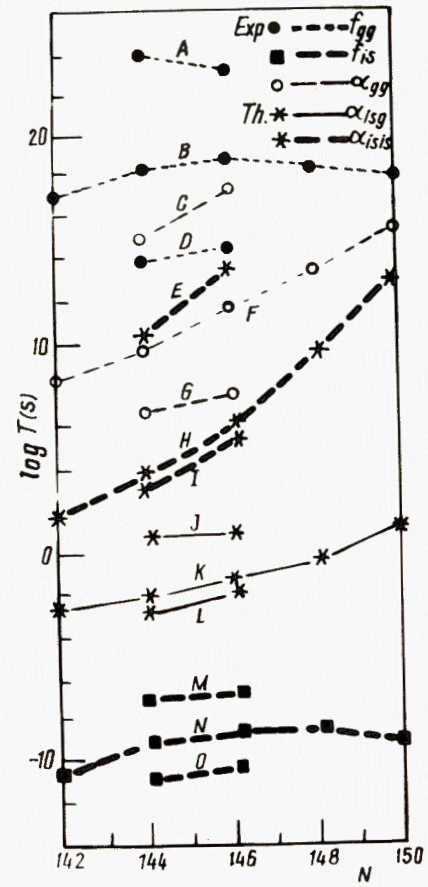

Fig.29. Half-lives for some fission (f) and alpha decay (a) processes for the ground state and shape isomeric states of some U (curves A, C, E, J and M), Pu (curves B, F, H, K and N) and Cm (curves D, G, I, L and O) even-N isotopes.

vantage of the analytical relationship for $E_d(R)$, in the LDM, when the fragments are separated ($R \geq R_t$).

The spheroidal deformation β of some even-even parent and daughter nuclei, calculated with the eq.(5.3) from the quadrupole and hexadecapole deformation parameters α_2 and α_4 (Seeger and Howard 1975) are plotted in fig.24. The arrows directed from the parents to the daughters (which are displayed at the same N as the parents).

Due to the deformation, Q_d increases, improving the agreement with experimental values. The reduction of the Q_{corr} with 0.6-1.2 MeV is clearly seen in fig.25.

Because of the increase of R_t, the LDM barrier height (fig.26) and consequently the zero point vibration energy are

now smaller (E_{vib} = 0.2 MeV for the case of constant reduced mass μ_f).

Another interesting effect is illustrated in fig.27 where an enlarged view of the residual discrepancies is displayed, without (a) or with (b) deformations taken into account. It is obvious that the dependence on Z of the discrepancies are greatly reduced in the presence of deformation. This is an argument that the neutron shell effects shadow the proton ones in this region. The same conclusion can be drawn from the figure 28 where the individual zero-point vibration energy of each nucleus, determined from the condition $T = T_{exp}$ were plotted, assuming a constant inertial mass parameter $\mu_A = \mu_f$.

5.7.2. Alpha decay of fission isomers

The parametrization of a spheroid for the parent and daughter nuclei and of a sphere for alpha fragment allowed us to study the alpha transition $\alpha_{is\,g}$ from a shape isomeric state (Vandenbosch 1977, Poenaru 1977, Metag et al.1980) of a parent nucleus to the ground state of the daughter. In this case

$$Q_{is\,g} = Q_{gg} + E_{IIp}\ , \qquad (5.25)$$

where E_{IIp} is the fission isomer excitation energy (Britt 1973, Ivaşcu and Poenaru 1981) of the parent nucleus and Q_{gg} is the Q-value for the alpha decay between ground states (called Q_{exp} above). The shape isomeric state has a large deformation $\beta_p \simeq 2$ (Bjørnholm and Lynn 1980), but the ground state deformation of the daughter nucleus is of the order of $\beta_d = 1.24$.

The results obtained for the known even N isotopes of U, Pu and Cm are plotted in fig.29. On the same figure one can see the measured lifetime for the decay by spontaneous fission from the isomeric state f_{is}. This process is much faster. The branching ratio for the alpha decay is lower than 10^{-8} - a figure which explains why the alpha particles of the fission isomers could not be found experimentally (Leachman and Erkkila 1966, Belov et al. 1973).

Another type of alpha transition $\alpha_{is\,is}$ between the shape isomeric states of the parent and daughter nuclei, has a lower Q-value

$$Q_{is\,is} = Q_{is\,g} - E_{II\,d} = Q_{gg} + (E_{IIp} - E_{IId}) \qquad (5.26)$$

and the shape of the daughter nucleus is also well deformed $\beta_d \simeq 2$. As it is shown in fig.29, the probability of this process is at least 5 orders of magnitude lower than that of $\alpha_{is\,g}$.

The measured lifetime of other processes occurring in these nuclei are drawn in fig.29: the spontaneous fission of the

ground state F_{gg} and the gs-gs alpha decay a_{gg}. For low neutron number the alpha decay dominates, but for large N values the fission process competition became stronger and stronger.

6. TIME DEPENDENT HARTREE-FOCK STUDY OF ALPHA DECAY

It was shown (Sandulescu et al.1983) that in TDHF approximation, the collision of an alpha particle with a lead nucleus leads to nuclear dynamical effects during the capture process and to periodic oscillations of the compound system. The oscillations were interpreted as zero point motions associated with the alpha decay collective mode. The computed frequency corresponds exactly with the experimentally deduced value based on the alpha decay description as a fission process.

6.1. The Model

It is known that in the time-dependent Hartree-Fock (TDHF) approximation only a very limited set of physical quantities can reasonably be compared with the experiment. Up to now, the contact with experiment was restricted to the fusion cross sections and to the gross behaviour of the Wilcynski plots.

Recently Weiss (1981) has suggested that the TDHF-approximation may include also some high energy collective excitations of the residual nuclei after a grazing collision. It was shown that the high frequency structures of the Fourier transform of the Cartesian moments of the density of the residual nuclei for several moments are correlated. This may explain the observed bumps in the cross section versus the final kinetic energy for different species in the system $^{40}Ca + ^{40}Ca$ at E_{lab} = 100 MeV (Roynette et al. 1981). From these calculations it is not clear if the frequency components represent nonlinearity effects, multiple phonon or primary collective excitations.

In the following we present the results of a study in the TDHF approximation of another collective mode, which cannot be simply described by multipole expansion of the surface, the collective mode associated with alpha decay. In order to excite such a collective mode, the central collision of an alpha particle with a lead nucleus at relative kinetic energy just above the Coulomb barrier, was considered.

The calculation has been done, due to the extremely large asymmetry of the considered system, only in two dimensions and using the advanced array processing techniques. A simplified Skyrme plus Yukawa interaction was used, the small Coulomb exchange correction energy was neglected and no spin-orbit interaction was included. The effective charge quartet model with

the filling approximation for the outermost shells (Cusson et al. 1980, Stöcker et al.1980), has been used.

6.2. Alpha Decay Collective Mode

The process was computer over a long period of time (3.315 fm/c). From the total number of the pictures taken in steps of 19.5 fm/c only few were selected, which were considered to be characteristic for the alpha decay process.

In fig.30, the first 10 shapes which illustrate the capture of the alpha particle by the lead nucleus have been plotted. It is evident that if we assume that the emission process is just the capture process reflected in time, the alpha decay process implies many dynamical effects, like the polarization of the heavy nucleus in the vicinity of the alpha particle and the formation of a long neck before the alpha particle is emitted.

In the usual description of alpha decay, based on the R-matrix theory of nuclear reactions, these dynamical effects are neglected. The barrier is considered to be a one-body process

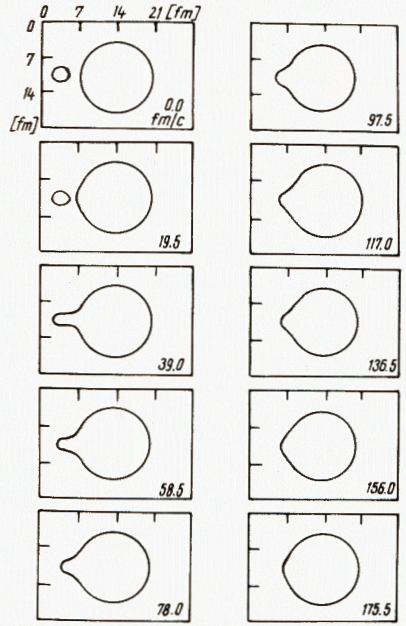

Fig.30. The capture of an alpha particle by the ^{208}Pb nucleus illustrated in time-steps of 19.5 fm/c.

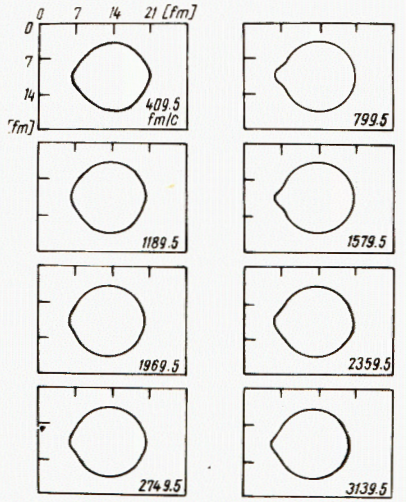

Fig.31. The shapes which appear periodically in the time evolution of the compound system ^{212}Po.

and the alpha reduced widths are evaluated in the one-center shell model.

From the TDHF calculations it was concluded that the whole process looks like a fission process. This gives a full support of the theory of alpha decay as a fission process based on the liquid drop model with phenomenological shell corrections (Poenaru et al. 1979a).

The dynamical effects suggested by the TDHF description of alpha decay, i.e., the modification of the self consistent field during the emission process have been recently taken into account by evaluating the alpha reduced widths in a very asymmetric two-center shell model. Comparatively to the one-center shell model, the asymmetric two-center shell model amplifies the single particle wave functions at the surface of the nucleus. Consequently the absolute values of the alpha reduced widths are increased. This increase may possibly explain the well-known theoretical underestimation of the alpha reduced widths, in the frame of R-matrix description of alpha decay, at least with two orders of magnitude.

After the capture process, the compound system has quite complicated shape oscillations. Looking at the time evolution of these shapes we can see clearly some shapes which appear periodically. First the compound system reaches a more or less symmetric shape, similar with a sphere with two bumps on the opposite sides and second an asymmetric shape which can be approximately described by a sphere with only one bump on the side on which the two partners come first in contact. These shapes which appear periodically with a half period $T/2 = 780$ fm/c $= 2.6 \cdot 10^{-21}$ s are given in fig.31.

These oscillations have been interpreted as zero point oscillations of the collective mode associated with alpha decay $E_{vib} = \hbar\omega/2 = 0.4$ MeV. We should like to stress that this value $E_{vib} = 0.4$ MeV corresponds exactly with the experimentally deduced value based on the description of alpha decay as a fission process (Poenaru et al. 1979a).

7. SEMIEMPIRICAL FORMULAE FOR ALPHA DECAY HALF-LIVES

During the last few years, the number of the known alpha emitters have been increased mainly by measuring the activity of the new neutron deficient nuclei produced in heavy ion reaction (Gauvin et al.1975, Cabot et al. 1978, Hagberg et al.1979, Hofmann et al. 1979, Ritchie et al. 1981, Schmidt et al.1979). A new island of alpha activity in the neighbourhood of the double magic nucleus ^{100}Sn was studied (Schardt et al.1979,1981).

Alpha decay competes usually with fission and beta decay in the disintegration of heaviest nuclei synthesized up to now

(Bemis et al. 1981) and it is expected to be frequently met in the superheavy region (Nix 1972).

As far back as 1911, Geiger and Nuttall have found a simple dependence of the alpha decay partial half-life, T, on the alpha particle range in air. Now the disintegration period can be estimated, if the kinetic energy of the emitted particle, E_α, is known, by using semiempirical relationships (Fröman 1957, Wapstra et al. 1959, Taagepera and Nurmia 1961, Viola and Seaborg 1966, Keller and Münzel 1972, Hornshoj et al.1974). Some of these formulae were derived only for a limited region of the parent proton and neutron numbers Z and N. Their parameters have been determined by fitting a given set of experimental data selected by the authors from the available measurements on large collectivity of even-even, even-odd and odd-odd nuclides.

Since then the precision of some measurements was increased and new alpha emitters were discovered. This process of improving both the quality and the quantity of data will continue in the future. Consequently it is interesting to have from time to time the possibility of changing some of the parameter values. In the following it will be shown that a better agreement with experimental results can be obtained by requiring a vanishing mean value of the absolute errors for each group of nuclei, leading to new parameters $\{C_k\}$ of the various formulae presented below.

In an attempt to improve the description of data even in the neighbourhood of the magic neutron and proton numbers, where the errors of the other relationships are large, a new formula with six parameters $\{B_k\}$, based on the fission theory of alpha decay have been derived (Poenaru et al. 1980b, Poenaru and Ivascu 1983a). This formula takes into consideration explicitly not only the dependence on the proton number, but also on the neutron number and their difference from magicity. A corresponding computer program (Poenaru et al.1982) allows us to improve automatically the parameters $\{C_k\}$ and $\{B_k\}$ mentioned above, every time a better set of experimental data is available (Poenaru and Ivascu 1984b).

7.1. A Basic Set of Experimental Data on the Strong Alpha Transitions

Our set of 376 data Q, T on the most probable (ground state to ground state or favoured) alpha transitions of 123 even-even, 111 even-odd, 83 odd-even and 59 odd-odd nuclei, is presented elsewhere (Poenaru and Ivascu 1983b). They are selected to meet in each of the four groups, the criteria of best fitting the systematics of Q-value, logT, of the quantity

χ_{exp} defined below, versus neutron number and the Geiger-Nuttall plot.

From these data, the parameters of our formula were obtained. Many of the alpha active nuclei have also other competing decay modes (beta decay, spontaneous fission, etc.), hence the partial alpha life time represents only a fraction, given by branching ratio, b_α, of the total disintegration period, T_t. From all the alpha transitions, we have selected the strongest ones: ground state to ground state transitions in even-even nuclei and the so-called favoured transitions in the odd-odd and odd-mass nuclei. The ratio of the intensity of this alpha line to the total alpha strength will be called i_p in the following. Consequently, the partial decay lifetime, T_α, of the most probable alpha transition is given by

$$T_\alpha = \frac{100}{b_\alpha} \cdot \frac{100}{i_p} T_t \ , \qquad (7.1)$$

where b_α and i_p are expressed in percent.

The released energy, Q, is related to the alpha particle kinetic energy, E_α, by the relationship

$$Q = E_\alpha A/A_d \ , \qquad (7.2)$$

where A and $A_d = A - 4$ are the mass numbers of the parent and daughter nucleus, respectively. For alpha transitions from the ground state of the parent nucleus to the ground state of the daughter, Q is given by the mass difference $Q = M(A, Z) - M(4,2) - M(A_d, Z_d)$; otherwise (for favoured transitions) one has to add also the difference of the excitation energies.

Except a small number of cases (some isotopes of Te, Xe, I, Cs, Hf, Ta, Os, Ir, and No), for the energy release in alpha decay, the Q-values - derived from the masses of nuclei tabulated by Wapstra and Bos (1977) were used. Some authors (Perlman and Rasmussen 1957, Keller and Münzel 1972) take into consideration a small term, ΔE_s, due to the electronic shielding

$$\Delta E_s = (85.3Z^{7/5} - 80Z^{2/5})\, 10^{-6} \text{ MeV}. \qquad (7.3)$$

They use an effective Q-value $Q_{eff} = Q + \Delta E_s$. The contribution of this term is only of the order of 15-30 keV. For a semiempirical relationship the complication introduced is not justified by an improvement of the agreement with experimental data. Consequently this term will be ignored in the following.

Informations concerning the quantities T_t, b_α and i_p of the eq.(7.1) were compiled by Rytz (1979). Our basic set of experimental data was selected from these tables and from the pub-

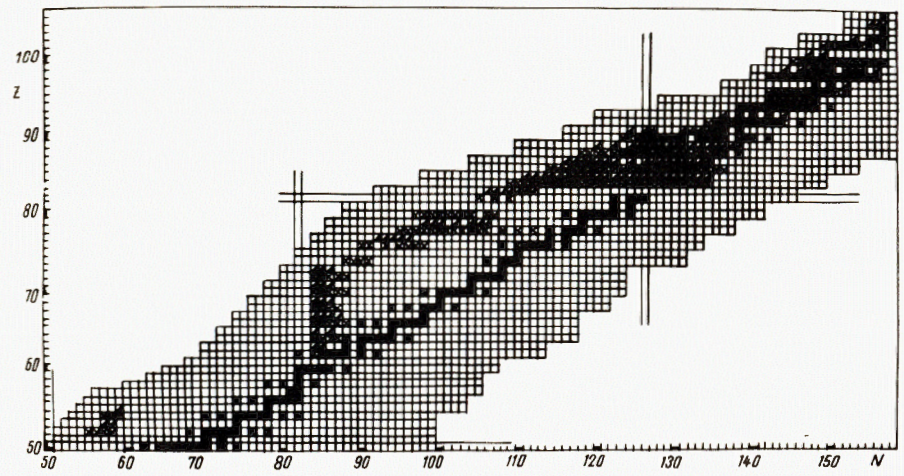

Fig.32. Selected alpha emitters ,(▣. ▣) and beta-stable nuclei. (■).

lications by Gauvin et al. (1975), Gorbachev et al. (1975), Cabot et al. (1978), Lederer and Shirley (1978), Hagberg et al. (1979), Hofmann et al. (1979), Schardt et al. (1979) and Schmidt et al. (1979). As the range of lifetimes of different nuclides extends over many orders of magnitude, it is more practical to use the decimal logarithm logT. The experimental values of T will be denoted by T_{exp}. Unlike the mass tables (Wapstra and Bos 1977), presenting only one value for a given nucleus, usually for a given transition there are many measurements of the quantities T_t, b_α and i_p, different from each other.

In each of the four groups of nuclides: even-even, even-odd, odd-even, and odd-odd, our selection was guided by the criteria of the best matching in the general trend of the following four systematics: Q, $\log T_\alpha$, χ_{exp} versus neutron number, N, and $\log T_\alpha$ versus $1/\sqrt{Q}$.

The quantity χ_{exp} is derived (Poenaru and Ivascu 1980) below from the experimental value $\log T_\alpha$ and the calculated K_S value.

The position of the selected alpha emitters in a N-Z system of coordinates, is shown in Fig.32 where the beta stable nuclei are marked with heavy squares. One can see that the majority of the alpha radioactive nuclei are neutron deficient.

The systematics of Q, $\log T_\alpha$ and χ_{exp} quantities versus the neutron number, N, for even-even nuclei, are shown in Fig.33a,b and c, respectively. For Q values between 2 and 9.8 MeV, the alpha disintegration lifetime variation extends over 30 orders

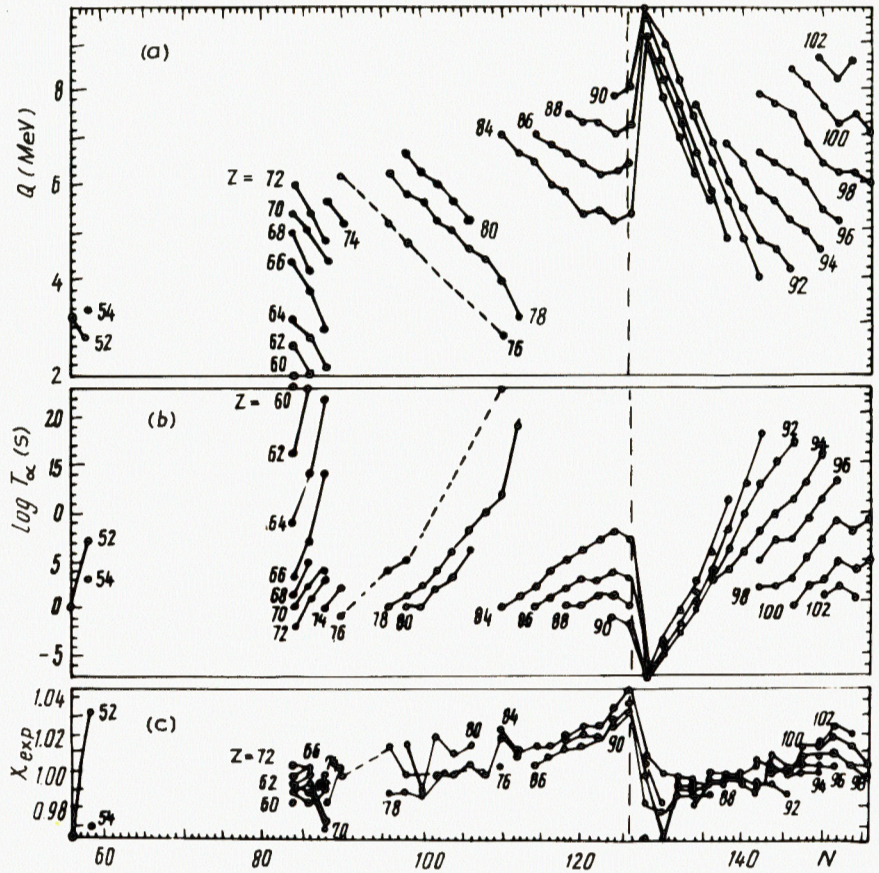

Fig.33. Systematics of Q *(a),* $\log T_\alpha$ *(b) and* χ_{exp} *(c) values of the even-even basic set of nuclei.*

of magnitude (from 10^{-7} to 10^{23}s) but χ_{exp} is only slightly different from unity; it ranges from 0.965 to 1.045.

The most unstable nuclides toward alpha emission have 128 neutrons leading to the magic neutron number of the daughter nucleus, but the maximum value of χ_{exp} corresponds to N = 126.

For various isotopes of Po, Rn, and Ra (Z = 84, 86, 88) the approach of the magic neutron number of the daughter nucleus N_d = 126 (N = 128) is felt beginning with N = 126, as the half-life for N = 126 (see Fig.33b) is lower than that for N = 124, but a dramatic decrease is noted when N is increased from 126 to 128. The Cf, Fm, and No (Z = 98, 100,102) isotopes show a discontinuity for N = 154 due to the subshell closure at N_d= 152.

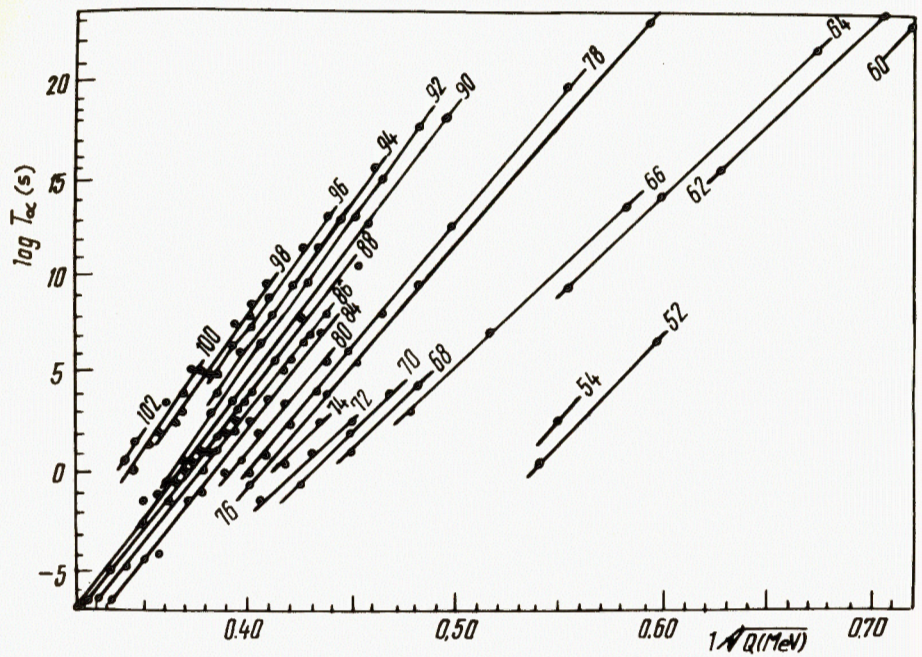

Fig.34. Geiger-Nuttall plot for even-even nuclei.

A Geiger-Nuttall plot for the same nuclei can be seen in Fig.34. Some of the points which deviate from the straight line systematics of the other isotopes of a given nucleus are connected with a short thin line with their common curve.

The figures similar with Fig.33 and 34 for even-odd, odd-even abd odd-odd nuclei and the detailed tables of experimentally determined quantities of our set of nuclei, are given by Poenaru and Ivaşcu (1983b).

7.2. New Additive Parameters of the Known Formulae

The formula given by Fröman (1957)

$$\log T = [139.8 + 1.83(Z-90) + 0.012(Z-90)^2]/\sqrt{Q} - 0.3(Z-90) - 0.001(Z-90)^2 + C_F \qquad (7.4)$$

is limited to the region of even-even nuclei with $Z \geq 84$. Q-values are expressed in MeV and T in seconds throughout this work. Consequently some additive parameter "old" values in table 1 could be different from the original if the author has used other units for T (years or minutes).

Table 1

Additive constants ($-c_i$) of semiempirical relationships

i	e - e		e - o		o - e		o - o	
	old	new	old	new	old	new	old	new
F	52.3	52.224	52.3	51.863	52.3	51.751	52.3	51.336
W	53	52.421	53	51.992	53	51.986	53	51.524
T	21.02	20.789	20.86	20.346	20.64	20.470	20.33	19.758
V	0	0.043	-1.066	-0.339	-0.772	-0.196	-1.114	-0.962
K	22.5	20.226	20.5	20.383	20.7	20.643	20.8	20.571
H	20.279	20.347	20.279	19.922	20.279	20.051	20.279	19.355

Almost all parameters $\{C_k\}$ are negative. Hence the values $-C_k$ are given in table 1. The original parameter value is called "old" and the new one is obtained from the condition that the mean value of the absolute error $(1/n)\sum_{i=1}^{n}\log(T_i/T_{i\,exp})$ vanishes in each group of the nuclei mentioned above. All diagrams presented in this section (except Fig.40a) are computed by using these new values.

The formula (7.4) gives a very good agreement with experimental data for $N \geq 128$, but for the new region of nuclei produced in heavy ion reactions, the errors as high as 5 orders of magnitude are obtained (Poenaru et al. 1984b), because the eq.(7.4) was not designed for lighter nuclei.

A better overall result, though the dispersion for heavy nuclei is larger, gives a very simple relationship of Wapstra et al. (1959).

$$\log T = (1.2Z + 34.9)/\sqrt{Q} + C_w \qquad (7.5)$$

also valid for even-even nuclei with $Z \geq 85$. This time the maximum error affects $Z = 60$ nucleus, not $Z = 52$ as in the preceding case.

In figure 35 the half-life of the even-even nuclei calculated with various equations is compared with the experimental one. To aid the eye, the consecutive isotopes of a given element are connected with a segment of line; a dashed line is used if one or more isotopes of a sequence are missing. From $N = 60$ to 82 there is a gap of stable nuclides toward alpha decay, or emitters undiscovered yet. Up to now only a few components of the new island of alpha activity, close to the double magic ^{100}Sn, have been found.

As can be seen from figure 35a, the formula presented by Taagepera and Nurmia (1961)

$$\log T = 1.61(Z_d/\sqrt{E_\alpha} - Z_d^{2/3}) + C_T\,, \qquad (7.6)$$

where $Z_d = Z - 2$ is the atomic number of the daughter nucleus, and C_T was allowed to vary in different groups of nuclei, remains one of the best; it is practically exceeded (Fig.35b) only by a new variant (Keller and Münzel 1972)

$$\log T = K_2(Z_d/\sqrt{Q} - Z_d^{2/3}) + C_k\,, \qquad (7.7)$$

where $H_K = 1.61$ for even-even (e-e); 1.65 for even-odd (e-o); 1.66 for odd-even (o-e) and 1.77 for odd-odd (o-o) nuclei.

The equation presented by Viola and Seaborg (1966) is of the form

$$\log T = (a_1 Z - a_2)/\sqrt{Q} - b_1 Z - b_2 + C_V\,, \qquad (7.8)$$

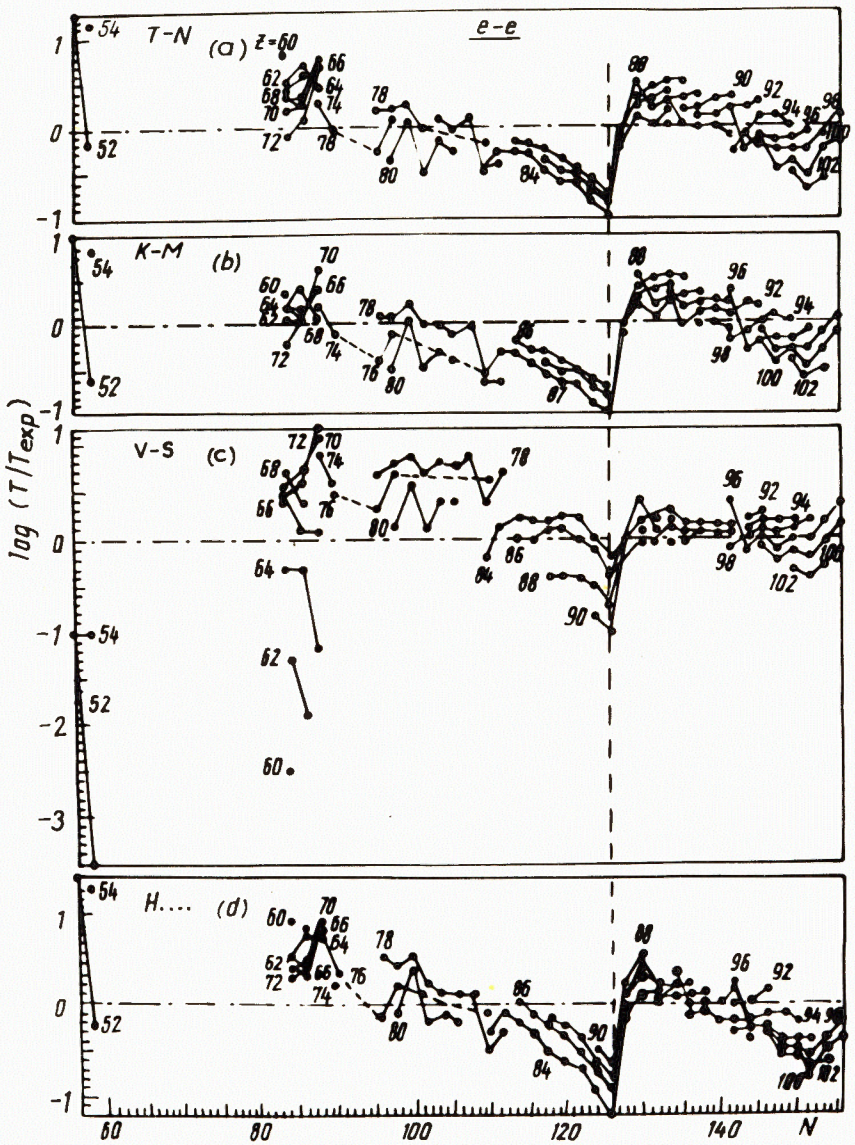

Fig.35. The errors of life-time predictions with Taagepera-Nurmia's (a), Keller-Münzel's (b), Viola-Seaborg's (c) and Hamshøj et al. (d) formula for even-even nuclei.

where $a_1 = 2.42151$; $a_2 = 62.3848$; $b_1 = 0.59015$; $b_2 = 4.2109$ for $N < 126$ and $a_1 = 2.11329$; $a_2 = 48.9879$; $b_1 = 0.39004$; $b_2 = 16.9543$ for $N > 126$, $Z > 82$. It gives excellent agreement in the region of actinides with $N > 128$, but as it can be seen from figure 35c for even-even nuclei it underestimates the lifetime of lighter nuclei in contrast with the overestimates of the eq.(7.4).

Hornshøj et al. (1974) have proposed the formula

$$\log T = 0.80307\left(\frac{A_d^{4/3} Z_d}{A}\right)^{1/2}\left(\frac{\arccos\sqrt{x}}{\sqrt{x}} - \sqrt{1-x}\right) + C_H \qquad (7.9)$$

in which $x = 0.538243\, Q A_d^{1/3}/Z_d$ and C_H is not changed in various groups of nuclei, like C_F of eq.(7.4) and C_W of eq. (7.5).

In spite of the strong influence of the neutron shell effects, in eqs. (7.4)-(7.9), mainly the Z dependence was stressed. From figure 35 (except the region of low Z up to 72 in figure 35c), one can see that for e-e nuclei in all equations a good enough dependence on Z was chosen, because at a given Z the spread of the results for various Z is not very large.

The dispersion of results for o-e, e-o and o-o (fig.36) nuclei is larger. In all cases one has a large negative peak at N = 126 or 127 which is approximately of one order of magnitude for o-e nuclei, but around 2 order of magnitude for e-o and 5 for o-o. In fig.36 there are very pronounced negative errors (-5.6; -5.2; -6.4 and -5.8 orders of magnitude) for Z = 83 N = 127. The fact that the neighbourhood of the magic number of nucleons is very badly described by all these formulae, is attested by the presence of the negative peaks in figures 35 and 36.

7.3. New Formula Based on Approximation of the Potential Barrier Penetrability

By applying the phenomenological fission theory with a Myers-Swiatecki's (1967) variant of the liquid drop model to the alpha decay, it was shown (Poenaru et al.1979a) that the potential barrier, for the split of a particular parent nucleus in its daughter and an alpha particle, is of the shape shown in figure 37, where $E' = Q + E_{vib}$ and E_{vib} is the zero point vibration frequency. For $E_{vib} = 0.4$ MeV one has

$$T = 3.58 \times 10^{-21} \exp(K) \qquad (7.10)$$

and the WKB formula of penetrability leads to the eq.(2.4) for the action integral K.

By choosing two intervals of integration (R_a, R_t) and (R_t, R_b), the action integral is split in two terms $K = K_i' + K_s'$ corresponding to the overlapping and to separated fragments,

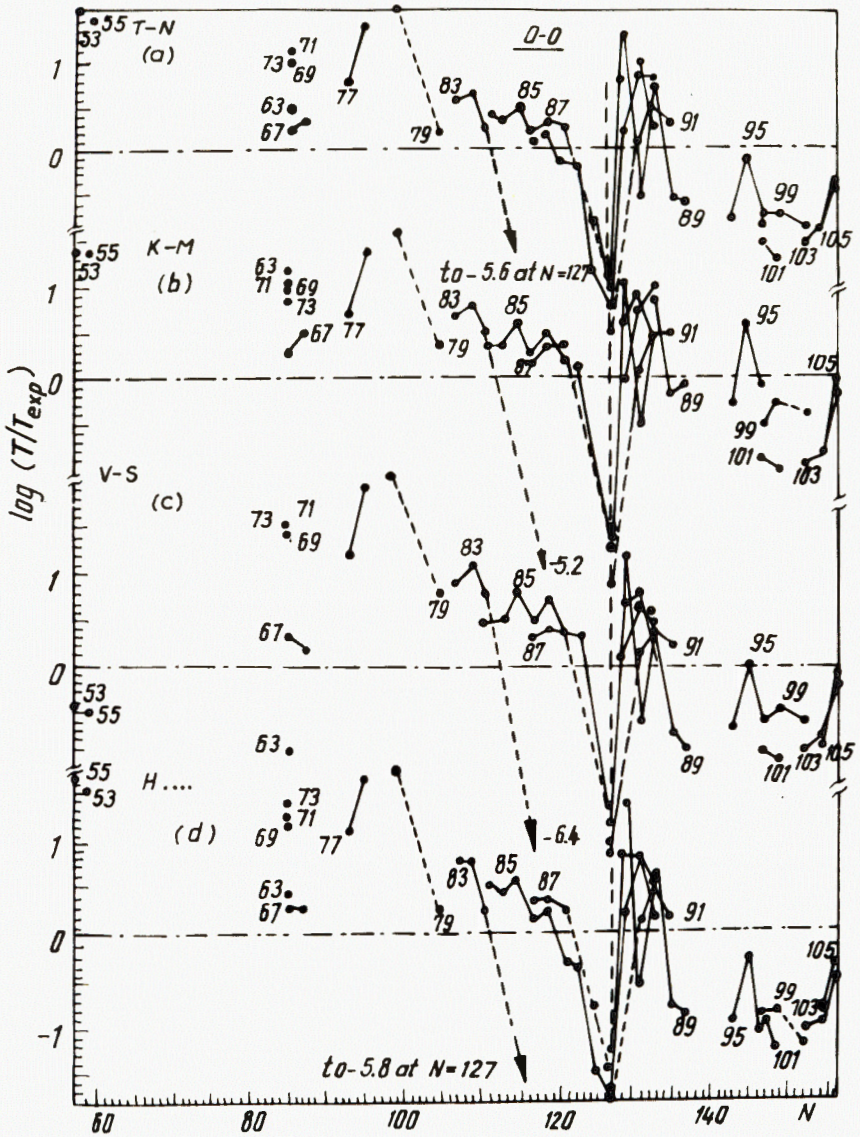

Fig.36. The same as in figure 35 for odd-odd nuclei.

respectively. The main contribution, K'_s, comes from the separated fragments, where the potential energy is the Coulomb interaction

$$E(R) = \frac{2Z_d e^2}{R}, \quad R \geq R_t = R_d + R_\alpha \qquad (7.11)$$

Fig.37. The barrier shape for alpha decay.

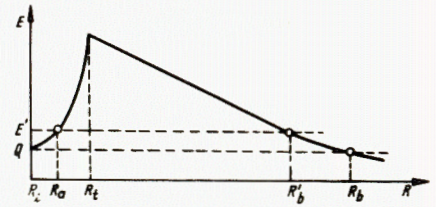

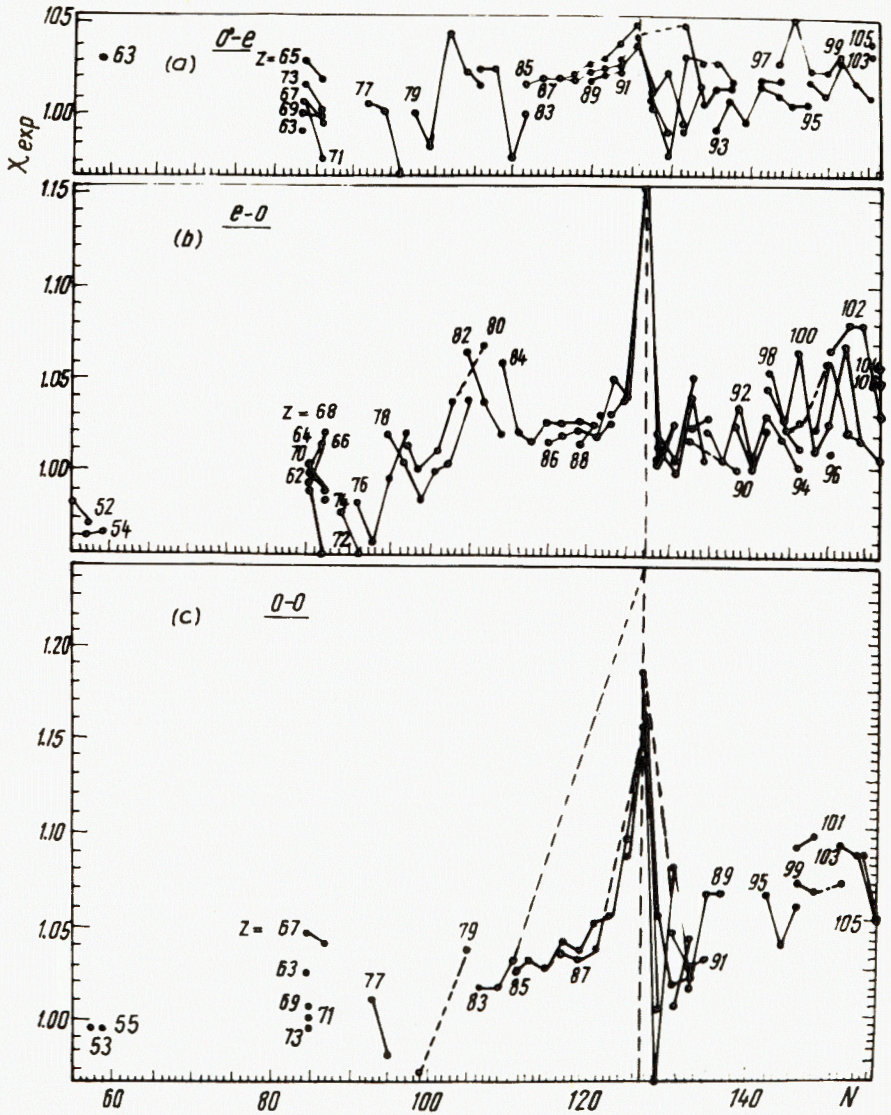

Fig.38. The "experimental" values of the coefficient χ_{exp} for odd-even (a), even-odd (b) and odd-odd (c) nuclei.

in which e is the electron charge and $R_d = r_0 A_d^{1/3}$, $r_0 = 1.2249$ fm. With the substitution $R = R'_b \cos^2\xi$, the integration K'_s is performed easily and leads to an analytical relationship. It is approximated by a larger quantity obtained by replacing E' by Q and consequently R'_b by $R_b = 2Z_d e^2/Q$. Now $K = K_i + K_s$ and

$$K_s = \frac{8e^2}{h}\sqrt{2m}\, Z_d \left(\frac{A}{AQ}\right)^{1/2} [\arccos\sqrt{x} - \sqrt{x(1-x)}\,], \qquad (7.12)$$

$$x = R_t/R_b = r_0(A_d^{1/3} + 4^{1/3})Q/(2Z_d e^2).$$

The term K'_i is a consequence of the strong interaction in the overlapping region; it was computed numerically and can be approximated as a small percent from K_s leading to

$$K = \chi K_s, \qquad (7.13)$$

where χ is different for various nuclides; it can be either greater or lower than unity, due to the fact that $K_s > K'_s$, hence sometimes it happens that $K_s - K'_s$ over compensates K'_i. For each of the nuclei of our set of experimental data one can determine an "experimental" value

$$\chi_{exp} = \ln 10(\log T_{exp} + 20.446)/K_s, \qquad (7.14)$$

where, after replacing the numerical constants, one has from eq.(7.12)

$$K_s = 2.52956 Z_d \left(\frac{A_d}{AQ}\right)^{1/2} [\arccos\sqrt{x} - \sqrt{x(1-x)}\,], \qquad (7.15)$$

$$x = 0.4253\, Q(1.5874 + A_d^{1/3})/Z_d.$$

The eq.(7.10) becomes

$$\log T = K_s/\ln 10 - 20.446. \qquad (7.16)$$

The figures 33c and 38a,b,c show the variation of the quantity χ_{exp} for e-e, o-e, e-o, and o-o groups of nuclei, respectively. For e-e nuclei (fig.33c), there is a systematic sawtooth variation; χ_{exp} increases slowly when N is increased between two successive magic numbers and decreases steeply from magic to magic plus two neutron numbers. The same thing happens for o-e nuclei (fig.38a), though the dispersion of data is more pronounced. For e-o (fig.38b) and o-o (fig.38c) nuclei the maximum value of χ_{exp} reached at the magic plus one number

of neutrons is greater. The e-o nuclei (fig.38b) show a very sharp peak at N = 127. The very special behaviour of the data for Z = 83, N = 127, which was observed in figure 36, is also present in the figure 38c.

The variation of χ_{exp} plotted in figures 33c and 38 suggests that the rising part of χ could be approximated by some simple laws of variation with Z and N: a constant value, a first order polynomial or a second order polynomial. The saw tooth is obtained if N and Z are replaced by the reduced variables y and z:

$$\chi = B_1 + B_2 y + B_3 z + B_4 y^2 + B_5 zy + B_6 z^2 \qquad (7.17)$$

expressing the distance from the closest magic-plus-one number N_i (or Z_i):

$$y \equiv (N - N_i)/(N_{i+1} - N_i);\ N_i < N \le N_{i+1},\ N_i = \ldots\ldots, 51, 83, 127, 185, \ldots\ldots \qquad (7.18)$$

$$z \equiv (Z - Z_i)/(Z_{i+1} - Z_i);\ Z_i < Z \le Z_{i+1},\ Z_i = \ldots\ldots, 29, 51, 83, 115, \ldots\ldots \qquad (7.19)$$

The parameters $\{B_k\}$ are obtained from the fit with our set of experimental data.

7.4. The Fit with Experimental Data

The value of the parameter B_1 for the simple constant approximation of $\chi = B_1$, can be obtained straightforwardly by using the least squares method. The sum $\sum_{i=1}^{n} \log(T_{i\,exp}/T_i)$ is minimized with respect to χ leading to

$$B_1 = \ln 10 \sum_{i=1}^{n} (\log T_{i\,exp} + 20.446) K_{si} / \sum_{i=1}^{n} K_{si}^2 \qquad (7.20)$$

in each of the four groups of nuclei (n = 123 for e-e, 83 for o-e, 111 for e-o and 59 for o-o nuclei). In this way, the following figures have been obtained: $B_1 = 1.002\,410$ for e-e; $B_1 = 1.016\,046$ for o-e; $B_1 = 1.019\,613$ for e-o and $B_1 = 1.049\,592$ for o-o nuclei.

For the first order and the second order polynomial $\chi = \chi(y,z)$, a numerical procedure (Poenaru et al. 1982) has been used in order to find the parameters $B = \{B_k\}$ minimizing the sum of the squared of the deviations. In case of the second order polynomial one seeks to minimize the functional $\sigma_x : R^6 \to R$, defined by

$$\sigma_x(B) = \sum_{i=1}^{n} [\chi_{exp}(y_i, z_i) - \chi(y_i, z_i)]^2 . \qquad (7.21)$$

From the condition of minimum, the set of normal equations of the least-squares problem is derived:

$$\sum_{i=1}^{n} [\chi_{exp}(y_i, z_i) - \chi(y_i, z_i)] \frac{\partial \chi}{\partial B_k}(y_i, z_i) = 0 . \quad (k = 1,2,...,6) . \qquad (7.22)$$

For the first order polynomial the similar set has only 3 equations. The Gauss elimination method with complete pivot has been used to solve these systems. The parameter values obtained in this way are given in table 2 (see section 7.6).

The capacity of our formula to describe the experimental data can be appreciated from figure 39. For even-even nuclei, fig.39a shows the constant approximation; fig.39b, the first order polynomial approximation, and fig.39c, the second order polynomial approximation. The increased error in the vicinity of the magic number of neutrons N = 126, which is present for all known formulae (see figures 35 and 36) and for the constant χ (fig.39a), is practically smoothed out by the second order polynomial approximation. This performance is only partly achieved for o-e (fig.39d), e-o (fig.39e) and o-o (fig.39f) nuclei. In any case a comparison with figures 35 and 36 demonstrates the advantage of using our formula. Even the very large errors of 5-6 orders of magnitude obtained for Z = 83, N = = 127 in figure 36 are greatly reduced below 0.4 orders.

An overall estimation of how well various formulae can describe the experimental data, could be quantitatively obtained by introducing the standard rms deviations of logT values:

$$\sigma = \{ \sum_{i=1}^{n} [\log(T_i / T_{exp})]^2 / (n-1) \}^{1/2} . \qquad (7.23)$$

This quantity was displayed in figure 40a for the original (old) and in figure 40b for the improved additive coefficients (new) in each of the four groups of nuclei. Only for some particular cases (hatched area at the top of the column) the reduction of σ is not larger than 0.02. This is a property of the experimental data used by various authors in comparison with our set.

Even the constant χ approximation of our formula has σ somewhat lower than the best of the known relationships (Keller-Münzel 1972). Of course the second order polynomial approximation leads to smaller standard deviations.

In the future when a better set of experimental data (more accurate or more complete) will be available, the parameters $\{B_k\}$ and $\{C_k\}$ could be automatically improved with a computer program (Poenaru et al, 1982).

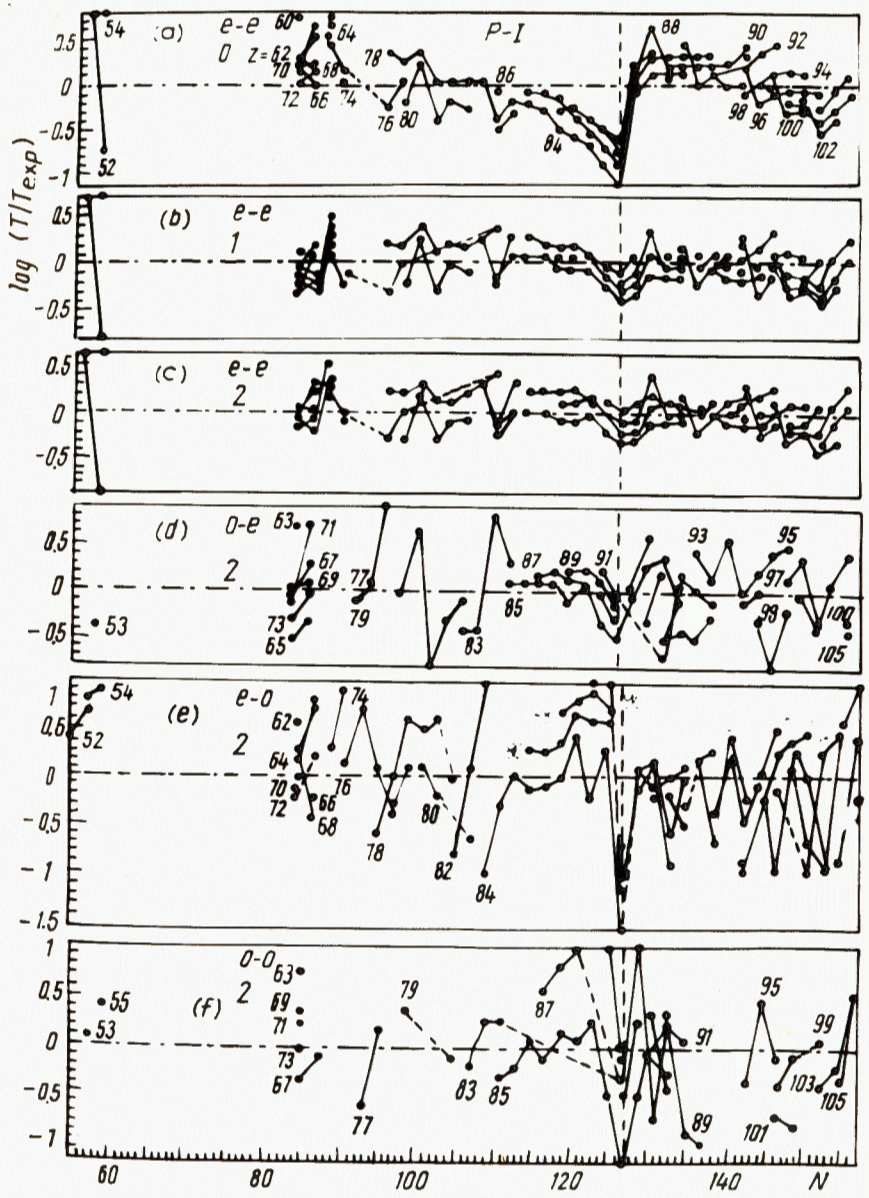

Fig.39. The errors of life-time prediction with our formula, when χ is approximated with a constant (a), first order (b) and a second-order (c) polynomial of two variables for even-even, odd-even (d); even-odd (e) and odd-odd nuclei (f).

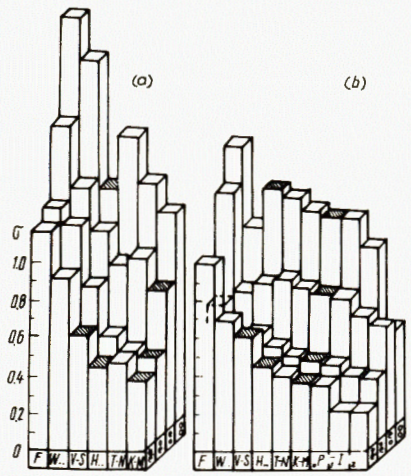

Fig.40. The standard deviation of various formulae in each group of nuclei for both old (a) and new (b) values of the additive parameters.

7.5. Partial Alpha Decay Half-Life of the Nuclei with Known Q-Values

For all parent and daughter nuclei with $Z \geq 48$, which have masses tabulated by Wapstra and Bos (1977) the Q values were calculated. By using our semiempirical formula it was possible to predict (Poenaru and Ivascu 1981a) the partial alpha decay lifetime T for all gs-gs transitions for which $Q>0$, by using our semiempirical relationship given above. Only the values $10^{-7} < T < 10^{30}$ (interesting from the experimental point of view, were plotted in figure 41. In this way, many isotopes with small Q-values and consequently very small probability to decay, are not present on this figure.

The systematics of the alpha decay half-life are shown separately for even-even (fig.41a), odd-even (fig.41b), even-odd (fig.41c), and odd-odd (fig.41d) nuclei. One can see that for a given Z, the lifetime rises when the neutron number increases, except in the neighbourhood of the magic numbers of the daughter nuclei, where it steeply decreases, from N = 82 to 84 and 126 to 128 when N is even, or from N = 81 to 85 and 125 to 129 when N is odd.

Fig.41. Systematics of the gs-gs transitions life-time predicted values in the interval 10^{-7} to 10^{3} s for our set of experimental data (x) and for the other alpha emitters (•) (a) even-even; (b) odd-even; (c) even-odd and (d) odd-odd nuclei.

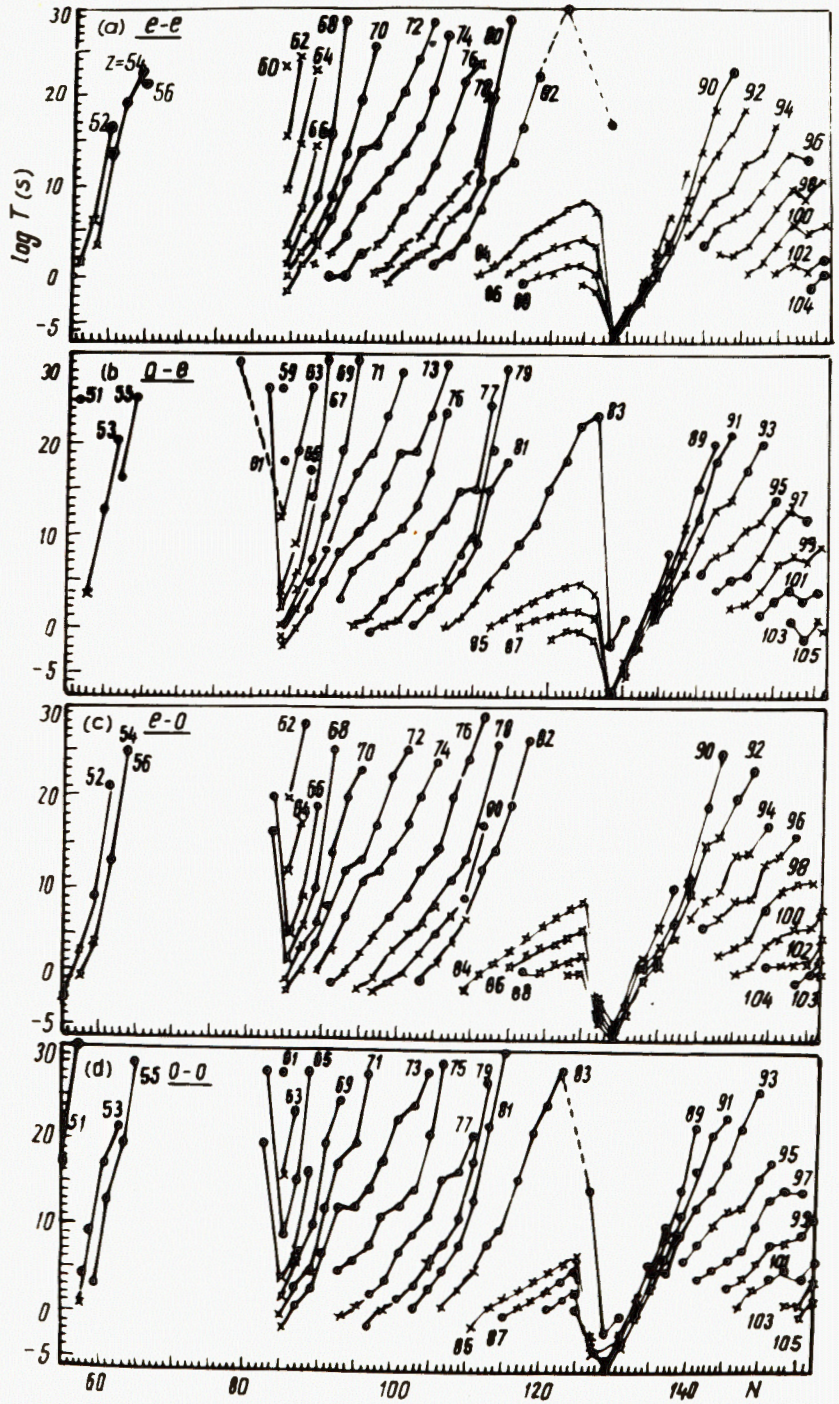

The nuclei with known values of the half-life, used to obtain by fit the coefficients $\{B_i\}$ were marked with a cross on the figure, where the estimated value of T is plotted.

After a small island of alpha emitters (Z = 51-56 and N = = 55-65), there is a gap of relative stability to the alpha decay (very long decay time) or even negative Q -values. After that, with Z = 59 and N = 83 begins the main region of alpha instability. It would be interesting to find also other competing modes of disintegration (beta decay or spontaneous fission) for those nuclei.

Predictions for nuclei with $62 < Z < 76$, have been made also by Rurarz (1982) who found good agreement of the results obtained by using our formula with experimental data. He extended the calculations for nuclei far off the beta stability line by using mass formulae to find the Q -values.

7.6. The Island of Alpha Activity Close to the Double Magic ^{100}Sn

The island of alpha emitters close to the double magic nucleus ^{100}Sn, has been extensively studied (Schardt et al. 1979, 1981) experimentally at the GSI on-line mass separator. Due to the double magicity the mass surface is lowered, leading to increased Q-values for alpha decay of nuclei with Z, N $\geq$ 52. Complex decay paths are presented by the very neutron deficient trans-tin isotopes, because the β^+ decay Q -value increases and the charged particles binding energies decrease with increasing distance from the line of β-stability. For example ^{114}Cs has an alpha transition from the ground state and β -delayed protons, alpha particles and γ-rays (Tidemans - Petersson et al. 1981).

At the beginning, the alpha activities detected following ^{96}Ru(^{16}O, xn) reaction (Macfarlane and Siivola 1965) have been assigned to the isotopes ^{107,108}Te. After that, Karnaukhov and Ter-Akopyan (1967) corrected this result showing that one has ^{108,109}Te. At the GSI UNULAC accelerator, 14 alpha emitters, isotopes of Te, I , Xe, and Cs, have been identified. These are not tabulated in the catalogues of alpha decaying nuclei, published by Gauvin et al. (1975) and Rytz (1979).

The alpha transitions between ground states of the nuclei with Z = 52-61 have been studied (Poenaru and Ivascu 1984b) by using our semiempirical formula based on the fission theory of alpha decay.

In our previous papers (Poenaru and Ivascu 1983a) we have used for Te, I , Xe, and Cs isotopes the data from Schardt et al. (1979) with which the old values "ov" of B_k given in table 2, have been obtained. Recently, the authors have pub-

Table 2

B_k *parameter values*

Group of nuclei		n	B_1	B_2	B_3	B_4	B_5	B_6
e - e	ov	122	0.987 722	0.021 227	0.017 407	0.023 342	0.001 546	-0.016 509
	nv	125	0.985 911	0.022 841	0.024 584	0.023 279	-0.000 716	-0.022 562
O - e	ov	83	1.003 660	0.021 626	0.034 805	0.000 870	0.039 190	-0.066 147
	nv	84	1.000 560	0.010 783	0.050 671	0.013 919	0.043 657	-0.079 999
e - o	ov	111	1.014 620	-0.119 094	0.030 606	0.156 507	0.228 848	-0.109 130
	nv	111	1.017 560	-0.113 054	0.019 057	0.147 320	0.230 300	-0.101 523
o - o	ov	59	1.008 070	-0.184 468	0.259 041	0.231 988	0.326 171	-0.406 200
	nv	60	1.007 740	-0.184 136	0.260 268	0.231 900	0.326 025	-0.407 280

Table 3

Comparison between experimental data and life time computations

Z	A	Experimental values				log (T/T_{exp})				
		$Q^{a)}$ MeV	$\log T_{exp}$ s	$Q^{b)}$ MeV	$\log T_{exp}$ s	P-1 ov	nv	T-N	V-S	K-M	H...
52(Te)	106			4.323	-4.22	0.44	0.41	1.04	-0.15	0.85	1.24
	108	3.406	0.49	3.448	0.49 c)	0.34	0.31	1.04	-1.21	0.78	1.14
	110	2.800	6.57	2.723	6.39 c)	-0.06	-0.09	0.65	-2.82	0.31	0.71
54(Xe)	110			3.878	-0.40 c)	-0.08	-0.10	0.48	-0.99	0.25	0.68
	112	3.303	2.51	3.329	2.97 c)	-0.06	-0.08	0.53	-1.61	0.25	0.67
52(Te)	107	3.982	-2.29	3.982	-2.29 c)	0.32	0.38	1.22	-0.42	0.87	1.36
	109	3.198	2.01	3.197	2.01 c)	0.64	0.72	1.68	-1.02	1.37	1.73
54	111	3.693	-0.05	3.714	0.54 c)	0.09	0.15	0.94	-0.79	0.62	1.10
	113	3.095	3.90	3.095	4.68 c)	0.09	0.17	1.01	-1.54	0.73	1.11
53(I)	111	3.270	3.45	3.270	2.74 c)	0.31	0.22	0.88	-1.54	0.59	0.95
	113			2.706	7.25 c)	0.46	0.34	0.94	-2.43	0.73	0.98
53	110	3.553	0.84	3.574	0.58 c)	0.23	0.23	0.74	-0.20	1.44	1.82
	112			2.987	4.84 c)	-0.02	-0.02	1.61	-1.19	1.51	1.65
55(Cs)	114	3.343	3.50	3.357	3.50	0.27	0.27	1.41	-0.55	1.24	1.53

a) Data from Schardt et al (1979); b) Data from Schardt et al (1981); c) b estimated ,Schardt et al (1981), by using transmission calculations from (Rasmussen 1959) assuming a reduced width $W_\alpha = (Pt)/(PT)_{212_{Po}}$

lished (Schardt et al. 1981) improved data. In table 3 the computed results, obtained for the new data both with the old and new B_k values, are compared with experiment. The errors obtained with other semiempirical formulae are also given.

Table 3 includes the new isotopes ^{106}Te and ^{110}Xe and more accurate data for ^{108,110}Te, , ^{110,112,113}I, ^{111,112}Xe and ^{114}Cs. There are two alpha lines for ^{111}Xe; that with lower energy and intensity was not introduced in table 2, assuming that it does not corresponds to transition between ground states. The lightest emitter discovered up to now is ^{106}Te. Its daughter, ^{102}Sn, is the closest isotope to the double magic ^{100}Sn reached till now.

As in our preceding paper (Poenaru et al. 1983b) where more data have been analysed, allowing to obtain the results shown in figure 40, from table 3 one can see that also for this island of 14 alpha emitters, smaller errors are given by our equation (PI), followed by Keller-Münzel (K-M), Taagepera-Nurmia (TN), Hornshøj et al. (H...) and Viola-Seaborg (VS).

The differences between the errors of our formula with the old and new B_k values, are not large. Concerning their variation trend, one can say that except the odd-N Te and Xe isotopes,for which one get a slight increase, for other groups of nuclei the errors become lower when the new B_k values are used.

7.6.1. Computation of Q-values with various mass formulae

Only three isotopes of Te and two of I, from that given in table 3, have alpha decay Q-values tabulated by Wapstra and Bos (1977): for ^{108,109}Te they correspond to older measurements and for ^{110}Te,, ^{112,113}I they have been estimated from systematics and are smaller than the experimental results.

The Q-value variation trend given by the liquid drop model is to increase when the distance from the line of beta stability is increased. The superposed shell effects produce an important rise of Q for nuclei having a daughter with magic number of neutrons (or protons), that is N = Z = 52 or N = 84. This shell effect explains the existence of the island of alpha emitters in the neighbourhood of the double magic nucleus ^{100}Sn, far off the main region of alpha emitters having $N \geq 84$.

When the Q-value for Te isotopes is splitted in two terms given by the droplet model (Myers 1977) and the shell effects, one obtains that 90% is given by the second term, which is an additional support for the double magicity of ^{100}Sn.

Concerning the proton drip line in this region Płochocki et al. (1982) predicts that ^{104}Sb or ^{105}Sb , ^{103}Te ,, ^{109}I , and ^{113}Cs are (very likely) protons emitters.

Table 4

Comparison between measured and computed Q-values (in MeV)

Z	A	Exp.	Calculations											
			M	GHT	SH	LZ	B	BIM	J	CK	JE	WB		
52(Te)	106	4.32	4.32	3.94	3.88	4.27		6.58	3.22	3.45	3.42			
	107	3.98	4.02	3.63	3.88	3.93	2.21	6.58	3.12	3.30	3.27			
	108	3.45	3.74	3.36	3.58	3.56	2.04	5.98	2.92	3.03	3.02	3.41		
	109	3.20	3.44	3.06	3.87	3.26	1.80	5.98	3.18	2.85	3.17	3.20	x)	
	110	2.72	3.16	2.77	3.38	2.92	1.60	5.38	3.05	2.75	2.99	2.80	x)	
53(I)	110	3.57	3.61	3.27		3.22			3.29	2.87	3.38			
	111	3.27	3.34	3.01	3.88	2.97		6.08	3.22	2.63	3.22		x)	
	112	2.99	3.03	2.72	3.47	2.68			2.94	2.28	2.95	2.54	x)	
	113	2.71	2.77	2.43	3.17	2.38	2.30	4.97	2.40	2.02	2.36	2.26	x)	
54(Xe)	110	3.88	4.10	3.80	4.17	3.64		6.47	3.15	2.88	3.60			
	111	3.71	3.80	3.52	4.27	3.30		6.38	3.43	2.72	3.75			
	112	3.33	3.56	3.25	4.18	3.05		5.87	3.21	2.52	3.60			
	113	3.09	3.24	2.84	3.38	2.71		5.57	2.99	2.28	3.34			
55(Cs)	114	3.36	3.08	2.72		2.69			3.12	2.40	3.95			
		n	14	14	12	14	5	11	14	14	14	5		
		Errors σ_Q (MeV)	0.21	0.29	0.53	0.33	1.46	2.69	0.50	0.76	0.42	0.36		
		$\sigma_{\log T}$	1.42	2.50	3.30	2.83	15.07	11.45	3.40	6.56	2.84			

x) From systematics

The computed Q-values with various mass formulae, are compared with the experimental ones (Schardt et al.1981)in table 4. One can see that systematically Beiner-Lombard-Mas (BLM) (1976) Q-values are too high and those obtained with Bauer (B) (1976) formula for Te isotopes, are too small. None of the nine mass formulae can reproduce all the experimental results, but one can say that many good estimates are obtained by Myers (M)(1977) followed by Groote-Hilf-Takahashi (GHT) (1976), Liran-Zeldes (LZ) (1976), Jänecke-Eynon (JE) (1976), and Jänecke (J) with Garvey-Kelson relationships (1976). The best description of Q-values for Te isotopes is given by LZ, for I isotopes by M, for Xe isotopes by GHT and J and for ^{114}Cs by J.

The small errors obtained with LZ for the masses of Cs isotopes, for which Wapstra-Bos (WB) masses estimated from systematics are too small, have been mentioned by Epherre (1983). Also the good results given by GHT have been stressed by Epherre (1983) and Schardt et al. (1981), by M - in ref. (Schardt et al.1981) and by GHT and JE in ref. (Płochocki et al.1982).

7.6.2. Predictions for alpha decay of some nuclides with Z = 52-61

In a previous work (Poenaru and Ivascu 1981a) we have computed the partial alpha decay lifetimes, by using Q-values calculated from WB masses (see figure 41). In this figure one can see that for the range of $T < 10^{30}$s, the island of alpha emitters with Z = 52-56, N = 55-65 is well separated from the main region of alpha radioactivity having $Z \geq 60$, $N \geq 82$.

Due to the fact that WB masses for neutron deficient nuclei, estimated from systematics do not allow a good reproduction for all the masses in this region and many nuclei far off the beta stability line have not been tabulated by WB, the estimations made in this section for Z = 52-61 alpha emitters, are based on the 1975 mass predictions (Maripuu 1976). The range Z = 62-76 has been analysed by Rurarz (1982).

The results for Q-values and partial alpha decay lifetimes computed with our semiempirical formula with old $\{B_k\}$ values, are plotted in figures 42-44 for various isotopes of an element versus the neutron number N.

In the figures 42 and 43, only the range of N values in which $Q > 0$, has been plotted. Due to the fact that all 10 curves could not be clearly shown at this scale, the regions in which many mass formulae give closer results have been hatched in figures 42-44; only the curves for which confusions could not arise, have been plotted in the usual manner. With full line are drawn the WB data for Q-values and the corresponding half-lives. In order to show very roughly a possible proximity of

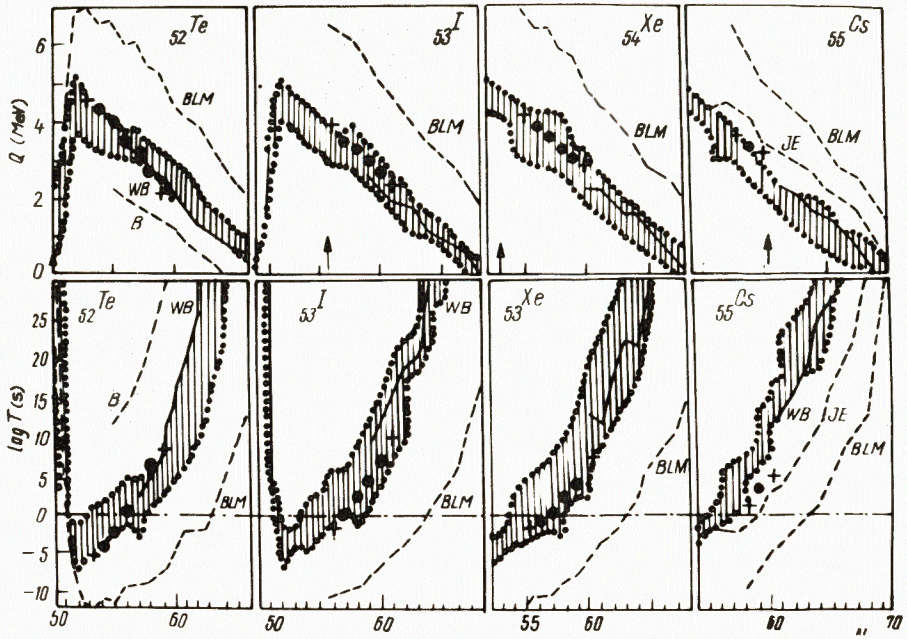

Fig. 42. Alpha decay **Q** *-values predicted by various mass formulae and the corresponding life-times computed with our formula versus neutron number* **N**, *for* **Te**, **I**, **Xe** *and* **Cs** *isotopes.*

the proton drip-line, an arrow has been placed at the distance of 18 units of N, from the closest stable isotope.

The increased stability of the closed shell nuclei is illustrated on figures 42-44 by the small Q-values for magic neutron numbers of the parent nuclei (N = 50 in figure 42 and N = 82 in figure 44) and large Q-values for the magic neutron numbers of the daughter (N = 52 in figure 42 and N = 84 in figure 44). For all other N values between these two extremes one obtains monotonously decreasing Q-values with increasing except for the steep increase between magic and magic-plus-two neutron numbers.

The dispersion of 1 MeV of the Q-values gives rise of 6-8 orders of magnitude dispersion of the half-lives. Hence, from this point of view, the nowadays mass predictions are not satisfactory.

The computations based on BLM masses are too optimistic (large Q-values and correspondingly small half-lives) for this range of Z values; moreover they lead to a very steep decrease with the neutron number, as it is shown in figure 44.

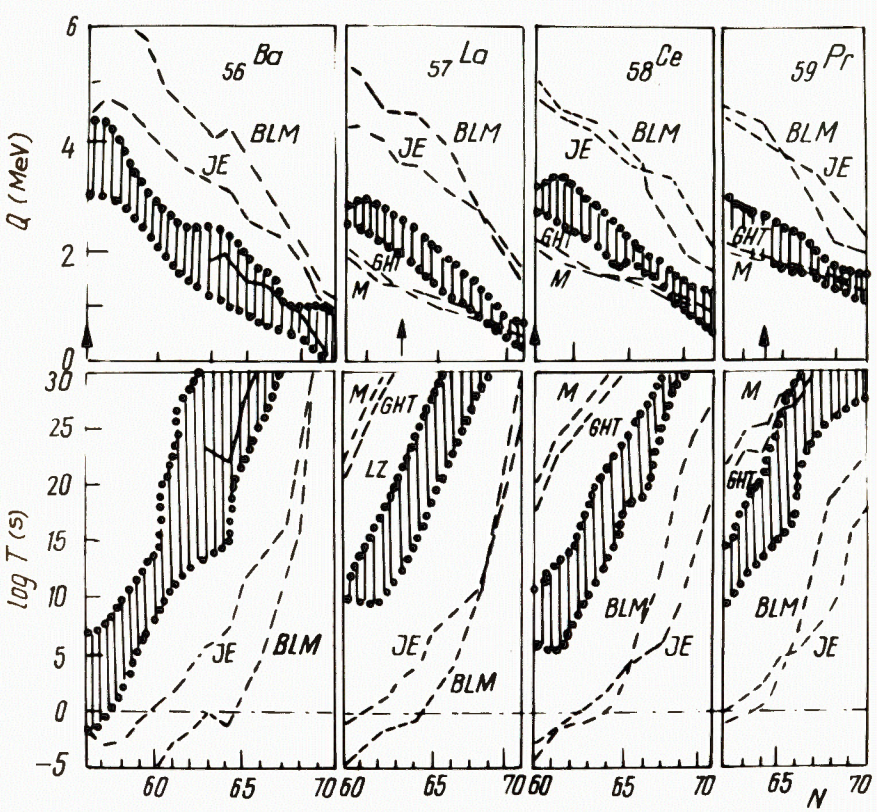

Fig. 43. The same quantities as in figure 42, for **Ba**, **La**, **Ce** *and* **Pr** *isotopes.*

Beginning with Z = 55, the JE Q-values are coming closer and for Z ≥ 57 they even surpass them.

The figure 42 shows the results for the isotopes of the elements with Z = 52-55, for which some alpha emitters have been already identified. The experimental data are plotted with heavy points and the predictions from ref. (Schardt et al.1981) with crosses. It was mentioned that the alpha branching ratio is small for the high mass number isotopes and is close to 100% for small mass number isotopes. Very likely, for ^{109}I and ^{113}Cs one has to consider also the competition of the proton radioactivity.

The figure 43 shows two extreme limits: the high Q-values and alpha decay probabilities given by BLM and JE and the low Q-values and alpha decay probabilities (long half-lives) of M and GHT. For the La and Ce isotopes, this trend is very clearly seen. From the results plotted in this figure, one can hope

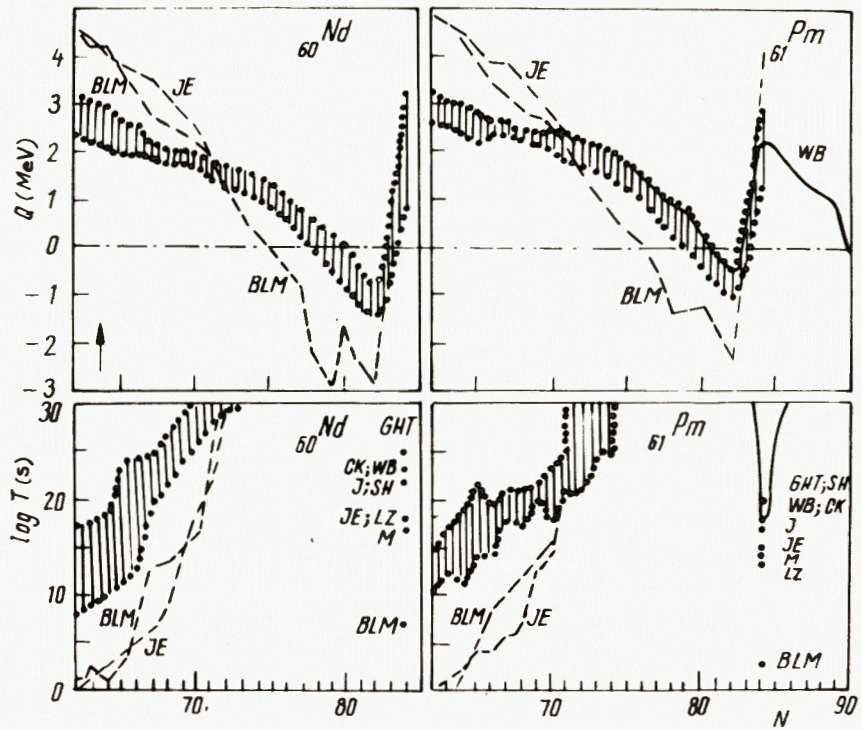

Fig.44. The same quantities as in figure 42, for Nd *and* Pm *isotopes.*

that some new alpha emitters could be found especially for the Ba and Ce isotopes.

The shell effects in the neighbourhood of N = 82 magic numbers are shown in figure 44. For N = 74-84 there is a gap in which no alpha activity could be detected wither because one has Q<0, or, if it is positive, its value is very low,leading to extremely long half-lives.

8. ANALYTICAL APPROXIMATION OF THE POTENTIAL BARRIER

We have performed (Poenaru and Ivascu 1984a) a systematic investigation of the stability of about 2000 nuclei, with known masses tabulated by Wapstra and Bos, toward the emission of isotopes (Z_2 = 2) with various mass numbers A_2= 3,4,...,10. It was possible to consider this large number of cases (about 16,000) by using a model leading to analytical results both for the states (potential energy) and the dynamics (barrier

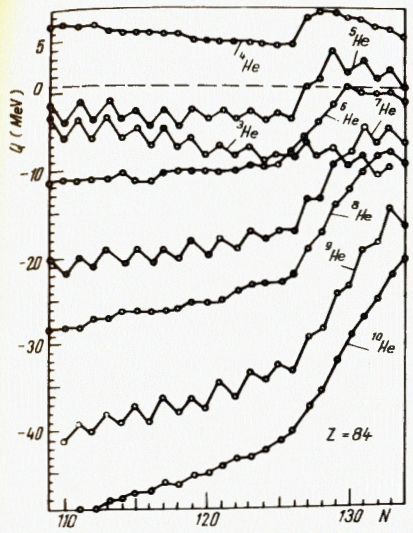

Fig.45. Q-values for the emission of various He *isotopes from* Z=84 *nuclides with different neutron numbers.*

penetrability) of the process. In the following we would like to present this model allowing to account for angular momentum and nuclear excitation effects. This version can be used to find new kinds of radioactivities, as will be shown below.

The figure 45 illustrates the fact that for some Po isotopes, besides the well-known alpha decay, the exotic ^{5}He spontaneous emission from the ground state is also energetically possible. All other He isotopes (A_2 = 3,6, 7,8,9,10) could be emitted only from excited states, because Q<0.

Unfortunately ^{5}He is not stable (see Ajzenberg-Selove and Lauritsen (1974) and the references cited therein). Its ground state has a width Γ = 600±20 keV (Nyman et al.1981). Consequently, the ^{5}He radioactivity could be experimentally determined by alpha-particles or the neutrons produced by its own disintegration, as well as by the presence of the daughter nucleus. In this respect it is encouraging that recently (Cable et al.1983) the existence of two-proton radioactivity predicted long time ago (Goldansky 1960) was experimentally confirmed. Of course, the diproton, like ^{5}He,is not a stable particle but from the analysis undertaken by Goldansky it seems that the two protons separates practically only after the passage of the cluster through the potential barrier. We presume that the same is true for ^{5}He, i.e., it disintegrates into a neutron and an alpha particle after tunnelling.

8.1. Parabolic Approximation of the Interaction Potential Containing a Centrifugal Term

In the framework of LDM two center spherical parametrization (see sections 5.1.1, 5.3 and 5.5) for separated fragments, $R \geq R_t$, only the Coulomb interaction energy $Z_1Z_2e^2/R$ has been considered for alpha decay of even-even nuclei. The maximum of the potential energy at $R = R_t$ was

$$E_c = Z_1 Z_2 e^2 / R_t , \qquad (8.1)$$

where e is the electron charge. In this way, a barrier shape like that shown in figure 37 was obtained.

Now, for ^{5}He, which has a spin $I_2 = 3/2$, the spin, $\vec{I}$, and parity, π, conservation must be fulfilled:

$$\vec{I} = \vec{I}_1 + \vec{I}_2 + \vec{\ell} \; ; \quad \pi = \pi_1 \cdot \pi_2 \cdot (-1)^{\ell} . \qquad (8.2)$$

Any quantity belonging to the parent nucleus is written without subscript, those of the daughter and emitted particle have the subscript 1 and 2, respectively.

To the Coulomb interaction E_c one has to add also the contribution of the angular momentum $\ell\hbar$ - the centrifugal term

$$E_\ell = \hbar^2 \ell (\ell + 1) / (2\mu R_t^2) , \qquad (8.3)$$

where $\mu = mA_1A_2/A$ is the reduced mass and m is the nucleon mass. By substituting the numerical values one obtains, for $R = R_t$ in fm, the total interaction energy at $R = R_t$, in MeV:

$$E_i = E_c + E_\ell = 1.43998 Z_1 Z_2 / R_t + 20.735 \ell (\ell + 1) A / (A_1 A_2 R_t^2) . \qquad (8.4)$$

In the overlapping region, a convenient analytical approximation of the potential energy curve E(R), leading from $E(R_i) = Q$ to $E(R_t) = E_i$, suggested by the potential barrier shape (fig.37) and allowing to get a closed formula for the lifetime T (see the next section), is a second order polynimial in R. Finally, one has

$$E(R) \simeq \begin{cases} Q + (E_i - Q)[(R - R_i)/(R_t - R_i)]^2 ; & R \le R_t \\ Z_1 Z_2 e^2 / R + \hbar^2 \ell (\ell + 1) / (2\mu R^2) ; & R \ge R_t , \end{cases} \qquad (8.5)$$

where E_i is given by eq.(8.4).

For a nonzero excitation energy (a nuclear temperature τ), the Coulomb energy is only slightly reduced (Sauer et al.1976), being multiplied by the factor $(1 - 10^{-3} \cdot \tau^2)$, where τ is expressed in MeV. Consequently, at relatively small excitation energies, it remains practically unchanged.

8.2. Closed Formula for the Lifetime

Like in fission the halflife of a metastable system is given by eqs. (2.3)-(2.5), in which $Q' = Q + E_{vib} + E^*$ and $E^* < E_i - (Q + E_{vib})$ is the fraction of the excitation energy concentrated in the separation degree of freedom. This barrier transmission model, used in the present work, describes only low excitations (Bjørnholm and Lynn 1980). Statistical equilibrium among all the degrees of freedom of the nucleus is reached for high excitation energies U. In this case $E^* = U - (E^i + E_{rot})$, where $U = a\tau^2$; $a \simeq A/10$ MeV^{-1} is the level density parameter, E^i is the internal energy available for other degrees of freedom; E_{rot} is the rotational energy. In a hot nucleus the energy concentrated on motion in the deformation mode is of the order of the nuclear temperature. Hence the residual nucleus is usually left in a highly excited state, too. According to the statistical model (Michaudon 1981) the probability to excite a collective state of E^* energy is roughly proportional to $\exp(-E^*/\tau)$. Due to the fact that $E(R_a) = E(R_b') = Q' = E'$ it follows that

$$R_a = R_i + (R_t - R_i)[(E_{vib} + E^*)/E_b^\circ]^{1/2} , \qquad (8.6)$$

$$E_b^\circ = E_i - Q , \qquad (8.7)$$

$$R_b' = (R_t E_c / Q')[0.5 + (0.25 + Q' E_\ell / E_c^2)^{1/2}] . \qquad (8.8)$$

According to the eq.(8.5), one can split the action integral in two terms $K = K_{ov} + K_s$ by integrating from R_a to R_t in the overlapping region and from R_t to R_b' for separated fragments. By expressing the time in seconds, the energies in MeV and the lengths in fm, one obtains, after replacing the numerical constants, the following relationships:

$$T = \frac{1.4333 \times 10^{-21}}{E_{vib}} [1 + \exp(K)] ; \quad K = K_{ov} + K_s , \qquad (8.9)$$

$$K_{ov} = 0.1296 (E_b^\circ A_1 A_2 / A)^{1/2} \left[\sqrt{b^2 - a^2} - \frac{a^2}{b} \ln \frac{b + \sqrt{b^2 + a^2}}{a} \right] , \qquad (8.10)$$

$$K_s = 0.4392 (Q' A_1 A_2 / A)^{1/2} R_b J_{cm} , \qquad (8.11)$$

$$J_{cm} = (c + m - 1)^{1/2} - [r(c - r) + m]^{1/2} + \frac{c}{2} \left(\arcsin \frac{c - 2r}{\sqrt{c^2 + 4m}} - \arcsin \frac{c - 2}{\sqrt{c^2 + 4m}} \right) + \sqrt{m} \ln \left\{ \frac{2\sqrt{m}\,[r(c - r) + m]^{1/2} + cr + 2m}{r[2\sqrt{m}\,(c + m - 1)^{1/2} + c + 2m]} \right\} , \qquad (8.12)$$

where

$$a \simeq R_a - R_i = b[(Q' - Q)/E_b^\circ]^{1/2} ; \quad b = R_t - R_i , \qquad (8.13)$$

$$c = rE_c/Q' ; \quad m = r^2E_\ell/Q' ; \qquad r = R_t/R_b . \tag{8.14}$$

If $\ell = 0$, one has $c = 1$, $m = 0$ and the well-known formula

$$J_{10} = \arccos\sqrt{r} - \sqrt{r(1-r)} \tag{8.15}$$

is obtained.

The zero point vibration energy, $E_{vib} = 0.51$ MeV, was determined by fit with experimental data, T_{exp}, on 376 alpha emitters the same given as input data in the computer program described by Poenaru et al.(1982). In the variation with E_{vib} of the r.m.s. deviation of logT values defined by the eq.(7.23) there is a minimum $\sigma_{min} = 1.02$ at $E_{vib} = 0.51$ MeV. For $E_{vib} = 0.2$ and 0.9 MeV, one has $\sigma = 2.20$. It is assumed that the optimum value for alpha decay could be used also for ^{5}He radioactivity. Of course, this assumption which presumably is an optimistic one, needs further theoretical (or experimental) support. Consequently, the absolute values for T given in the following sections should be taken only as tentative lower limits.

8.3. ^{5}He Radioactivity

The variation of Q-values for the emission of ^{5}He from the ground states of nuclei with masses tabulated by Wapstra and Bos (1977) is plotted in figure 46. One can see the pronounced odd-even effect, which is present for all odd-mass He isotopes (see also figure 45).

There are two islands (in fact two archipelagos due to odd-even effects) of ^{5}He radioactivity. The figure 46 shows the detailed position of ^{5}He emitters, relative to the Green approximation for the line of beta stability. The main archipelago formed from two islands involves the medium-mass nuclei with $Z = 83$-92 and $N = 127$-137. The enhanced Q of $N = 129$, $Z = 84$ nucleus, leading to the double magic daughter $N_1 = 126$, $Z_1 = 82$, is a strong shell effect, disturbing the smooth LDM-like trend, toward larger Q-values of the neutron deficient nuclei. This trend is manifested in the second archipelago of 4 islands heavy transcurium nuclei with $Z = 97$-105, $N = 145$-157. Similarly, the neutron subshell $N_1 = 152$ explains the larger Q-values for $N = 155$.

Unfortunately the lifetimes for ^{5}He spontaneous emission from the ground states of the above-mentioned nuclei, are very long even with the optimistic assumption mentioned above. Only 15 of all 110 emitters have the disintegration period, T, smaller than 10^{45} s (see figure 47). Such a reduced probability, as in the case of spontaneous fission of some actinides, will make difficult to observe experimentally this phenomenon, in the

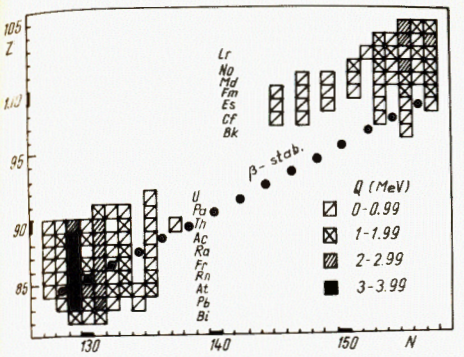

Fig.46. The ^{5}He emitters. The heavy dotts corresponds to the Green approximation for the line of beta stability.

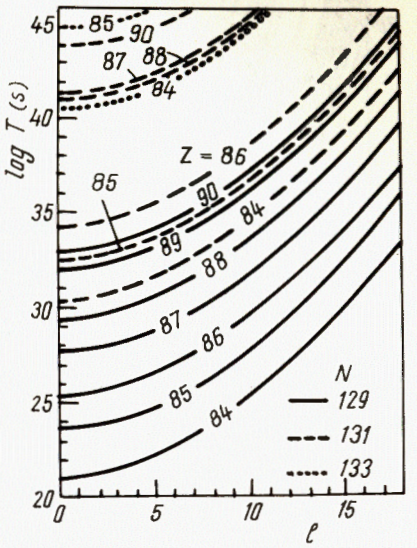

Fig.47. Variation of the life-times of some ^{5}He emitters with the angular momentum.

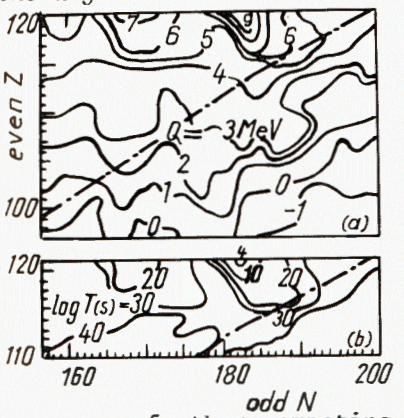

Fig.48. Q-values and life-times for some superheavy nuclei with binding energies predicted by Seeger and Howard (1975).

presence of other competing decay modes. For example the partial lifetime, for ^{5}He radioactivity of ^{213}Po is $10^{20.9}$ s, but its total half-life due to α emission is only 4.2 μs.

One has to consider also the contribution of the angular momentum $\ell\hbar$, rising the potential barrier. This is determined from the spin and parity conservation condition (see eq.(8.2)). For example when ^{5}He is emitted from ^{213}Po, one obtains $\ell = 3$ or 5, because $I^\pi = 9/2^+$, $I_1^{\pi_1} = 0^+$ and $I_2^{\pi_2} = 3/2^-$. Five units of angular momentum produce an increase of about an order of magnitude of the lifetime as it is shown in figure 47. In the opposite direction acts the energy E^*, as will be shown below.

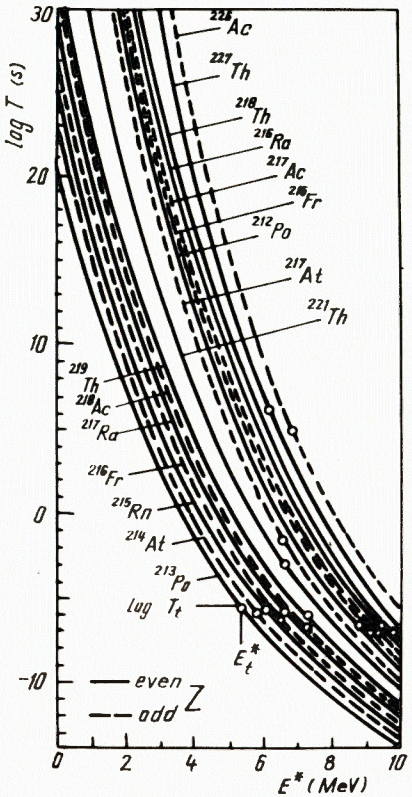

Fig.49. Variation of the partial half-lives of some ^{5}He emitters, with the energy E. The total life-time T_t of each isotope is given on the curves.*

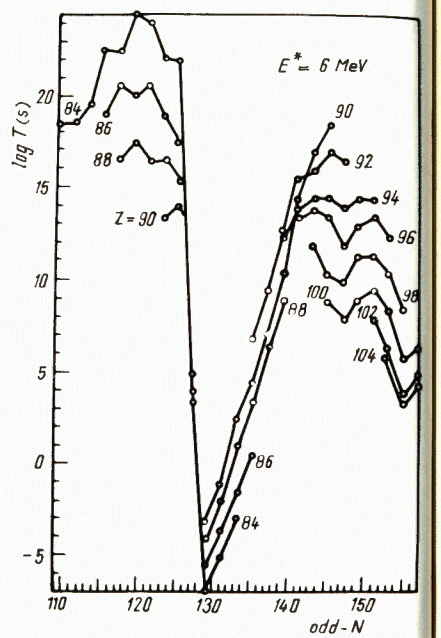

Fig.50. Partial lifetimes for ^{5}He emission from excited states with E = 6 MeV. E* is the fraction of the excitation energy concentrated in the separation degree of freedom.*

Shorter lifetimes are expected to be met in the region of superheavy nuclei. The results presented in figure 48a, obtained by using the binding energies calculated by Seeger and Howard (1975) show that the island of ^{5}He radioactive heavy nuclei continue in the superheavy region. Larger Q-values lead to shorter lifetimes (fig.48b). Of course, the partial half-lives of ^{5}He disintegration computed in this work has to be composed with the lifetimes of other competing decay modes like α or β decay, spontaneous fission. etc., in order to obtain the total disintegration period T_t. The variation of T with the energy E* (fraction of the excitation energy concentrated in this collective mode), plotted in figure 49 for some nuclei, suggests

that a convenient method to obtain shorter lifetimes is to excite the ^{5}He emitters.

As it was expected from the beginning, the odd- N nuclei are better candidates, for ^{5}He emission, than their even- N neighbours. At E* = 6 MeV energy, lifetime of some ^{5}He emitters becomes measurable. This can be seen from the figure 50, given only to illustrate that in principle, by raising the tunnelling energy, the partial half-lives for ^{5}He emission could be conveniently diminished. A more detailed analysis, of both probabilities to excite the nuclear states and to compete with other disintegration modes of these states, should be undertaken in order to plan an experiment. Such an analysis can be made similarly with that of a β-delayed proton emission (Karnaukhov 1974).

One way to excite the parent nucleus is to populate some of its excited levels by β-decay of a precursor. The β-delayed ^{5}He radioactivity (Poenaru and Ivascu 1984a) has a better chance to be experimentally determined. In this respect, from the available energy of the analysed nuclei, one can say that ^{155}Yb, ^{175}Pt and ^{209,217}Ra after β^{+}-decay, as well as $^{9\text{-}11}$Be, $^{13\text{-}14}$B, $^{13\text{-}17}$C,, $^{19\text{-}21}$O etc., after β^{-}-decay, are in a privileged position.

The ^{5}He decay of the ^{9}Be excited states fed by the β^{-}-decay of the ^{9}Li precursor have been already experimentally determined (Nyman et al.1981).

Up to now we have considered only the nuclei with masses tabulated in 1977 by Wapstra and Bos. Taking into account that the beta decays of exotic nuclei (far off the β-stability line) have high Q-values and can populate a large number of excited levels, it is expected that many other β-delayed ^{5}He radioactive nuclei could be found in the yet unexplored regions.

8.4. Emission of Heavy He Isotopes from Excited States

The light He isotopes, like alpha particles, are easily emitted usually by neutron deficient nuclei: in figure 51 the trend of increasing Q-value is clearly seen. The same is true for ^{5}He, but this trend is weaker.

On the contrary, the neutron-rich nuclei have larger Q-values for the heavy isotopes ^{8}He, ^{9}He (figure 52) and ^{10}He (figure 53). For ^{10}He, the mass excess of 50.13 MeV estimated by Jänecke (1976) have been used. Due to the fact that Q<0, these heavy He isotopes could not escape spontaneously from heavy nuclei, but they could be emitted from excited states.

If we assume that the fraction of the excitation energy concentrated in this collective mode is E* = 40 MeV, one finds, very tentatively, the lifetime for ^{10}He emission, given in

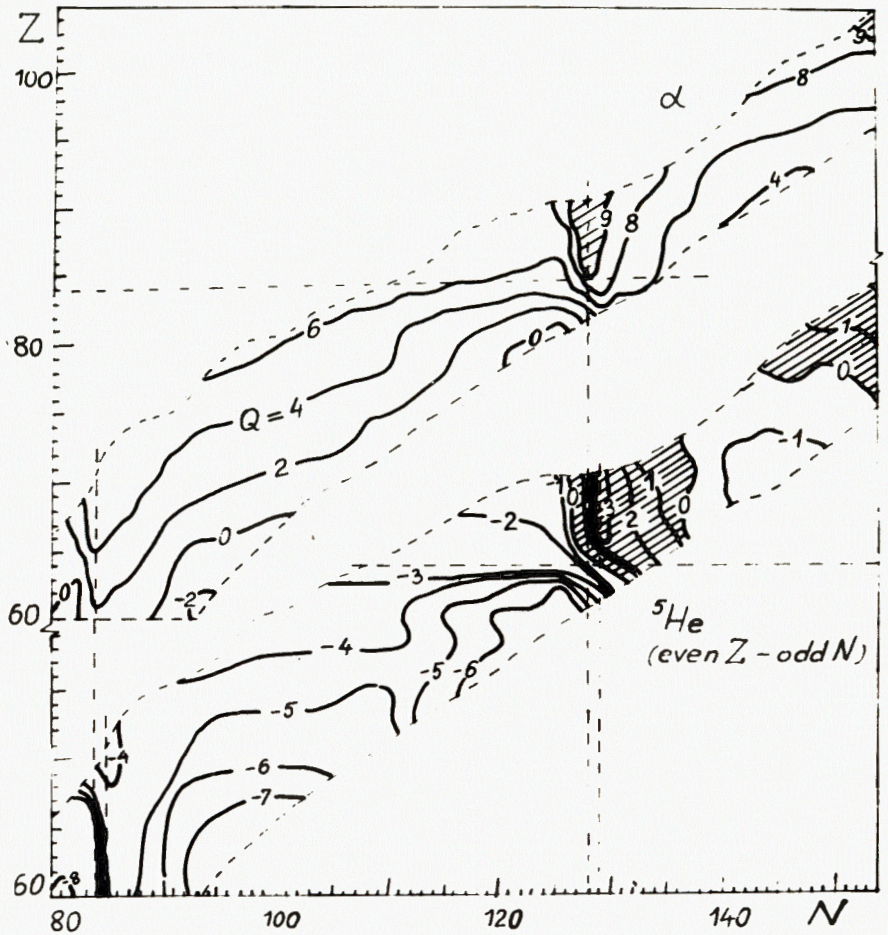

Fig. 51. **Q** *-values for the emission of alpha particles and* ^{5}**He** *from heavy nuclei. Only even* **Z** *and odd* **N** *nuclei are considered for* ^{5}**He.**

figure 53 (Poenaru et al.1983a). Due to the shell effects, the smallest lifetime is obtained for a parent nucleus like ^{218}Po, leading to the double magic daughter ^{208}Pb.

In spite of the experimental effort, the exotic nucleus ^{10}He is undiscovered up to now and moreover, it is not definetly settled whether it is stable or not. Our calculations show that in order to obtain the minimum lifetime (for E* under the barrier height), the region best suited for experimental search is that of excited compound neutron-rich isotopes of the trans-lead elements.

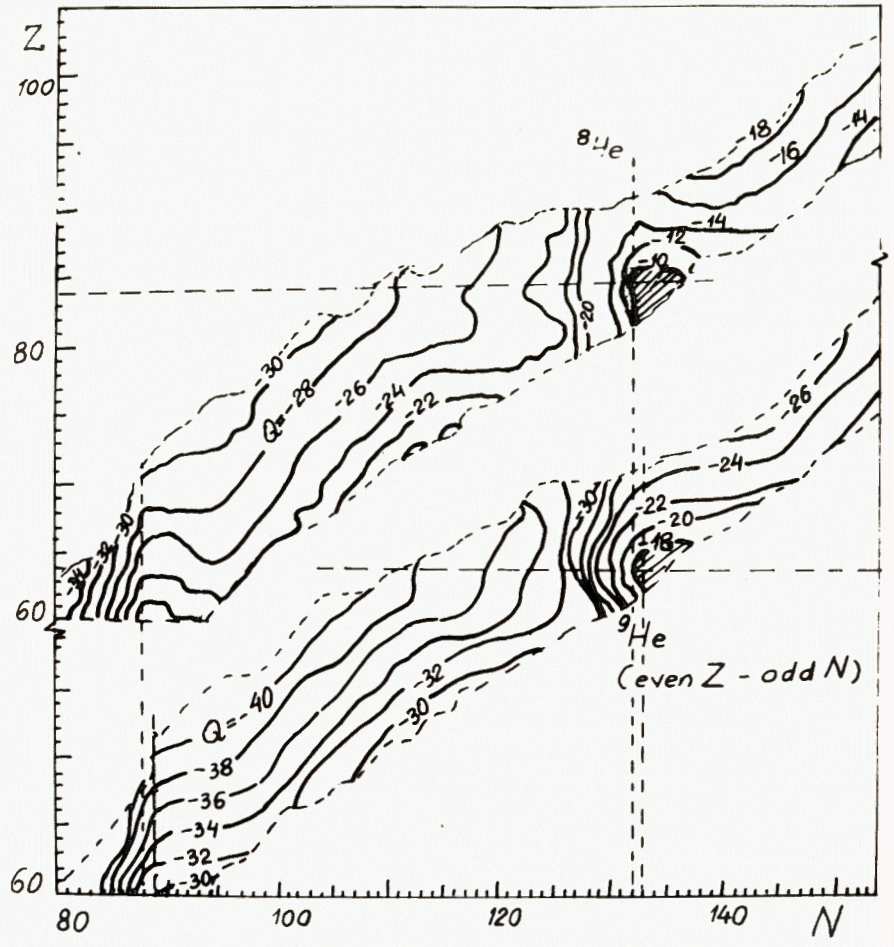

Fig. 52. **Q** *-values for the emission of* ^{8}**He** *and* ^{9}**He** *from heavy nuclei. Only even* **Z** *and odd* **N** *nuclides are considered for* ^{9}**He.**

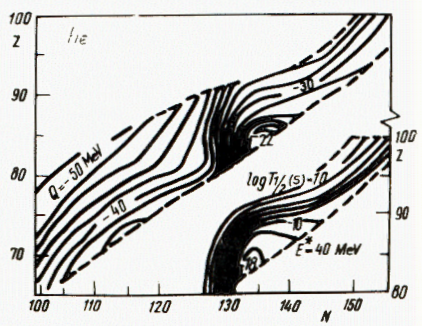

Fig. 53. **Q** *-values for* ^{10}**He** *emission from ground states and the lifetime for the fraction of the excitation energy concentrated in this collective mode* **E*** *= = 40 MeV.*

8.5. Spontaneous Emission of ^{14}C and of Other Heavy Clusters

In two papers entitles "New Type of Decay of Heavy Nuclei Intermediate between Fission and Alpha Decay" (Sandulescu et al. 1980) and "Emission of Alpha Particles and Other Light Nuclei as a Fission Process" (Poenaru and Ivascu. 1980), we have shown that for many heavy nuclei, the ground state is metastable (the released energy $Q > 0$) with respect to the very asymmetric spli and this phenomenon, like alpha decay (Poenaru et al.1979) coul be considered a fission process described with the Strutinsky (1967) macroscopic-microscopic method adopted for this super-asymmetric case.

Initially (Sandulescu et al.1980), the emission of various heavy clusters like ^{14}C, ^{24}Ne, ^{24}Mg, $^{32,34}Si$, , ^{46}Ar, ^{48}Ca, etc., from some particular parents like $^{222,224}Ra$, $^{230,232}Th$ and heavier nuclides up to ^{254}No have been predicted on the basis of very simple calculations of penetrability. Then, an analytical expression of the lifetime have been obtained (Poenaru and Ivascu 1980) and was used to made a systematic study of various cluster emission from the ground state or low excited states populated by beta decay of a precursor (beta delayed heavy clus ter radioactivity). If we consider all nuclei (~2000) with masses tabulated by Wapstra and Bos (1977) and the 100 isotopes of the emitted elements with $Z = 1$-10, the number of the possible combinations ground state parent - cluster emitted is of the order of $2 \cdot 10^5$. Of course, only a closed formula can be used for such a purpose, but in the future the most interesting cases revealed in this way could be studied with more refined methods.

As was shown in the preceding sections, the He isotopes with $A = 3$-10 have been studied firstly, allowing to predict ^{5}He radioactivity and deta delayed ^{5}He-radioactivity (Poenaru and Ivascu 1983b, 1984a) and to show the regions of the nuclear chart where ^{10}He emission from excited states has the most important chance to be met (Poenaru et al.1983). It was stressed that the maximum probability is encountered for the processes leading to a double magic daughter.

This conclusion was also advanced by Rose and Jones (1984) whi discovered the ^{12}C radioactivity * of ^{223}Ra - giving the first evidence for such a new type of decay mode.

In our computations, initially, the zero point vibration energy $E_{vib} = 0.51$ MeV was determined by fit with experimental data on 376 alpha emitters - the same given as input in the computer program described by Poenaru et al.(1980). With this value one obtains (Poenaru and Ivascu 1984b) the results from which the optimum-optimorum cases are shown in Table 5. For

* Confimed also by Dr.Ogloblin (1984) and coworkers from Kurchatow Institute in Moscow (see p.2 of the present paper).

Table 5

Some high probability heavy cluster emissions ($N_1 = 126$); $E_{vib} = 0.51$ MeV

N_2	Z_2	Z_1	Q (MeV)	log T(s)	N_2	Z_2	Z_1	Q (MeV)	Log T(s)
2	2	82	8.95	-6.52*)	2	3	86	5.69	34.61
3	(He)	82	3.71	20.88	3	(Li)	86	5.42	42.08
					4		82	5.59	41.09
3	4	86	7.37	57.55					
4	(Be)	85	18.27	11.96	5	5	86	18.57	32.82
5		82	14.06	23.90	6	(B)	82	21.71	21.99
					7		82	19.86	28.97
5	6	85	22.96	37.70					
6	(C)	85	33.98	14.98	7	7	84	36.90	24.49
7		82	31.59	17.86	8	(N)	82	39.48	19.15
8		82	33.05	16.37	9		82	36.30	26.11
		82	33.62 +)	18.57 +)					
7	8	83	39.21	33.64	10	9	82	50.08	30.58
8	(O)	83	47.32	20.79	11	(F)	82	50.65	30.68
9		82	44.87	24.76	12		82	51.69	29.89
10		82	45.73	24.37	13		82	51.10	31.86
10	10	82	58.02	30.83	11	10	82	58.69	30.79
12	(Ne)	82	61.39	27.63	13	(Ne)	82	60.69	29.51
14		82	62.30	27.87	15		82	60.82	30.90

*) Experimental value

+) For $N_1 = 127$

a very large number of cases taken into consideration (approximately 2×10^5) only that leading to shortest lifetimes are given in this table. One can see that the high probability processes are encountered for that combination leading to a daughter nucleus ($A_1 Z_1$) with magic number of neutrons $N_1 = 126$. The Z_1 optimum proton number is not always a magic one, $Z_1 = 82$; it can be also 83, 84, 85 or 86. This shown once more that in the lead region of the nuclear chart of neutron shell effects, included in Q-values by this model, are stronger than the proton ones. The shell effects at $N_1 = 126$ are much stronger than that for lighter nuclei.

A pairing effect is also observed: the even Z_2 clusters have higher probability then their odd Z_2 neighbours to escape from heavy nuclei.

The absolute values of logT presented in table 5 are only tentative estimates, due to the fact that the potential barrier is overestimated and the parameter E_{vib}, which can be chosen by a fitting procedure to compensate this effect, was taken as for the alpha decay (0.51 MeV). In this way the heavier is the nucleus, the highest is the error in logT. For example in case of ^{14}C radioactivity of ^{223}Ra, one has for the lifetime relative to the alpha decay $\log T_\alpha = 6.3$ and from the measured (Rose and Jones 1984) branching ratio $(8.5 \pm 2.5) \cdot 10^{-10}$ one has $\log T^{exp} = 15.1$. The corresponding calculated value for $N_1 = 127$ is $\log T = 18.6$ - about three orders of magnitude too pessimistic. This means that in the experiment we can expect to find for lifetimes lower values, than that given in table 5 and this is especially true for heavy clusters far from alpha particle. Nevertheless one can conclude the discussion concerning table 5 by saying that besides the well-known alpha decay, one proton and two-protons emission, one can observe many other charged particle radioactivities like: ^{8}Be, $^{12,14,13}C$, , ^{15}N, ^{16}O, ^{5}He, ^{11}B, , ^{9}Be, ^{22}Ne, ^{18}O, ^{14}N, ^{17}O, ^{16}N, ^{24}Ne, ^{12}B, ^{23}Ne, $^{21,20}F$, etc., if we refer only to $Z_2 = 2$-10 for which the search was initially made. Of course, the intensities of these processes are by many orders of magnitude weaker than those of the alpha decay.

Now the first measured branching ratio, allows us to improve our estimations. In the following we present some results obtained by considering that in order to compensate the barrier overestimations for various clusters $E_{vib} = 0.51\, A_2/4$, with which $\log T = 14.9$ for the ^{14}C emission from ^{223}Ra.

The absolute values of logT estimated in this way for the emission of ^{14}C from various isotopes of Rn, Fr, Ra, Ac, Th, Pa, and U are plotted in the lower part of the figure 54, where (-logT) was plotted in order to have an indication about the relative intensities. One can see that the minimum lifetime is obtained at $N = 134$ ($N_1 = 126$) for Ra isotopes ($Z_1 = 82$), followed by Ac, Th, Fr, Pa, U, and Rn.

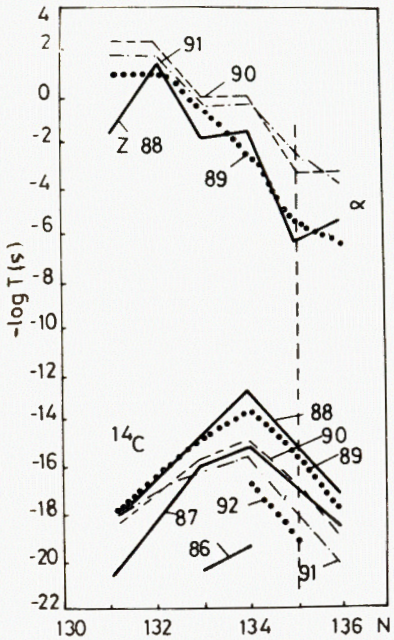

Fig.54. Variation with parent nucleus neutron number of the lifetime for ^{14}C and alpha radioactivities of some isotopes of Rn, Fr, Ra, Ac, Th, Pa *and* U.

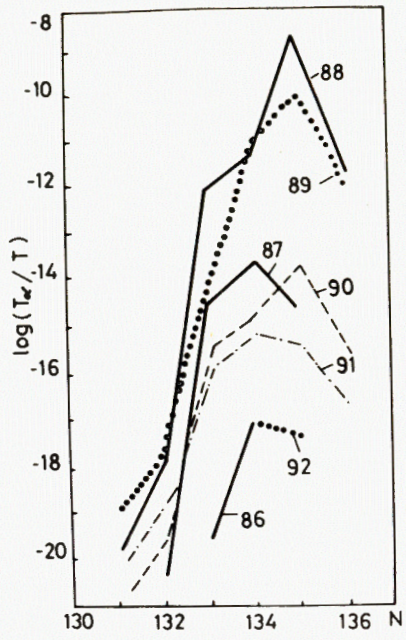

Fig.55. The ratio T_α/T for the same nuclides as in figure 54.

Usually, the most important competitor of heavy cluster emission is alpha decay and, from the experimentalist point of view, it is most important to know the ratio T/T_α, as it is presented in figure 55. From this figure, one can see that for some elements like Ra, Ac, and Th, the minimum value of T/T_α is not obtained at $N_1 = 126$ ($N = 134$), where T has its minimum, but at $N_1 = 127$ ($N = 135$) because T_α, plotted in the upper part of the figure 1, has steepest variation with N.

Another conclusion is that Rose and Jones (1984) discovered the best ^{14}C emitter. Nevertheless, we found that some other isotopes of Ra and Ac, like $^{224,223}Ac$, $^{222,224}Ra$, ^{225}Ac and ^{221}Ra, have also good ratio T/T_α.

To illustrate the answer to the other problem which is important for someone planning an experiment, we present in table 6 the most probable emissions from several long-lived nuclides. One can see that in all cases the daughter nucleus has magic number of neutrons or protons, or it is not far from it. Besides ^{223}Ra already measured, for which $\log(T/T_\alpha^{exp})$ has the lowest

Table 6

Most probable cluster emission from some parent nuclei

Parent	Daughter		Emitted		$\log T(s)$	$\log T_\alpha^{exp}$	$\log(T/T_\alpha^{exp})$
	N_1	Z_1	Cluster	E(MeV)			
^{223}Ra	127	82	^{14}C	31.84	14.9	6.3	8.6
^{224}Ra	128	82	^{14}C	28.21	21.9	10.7	11.2
^{227}Ac	130	83	^{14}C	28.07	23.2	11.0	12.2
	126	81	^{20}O	43.09	24.0		13.
^{230}Th	126	80	^{24}Ne	57.76	25.3	12.5	12.8
	126	82	^{22}O	43.13	26.2		13.7
^{232}Th	126	80	^{26}Ne	56.59	27.9	17.8	10.1
^{231}Pa	126	82	^{23}F	51.83	24.7	12.0	12.7
^{232}U	126	82	^{24}Ne	62.30	21.3	9.5	11.8
^{233}U	127	82	^{24}Ne	60.49	23.9	12.8	11.1
	126	82	^{25}Ne	60.82	23.8		11.0
^{234}U	126	82	^{26}Ne	60.09	25.2	13.0	12.2
	128	82	^{24}Ne	58.83	26.3		13.3
	126	80	^{28}Mg	74.11	25.8		12.8
^{235}U	127	82	^{26}Ne	58.73	27.3	16.3	11.0
	128	82	^{25}Ne	57.80	28.3		12.0
	125	80	^{30}Mg	73.00	28.0		11.7
^{238}U	126	80	^{32}Mg	71.15	31.0	17.3	13.7
^{237}Np	126	81	^{30}Mg	75.70	25.7	14.2	11.5
^{252}Cf	126	80	^{46}Ar	126.72	24.1	8.0	16.1

value, there are some other cases deserving attention, like: ^{14}C radioactivity of ^{226}Ra; ^{26}Ne radioactivity of ^{232}Th; $^{24,25}Ne$ emission from ^{233}U; ^{26}Ne emission from ^{235}U; ^{30}Mg emission from ^{237}Np, etc. It is possible to find other more favourable cases by doing more systematic search. Of course, one must stress again that all absolute values given in this section are only tentative estimates because the parameter E_{vib} was fitted only for alpha particles and ^{14}C.

9. CONCLUSIONS

In order to show that the gap between $A_2 = 4$ and $A_2 \simeq 70$ ($Z_2 = 2$ and $Z_2 \simeq 30$) in the fission fragment mass distribution can be fitted by new kinds of radioactivities, we have studied systematically the nuclear stability toward very asymmetric split. The extension of the fission theory to these superasymmetric processes was tested at the beginning on alpha-decay, due to the large wealth of experimental data available at the time.

Promising results have been obtained by applying the fission theory for the calculation of the alpha disintegration half-lives between ground states or low excited states below the barrier. Consequently, the traditional picture of the alpha preformation, followed by tunneling through the potential barrier, can be replaced by the larger amplitude oscillations (asymmetric fission mode) of the nuclear surface favoured energetically by the shell effects and leading to a very asymmetric split also by the quantum mechanical tunnel effect. The preformation factor role is played by the zero point vibration frequency.

For a very large mass asymmetric fission, the charge density asymmetry plays an important part. Three macroscopic models have been extended for nuclear systems with different charge densities. A phenomenological correction was introduced, accounting for both the shell effects, the nuclear deformation and the neglected terms of the mass formula. The shell correction part could be also described by Schultheis cluster prescription.

The fact that the macroscopic models, having the parameters obtained from a fit of experimental data for masses and almost symmetrical fission and fusion barriers, with a suitable phenomenological correction, reproduce the potential barrier shape is attested by the good agreement of the theoretical lifetimes for alpha decay with the experimental ones, over a range of some 24 orders of magnitude. The time dependent Hartree-Fock method gives the same zero point vibration frequency with that obtained from a fit with experimental data.

By taking into account the nuclear deformation of the parent and daughter nuclei, the agreement of Q-values with experi-

mental results was improved and it was possible to predict for the first time the lifetime of the alpha decay from a shape isomeric shate. This is many orders of magnitude larger than that of isomeric spontaneous fission, which explains the unsuccessful experimental research.

In principle this theory can explain both the Q-values and the half-lives. It has to be improved by extending the microscopic shell correction method for light nuclei or very asymmetric fission. Also the mass parameters and the zero point virration energy of this mode need further investigation.

The new semiempirical relationship for the lifetime takes into consideration explicitly the dependence not only on the proton number but also on the neutron number and their departure from magicity. In comparison with other formulae for the known regions of alpha emitters it gives the best estimates.

The estimation of the general trend of nuclear stability with respect to the emission of charged particles revealed many interesting facts. For the spontaneous emission of $^{2,3}H$, $^{3,6-10}He$, ^{4}Li, ^{7}N, ^{9}C and some other clusters, all nuclei with masses tabulated by Wapstra and Bos are stable ($Q<0$) in the ground state. ^{5}He radioactivity is energetically possible for some 110 nuclides grouped in two archipelagos with Z = 83-92, N = = 127-137, Z = 97-105, N = 145-157. The last region extends also for superheavy nuclei.

The analytical formula accounting for angular momentum and low excitation energies, allow to handle a large number of cases to search for other new kinds of radioactivities. Among the elements with Z = 3-8, good chances to be emitted have ^{8}Be, $^{12,13,14}C$, ^{15}N, ^{16}O, ^{5}He, etc. The most favourable case for ^{14}C emission in competition with alpha decay was already measured, but there are some other possible candidates like $^{224,223,225}Ac$ and $^{222,224,221}Ra$. By analysing several long-lived heavy elements, it was found that other clusters like $^{20,22}O$, ^{23}F, $^{24,25,26}Ne$, $^{28,30,32}Mg$ could have the ratio T/T_{α} within 10-13 orders of magnitude. In all cases this phenomenon, like the usual small asymmetry well-known in fission is a new manifestation of the nuclear shell structure, being stronger for the combinations parent-cluster leading to a magic-daughter or not too far from it.

REFERENCES

Abromowitz M. and Stegun I.A. (editors) 1964 Handbook of Mathematical Functions (Washington: National Bureau of Standards).

Adeev G.D., Filipenko L.A., Cserdantsev P.A. 1976 Yad.Fiz., 23, 30.

Adeev G.D., Gamalya I.A., Cherdantsev P.A. 1970 Yad.Fiz., 12,272.

Ajzenberg-Selove P., Lauritsen T. 1974 Nucl.Phys. A227 1.

Bauer M. 1976 At.Data Nucl.Data Tables 17 443.

Becquerel H. 1896 Compte Rendue 122.

Beiner M., Lombard R.J. and Mas D. 1976 At.Data Nucl.Data Tables 17 450.

Below A.G., Gangrsky Yu.P., Dalkhsuren B., Kucher A.M. and Nguen Kong Khan 1973 Xad.Fiz, 17 942.

Bemis C.R.(Jr.), Dittner P.F., Ferguson R.L., Hensley D.C., Plasil F. and Pleasonton F. 1981 Phys.Rev. C23 555.

Beringer R. 1963 Phys.Rev. 131 1402.

Beringer R. and Knox W.J. 1961 Phys.Rev. 121 1195.

Bjørnholm S. and Lynn J.E. 1980 Rev.Mod.Phys. 52 725.

Blatt J.M. and Weisskopf V.F. 1956 Theoretical Nuclear Physics (New York: John Wiley).

Bohr N., Wheeler J.A. 1939 Phys.Rev. 56 426.

Brack M., Damgaard J., Jensen A.S., Pauli H.C., Struntinsky V.M. and Wong C.Y. 1972 Rev.Mod.Phys. 21 109.

Britt H.C. 1973 At.Data Nucl.Data Tables 12 408.

Cable M.D., Honkanen J., Parry R.F., Zhou S.H., Zhou Z.Y. and Cerny J. 1983 Phys.Rev.Lett. 50 404.

Cabot C., Della Negra S., Deprun C., Gauvin H. and Le Beyec Y. 1978 Z.Physik A287 71.

Carlson B.C. 1961 J.Math.Phys. 2 441.

Cody W.J. 1965 Math.Comp. 19 105.

Comay E. and Kelson I. 1976 At.Data Nucl.Data Tables 17 463.

Cohen S. and Swiatecki W.J. 1962 Ann.Phys.(N.Y.) 19 67.

Condon E.U. and Gurney R.W. 1929 Phys.Rev. 33 127.

Cusson R.Y., Maruhn J.A. and Stöcker H. 1980 Z.Physik A294 245.

Davies K.T.R. and Sierk A.J. 1975 J.Comput.Phys. 18 311.

Davis P.J. and Rabinowitz P. 1975 Methods of Numerical Integration (New York: Academic Press).

Epherre M. 1983 in Proc. 7e session d´etudes biennale de Phys. Nucl. - (Aussois, IPN Lyon) c.4.1.

Fink H.J., Maruhn J., Scheid W. and Greiner W. 1974 Z.Physik 268 321.

Fiset E.O. and Nix J.R. 1972 Nucl.Phys. A193 647.

Frenkel J. 1946 Journal of Physics 10 533.

Fröman P.O. 1957 Mat.Fys.Sk.Dan.Vid.Selsk. 1 3.

Galeriu D. and Poenaru D.N. 1976 Rev.Roum.Phys. 21 109.

Gamow G. 1928 Z.Physik 52 510.

Gauvin H., Le Beyec Y., Livet J. and Reyss J.L. 1975 Ann.Phys. (Paris) 9 241.

Goepert-Mayer M. 1949 Phys.Rev. 75 1969.

Goldansky V.J. 1960 Nucl.Phys. 19 482.

Gorbachev V.M., Zamiatnin Yu.S. and Lbov A.A. 1975 Osnovnye harakteristiki izotopov tiajelyh elementov (Moscow: Atomizdat).

Groote H. von, Hilf E.R. and Takahashi K. 1976 At.Data Nucl. Data Tables 17 418.

Gupta R.K. 1977 Z.Phys. A281 159.
Gupta R.K., Scheid W. and Greiner W. 1975 Phys.Rev.Lett. 35 353.
Hagberg E., Hansen P.G., Hornshøj P., Jonson B., Mattson S. and Tiedemand-Petersson P. 1979 Nucl.Phys. A318 29.
Hahn O. and Strassmann F. 1939 Naturwiss 27 11, 89.
Hill D.L. and Wheeler J.A. 1953 Phys.Rev. 89 1102.
Hofmann S., Faust W., Münzenberg G., Reisdorf W., Armbruster P., Güttner K. and Ewald H. 1979 Z.Physik A291 53.
Holm G. and Greiner W. 1970 Phys.Rev.Lett. 24 404.
Hornshøj P., Hansen P.G., Jonson B., Ravn H.L., Westgaard L. and Nielsen O.N. 1974 Nucl.Phys. A230 365.
Ivascu M. and Poenaru D.N. 1978 in Proc. Predeal International School on Heavy Ion Physics (editors A.Berinde, V.Ceausescu and I.A.Dorobantu) 1119.
Ivascu M. and Poenaru D.N. 1981 Nuclear Deformation Energy and Shape Isomers (in romanian) (Bucharest: Romanian Academy Publ.House).
Jänecke J. 1976 At.Data Nucl.Data Tables 17 463.
——— 1980 private communication.
Jänecke J. and Eynon B.P. 1976 At.Data Nucl.Data Tables 17 467.
Junker K. 1974 Acta Phys.Austriaca 40 335.
Karnaukhov V.A. 1974 Nukleonika 19 425.
Karnaukhov V.A. and Ter-Akopyan G.M. 1967 Ark.Fys. 36 419.
Keller K.A. and Münzel H. 1972 Z.Physik 255 419.
Krappe H.J. 1976 Nucl.Phys. A269 493.
Krappe H.J. and Nix J.R. 1974 in Proc. Symp.on Phys. and Chem. of Fission (Vienna: IAEA) vol.1, p.159.
Krappe H.J., Nix J.R. and Sierk A.J. 1979 Phys.Rev. C20 992.
Lawrence J.N.P. 1965 Phys.Rev. 139 B1227.
Leachman R.M. and Erkkila B.H. 1966 Bull.Am.Phys.Soc. 10 1204.
Lederer C.M. and Shirley V.S. 1978 Table of Isotopes (New York: John Wiley & Sons).
Liran S. and Zeldes N. 1976 At.Data Nucl.Data Tables 17 431.
Macfarlane R.D., Siivola A. 1965 Phys.Rev.Lett. 14 114.
Maripuu S. (editor) 1976 At.Data Nucl.Data Tables 17 411.
Maruhn J.A. and Greiner W. 1976 Phys.Rev. C13 2404.
Meitner L. and Frisch O.R. 1939 Nature 143 239.
Metag V., Habs D. and Specht H.J. 1980 Phys.Rep. 65 1.
Michaudon A. 1981 Nuclear Fission and Neutron-Induced Fission Cross-Sections (Oxford: Pergamon Press).
Möller P. 1972 Nucl.Phys. A192 529.
Möller P. and Aberg S. 1980 Phys.Lett. 92B 223.
Möller P. and Nilsson S.G. 1970, Phys.Lett. 31B 283.
Möller P. and Nix J.R. 1976 Nucl.Phys.A269 493.
——— 1977 Nucl.Phys. A281 354.
——— 1981 Nucl.Phys. A361 117.
Möller P., Nilsson S.G. and Nix J.R. 1974 Nucl.Phys. A229 292.
Moretto L.G. 1975 Nucl.Phys.A247 211.

Mustafa M.G., Mosel U. and Schmitt H.W. 1972 Phys.Lett. 28 1536.
Myers W.D. 1977 Droplet Model of Atomic Nuclei (New York: Plenum).
Myers W.D. and Swiatecki W.J. 1966 Nucl.Phys. 81 1.
——— 1967 Ark.Fys. 36 343.
Nix J.R. 1972 Ann.Rev.Nucl.Sci. 22 65.
Nyman G., Azuma R.E., Jonson B., Kratz K.L., Larsson P.O., Mattsson S. and Ziegert W. 1981 CERN 81-09, 312.
Pashkevich V.V. 1971 Nucl.Phys. A169 275.
Perlman J. and Rasmussen J.O. 1957 in Handbuch der Physik (Berlin: Springer) band XLII, p.109.
Petryak K.A. and Flerov G.N. 1940 J.E.T.F. 10 1013.
Ptochocki A., Zylicz J., Kirchner R., Klepper O., Roeckl E., Tidemand-Pettersson P., Grant I.S. and Misaelides P. 1982 Nucl.Phys. A388 91.
Poenaru D.N. 1977 Ann.Phys. (Paris) 2 133.
Poenaru D.N. and Galeriu D. 1975 Inst. for Atomic Physics, Bucharest, report CRD-60.
Poenaru D.N. and Ivascu M. 1978 Comp.Phys.Commun. 16 85.
——— 1979 Rev.Roum.Phys. 24 119.
——— 1980 Lecture at Poiana-Brasov Int.School "Critical Phenomena in Heavy Ion Physics", p.743.
——— 1981a in Proc. of the EPS Div.Conf. "Nuclear and Atomic Physics with Heavy Ions" Bucharest p.681.
——— 1981b J.Phys.G: Nucl.Phys.7 965.
——— 1982 Rev.Roum.Phys. 27 129.
——— 1983a J.Phys. 44 791.
——— 1983b Rev.Roum.Phys. 28 309.
——— 1984a J.Phys.45.
——— 1984b Central Inst. of Physics, Bucharest, report NP-31-1984.
Poenaru D.N., Ivascu M. and Mazilu D. 1980a Comp.Phys.Commun. 19 205.
——— 1980b J.Phys.Letters 41 L-589.
——— 1982 Comp.Phys.Commun. 25 297.
Poenaru D.N., Ivascu M., Mazilu D. and Sandulescu A. 1980c Rev. Roum.Phys. 25 55.
Poenaru D.N., Ivascu M. and Sandulescu A. 1979a J.Phys.Letters 40 L-465.
——— 1979b J.Phys.G: Nucl.Phys. 5 L-169.
——— 1979c Rev.Roum.Phys. 24 917.
——— 1981 Rev.Roum.Phys. 26 253.
——— 1983a in Proc.Int.Conf. on Nucl.Phys., Florence, vol.1, p.662.
——— 1983b JINR, Dubna, report E4-83-858.
——— 1984 to be published.
Poenaru D.N., Mazilu D. and Ivascu M. 1979d J.Phys.H: Nucl.Phys. 5 1093.

Polikanov S.M., Druin V.A., Karnaukhov V.A., Mikheev V.M., Pleve A.A., Skobelev N.K., Subotin V.G., Ter-Akopyan G.M. and Fomichev V.A. 1962 JETF 42 1464.
Rasmussen J.O. 1959 Phys.Rev. 113 1593.
Ritchie B.G., Toth K.S., Carter H.K., Mlekodaj R.J. and Spejevski E.H. 1981 Phys.Rev. C23 2342.
Rose H.J. and Jones G.A. 1984 Nature 307 245.
Roynette J.C., Frascaria N., Blumenfeld Y., Jacnart J.C., Plagnol E., Garron J.P., Gamp A. and Fuchs H. 1981 Z.Phys. A299 73.
Rurarz E. 1982 Warszawa Inst.Nucl.Res. report INR 1950/IA/PL/A.
Rutherford E. and Geiger H. 1908 Proc.Roy.Soc. (London) A81 141.
Rytz A. 1979 At.Data Nucl.Data Tables 23 507.
Sandulescu A., Cusson R.Y. and Greiner W. 1983 Lett. Nuovo Cimento 36 321.
Sandulescu A., Poenaru D.N. and Greiner W. 1980 E.Ch.A.Ya. 11 1334 translated Sov.J.Part.Nucl.11(6) 528.
Sauer G., Chandra H. and Mosel U. 1976 Nucl.Phys. A264 221.
Schardt D., Batsch T., Kirchner R., Klepper O., Kurcewicz W., Roeckl E. and Tidemand-Petersson P. 1981 Nucl.Phys. A368 153.
Schardt D., Kirchner R., Klepper O., Reisdorf W., Roeckl E., Tidemand-Petersson P., Ewan G.T., Hagberg E., Jonson B., Mattson S. and Nyman G. 1979 Nucl.Phys. A326 65.
Schmidt K.H., Faust W., Münzenberg G., Clerc H.G., Lang W., Pielenz K., Vermeulen D., Wohlfarth H., Ewald H. and Güttner K. 1979 Nucl.Phys. A318 253.
Schultheis H. and Schultheis R. 1973 Nucl.Phys. A215 329.
Schultheis H., Schultheis R. and Süssmann G. 1970 Nucl.Phys. A144 545.
Seeger P.A. and Howard W.M. 1975 Nucl.Phys. A238 491.
Seelmann-Eggebert W., Pfennig G., Münzel H. and Klewe-Nebenius H. 1981 Nuklidkarte (Karlsruhe: Kernforschunszenrum).
Sobotka L.G., Padgett M.L., Wozniak G.J., Guarino G., Pacheco A.J., Moretto L.G., Chan Y., Stokstad R.G., Tserruya J. and Wald S. 1983 Phys.Rev.Lett.51 2187.
Stöcker H., Cusson R.Y., Maruhn J.A. and Greiner W. 1980 Z.Phys. A294 125.
Strutinsky V.M. 1967 Nucl.Phys. A95 420.
Taagepera R. and Nurmia M. 1961 Ann.Acad.Sci.Fennicae, Ser.A, Physics nr.78.
Tidemand-Petersson P., Kirchner R., Klepper O., Roeckl E., Ptochocki A., Zylicz J. and Schardt D. 1981 CERN 81-09 vol.1 205.
Vandenbosch R. 1977 Ann.Rev.Nucl.Sci. 27 1.
Viola V.E. (Jr.) and Seaborg G.T. 1966 J.Inorg.Nucl.Chem. 28 741.
Wapstra A.H. and Bos K. 1977 At.Data Nucl.Data Tables 19 215.

Wapstra A.H., Nijgh G.J., and Van Lieshout R. 1959 in Nuclear Spectroscopy Tables (Amsterdam: North Holland).
Weiss M.S. 1981 in Dynamics of Heavy Ions Collisions (editors N.Cindro, R.A.Ricci and W.Greiner) (Amsterdam: North Holland) p.115.
Zohni O. and Blann M. 1978 Nucl.Phys. A297 170.

◇

CONTENTS

Received by Publishing Department
on June 27, 1984.

Познару Д.Н. и др. E4-84-446

Ядерный распад как эмиссия заряженных частиц -суперасимметричный процесс деления

Макро-микроскопический метод, рассчитанный для суперсимметричного деления, был применен к альфа-распаду и другим видам испускания заряженных частиц, которые возможны благодаря структуре ядерных оболочек. Три макроскопические модели /жидкокапельная модель, модель ядерных сил конечного предела и Юкава-экспоненциальная модель/ были применены к ядерным системам с различными плотностями заряда. Представлены различные цифровые методы для расчета кулоновской и поверхностной энергии ядра общей конфигурации, а также аналитические результаты для некоторых особых конфигураций. Для получения экспериментальной величины Q использовалась феноменологическая коррекция.Этот формализм был применен к альфа-распаду из основного состояния и изомерного состояния,распределяющегося путем деления.Для оценки энергии нулевых колебаний использовался временнозависимый метод Хартри-Фока. Выведена новая полуэмпирическая формула, дающая лучшие оценки времен жизни альфа-распада для предсказания новых альфа-излучателей. Для этого нового способа распада, промежуточного между альфа-распадом и традиционным делением, получены большие вероятности комбинаций родительское ядро-тяжелый кластер, приводящие к дочерним магическим ядрам или близким к ним.

Работа выполнена в Лаборатории теоретической физики ОИЯИ.

Сообщение Объединенного института ядерных исследований. Дубна 1984

Poenaru D.N. et al. E4-84-446

Nuclear Decay by Emission of Charged Particle - Superasymmetric Fission Process

The macroscopic-microscopic method, adapted for superasymmetric fission was applied to the alpha decay and other kinds of charged particles radioactivities, which are possible due to the nuclear shell structure. Three macroscopic models (the liquid drop model, the finite range of nuclear forces model and the Yukawa-plus-exponential model) are extended for nuclear systems with different charge densities. Various numerical methods for the computation of Coulomb and surface energy of a general shape nucleus are presented along with analytical results for some particular configurations. A phenomenological correction was used to obtain the experimental Q-value. This formalism was applied to the alpha decay from the ground state and from a fission isomeric state. A time dependent Hartree-Fock method is used to estimate the zero point vibration energy. A new semiempirical formula giving the best estimates for the alpha decay lifetimes was derived and used to predict new alpha emitters. For this new mode of decay intermediate between alpha decay and the traditional fission, larger probabilities are obtained for the combinations parent-heavy cluster leading to a magic daughter or not too far from it.

The investigation has been performed at the Laboratory of Theoretical Physics, JINR.

Communication of the Joint Institute for Nuclear Research. Dubna 1984